universität wien

DISSERTATION

Titel der Dissertation

Structure and function of P-glycoprotein

angestrebter akademischer Grad

Doktorin der Naturwissenschaften (Dr. rer. nat.)

Verfasserin / Verfasser:	Mag. rer. nat. Sandra Pferschy
Matrikel-Nummer:	9545056
Dissertationsgebiet (lt. Studienblatt):	A 091 441 Genetik-Mikrobiologie
Betreuerin / Betreuer:	Ao. Univ.-Prof. Dr. Chiba / Ao. Univ.-Prof. Dr. Ecker

Wien, am 09. Juli 2009

Für Matthias

„Sicherlich gibt es mich: ICH BIN ICH!“ (Mira Lobe: Das kleine ICH BIN ICH)

TABLE OF CONTENTS

List of figures

List of tables

Acknowledgements

I would like to express my gratitude to all those who gave me the possibility to complete this thesis.

First of all I would like to thank my supervisor Prof. Dr. Peter Chiba for providing help and advice whenever I needed it, for providing the facilities and the means to do this thesis.

…because of this thesis I gained the friendship of amazing people…
Especially, I would like to give my special thanks to Matthias for his encouragement and motivation and for making the cell culture room such a great place to work. He made it his business to make me laugh… ☺ It was a pleasure to work with you.

Thank you Stephan for being such a good colleague. I will keep in mind our coffee breaks and discussions about "all the world and his brother". Such a really great friendship is not found every day!

My colleagues from the Institute of Medical Chemistry supported me in my research work. I want to thank them for all their help, support, interest and valuable hints. Thank you Nina, thank you Sabine and especially I would like to thank Angelika. She was the one keeping up my spirits drinking one or two or three "white spritzer" in the cafe Stein with me after a long working day.

I would like to thanks my colleagues from our cooperation group from the Department of Specific Prophylaxis and Tropical Medicine. Thank you Matthias again, thank you Bene and thank you Peter.

Thanks to my family for always being there for me. Thank you dad for your support and believing in me. Danke Mama für die vielen Telefonate, die mich immer für ein paar Minuten all meine Probleme vergessen ließen und für all deine guten Köstlichkeiten, die mir bei jedem kurzen Besuch das Gefühl gaben, daheim zu sein. Thank you Martina for being there.
…without you this would not have been possible.

Thank you Reini for your help in solving genetic problems.

And then there is a string of independent friends, spread all over the world, whom I want to say Thank you for their listening ear and cheer-ups.

Thank you very much!

1 Abstract

The human multidrug resistance P-glycoprotein (P-gp), the product of the *MDR1* gene, is an ATP-binding cassette (ABC) protein that uses ATP to transport a variety of cytotoxic compounds without a common structure or intracellular target, out of the cell. The protein is clinically important since it contributes to the phenomenon of multidrug resistance during chemotherapy of human cancers. It has two homologous halves that are joined by a linker. Each half consists of a hydrophobic transmembrane domain containing six transmembrane (TM) segments and a hydrophilic nucleotide-binding domain (NBD) containing the nucleotide binding site.

The aim of this project was the identification and characterization of TMD1/TMD2 contact interface residues, which are important for transport of solutes. Functional assays were performed with P-gp mutants, in which the TMD1/TMD2 contact interface residues were mutated to residues other than cysteine by site directed mutagenesis based on overlap extension polymerase chain reaction (OE-PCR). The mutational concept was guided by photoaffinity labeling, availability of protein homology models, *in-silico* importance prediction of residues by real valued evolutionary trace and data-driven docking results based on previous site-directed mutagenesis data. Thus, hypothesis driven generation of P-gp mutants with amino acid residues that will be tolerated in the protein to obtain a high number of correctly targeted and functional transporters was performed. The glutamine residues Q132 (TM2) in the N-terminal half and Q773 (TM8) in the C-terminal half of P-gp were found in predicted TM segments. Homology models of P-gp suggested that these Q-residues are located between highly photolabelled residues at the TM2/11 interface and the contralateral TM5/8 interface. In some species one of these Q residues is mutated to R or E, indicating that a charge is tolerated in this position of the protein. Thus, Q132 was mutated to Q132A, Q132E and Q132R, and Q773 was mutated to Q773A, Q773E and Q773R. In addition Q132A/Q773A, Q132E/Q773E and Q132R/Q773R double mutants were generated. Mutants were characterized using efflux studies, MRK16 staining and cytotoxicity assays. The Q773R mutant was deficient for rhodamine 123 transport, while the Q773E and Q773A mutants were active. Similarly the A, E and R mutants in position 132 showed unimpaired rhodamine 123 transports. The Q132R/Q773R double mutant was also transport deficient.

2 Introduction

2.1 ABC transporters

Transport proteins form 15% to 30% of membrane proteins in a cell (Sauna and Ambudkar 2007). Decreased accumulation of natural product toxins in the cells improves the likelihood of an organism's survival. Most of these cytotoxic compounds are lipophilic and thus able to enter cells by passive diffusion across the plasma membrane. This way of self-defence is aided by active efflux pumps, which intercept toxins at the level of the membrane and extrude them back to the cell exterior. These pumps are either adenosine triphosphate (ATP)-dependent (primary active) or driven by proton or sodium motive force (secondary active). The first group of proteins belongs to the subfamily of ATP-binding cassette (ABC) transporters (Hyde, Emsley et al. 1990). The ATP-binding cassette is found in a variety of prokaryotic and eukaryotic transporters (Pohl, Devaux et al. 2005) and thus the ABC protein family represents one of the largest and most diverse families of transport proteins.

Based on the direction of the transport reaction, ABC transporters are separated into two subtypes. ABC importers require a binding protein that delivers captured substrates to the external face of the transporter. These transporters are only present in prokaryotes. (Hollenstein, Dawson et al. 2007) In contrast, ABC exporters capture their substrates directly from the cytoplasm or from the inner leaflet of the lipid bilayer (Locher 2004). While human cells express only ABC exporters, which facilitate the export of compounds, in bacterial cells many ABC importers can be found, catalyzing the import of nutrients into the cell (Loo and Clarke 2008).

Based on sequence similarities, the human ABC protein family is categorized into seven subfamilies, denoted ABC A-G, and consists of 49 members (Dean, Hamon et al. 2001; Loo and Clarke 2008), 17 of them are implicated in diseases (Sauna, Kim et al. 2007). The ABC transporters bind ATP and use the energy to drive the translocation of various substrates such as ions, lipids, peptides, metabolites, chemotherapeutic drugs and antibiotics across the plasma membrane as well as intracellular membranes of the endoplasmic reticulum (ER), peroxisome and mitochondria, and as such can be associated with many disorders in humans (examples are shown in Table 2.1).

Protein	Transport substrate	Disorder	Species
ABCA1	Cholesterol	Tangier disease	Human
ABCA4	Retinal	Stargardt disease	Human
P-gp (ABCB1)	Hydrophobic drugs	Multidrug resistance	Human
TAP1/2 (ABCB2/3)	Peptides	Wegener's granulomatosis	Human
MRP1 (ABCC1)	Leukotrienes	Multidrug resistance	Human
MRP2 (ABCC2)	GSH conjugates	Dubin-Johnson syndrome	Human
CFTR (ABCC7)	Chloride channel	Cystic fibrosis	Human
SUR1 (ABCC8)	K^+ channel regulation	PHHI	Human
BtuCD	Vitamin B12		*E. coli*
$HisJQMP_2$	Histidine		*S. typhimurium*
LmrA	Hydrophobic drugs		*L. lactis*
$MalEFGK_2$	Maltose		*E. coli*
MsbA	Lipid A		*E. coli, V. cholera*

Table 2.1: ABC transporters, transported substrates and associated disorders.

Understanding how ABC transporters work to mediate directional transport of substrates across lipid membranes has been a challenge since the first sequence of a complete ABC transporter gene was published in 1982 (Higgins, Haag et al. 1982).

2.1.1 Structural organisation of ABC transporters

All ABC transporters are composed of four protein domains or subunits: two hydrophilic nucleotide-binding domains (NBDs), also known as ATP-binding cassettes, and two hydrophobic transmembrane domains (TMDs) (Higgins, Hiles et al. 1986). These four core domains are both necessary and sufficient for transport. The NBDs, located in the cytoplasm, are the site of ATP binding and hydrolysis, providing the energy needed for solute translocation. Despite the high diversity of transport substrates, the sequences of the NDBs are remarkably well conserved among the ABC transporter family. These conserved motifs include the Walker A (or P-loop) and Walker B sequence, common to most proteins that bind nucleotide, and the ABC signature motif (also called LSGGQ

motif, linker peptide, or C motif) that contacts the nucleotide in the ATP-bound state. In addition, the NBDs of ABC transporters contain the A-loop, D-loop, H-loop, and Q-loop. In contrast to the NBDs, the TMDs which form the transport pathway mediating accessibility to either side of the membrane have higher sequence diversity and vary in the total number of transmembrane (TM) helices, length, and architecture (reviewed in (Hollenstein, Dawson et al. 2007)).

The TMDs and the NBDs are separate polypeptide chains in ABC importers. In bacterial exporters a TMD is fused to an NBD, representing a so-called "half-transporter", which as a homodimer or heterodimer forms the functional four-domain canonical structure of the ABC transporter (Saurin, Hofnung et al. 1999). In many eukaryotic ABC exporters all four domains are expressed as a single polypeptide chain.

2.2 P-glycoprotein

Mammalian P-glycoprotein is the most well characterized ABC transporter. P-glycoprotein (P-gp) was discovered by Juliano and Ling (Juliano and Ling 1976) and is encoded by the human multidrug resistance (*MDR1*, *ABCB1*) gene (Ueda, Cornwell et al. 1986; Borst, Evers et al. 2000). Human *MDR1* spans over 100 kb on human chromosome 7q21 (Yang, Wu et al. 2008). The MDR1 genome contains 29 exons that produce a 3843 bp sequence of transcripts encoding the 1280 amino acids P-gp protein with a molecular weight of 170 kDa (Yang, Wu et al. 2008).

P-gp is an ideal model system for studying processes involved in folding and trafficking of ABC transporters because these processes can be manipulated by using specific chemical/pharmacological chaperones. Processing mutants can be rescued by expression in the presence of a chemical/pharmacological chaperone such as cyclosporin A (Loo, Bartlett et al. 2004). These chaperones also are substrates or modulators of P-gp (Loo and Clarke 1997). In many cases, such as ΔF508 in CFRT, the processing mutations are located outside the critical functional domain of the protein so that the mutant protein remains functional, but does not traffick to its final destination at the plasma membrane (Denning, Anderson et al. 1992).

P-gp was the first identified eukaryotic ABC transporter and is clinically important because of its role in conferring multidrug resistance (MDR) to cancer cells (Sauna and Ambudkar 2007). The overexpression of P-gp in human cancer cells can make the cells simultaneously resistant to a variety of chemically unrelated cytotoxic drugs due to its ability to transport these compounds out of the lipid bilayer of the cell.

2.3 A medical role in physiology and medicine

The ability of a cell to protect itself against environmental toxins is an essential biological function because many organisms produce toxins to repel ecological competitors, and plants rely on toxic secondary metabolites to make themselves unappetizing (Higgins 2007). To survive, most organisms have evolved multidrug transporters to prevent cytotoxic molecules entering cells and to clear membranes of unwanted agents.

2.3.1 Cancer chemotherapy

Chemotherapy is a major form of treatment for many cancers. There are two forms for development of resistance to chemotherapy: (I) the single-agent resistance as a result of mutations to the target molecule of the chemotherapeutic drug, for example single amino acid changes in topoisomerase II result in epipodophyllotoxin resistance (Campain, Gottesman et al. 1994), and (II) a broad resistance to compounds of diverse structure and unrelated mechanism of action termed multidrug resistance (MDR) (Dano 1973). Multidrug resistance is a serious medical problem and presents a major obstacle for effective chemotherapeutic treatment of malignant diseases. The remission of a tumour during chemotherapy is successful in tumours that do not express endogenous P-gp (Loo and Clarke 1999). Tumours that express endogenous P-gp usually compromise effectiveness of the chemotherapeutic regimen. First studies showed that P-gp expression was increased in tumours from colon, adrenal, pancreatic, mammary and renal tissue, even prior to chemotherapy (Cordon-Cardo, O'Brien et al. 1989; van der Valk, van Kalken et al. 1990).

There are many clinical problems associated with over- or underexpression of ATP-binding cassette transporters on the cell surface (Loo, Bartlett et al. 2005). Overexpression of ABC multidrug transporters such as the multidrug resistance P-glycoprotein (P-gp, also known as MDR1 or ABCB1), multidrug resistance-associated protein (MRP1, also known as ABCC1), or the breast cancer resistance protein (BCRP, MXR) interferes with drug delivery to target organs and/or contribute to the development of multidrug resistance of cancer cells by catalysing the extrusion of cytotoxic compounds during chemotherapy (Gottesman, Fojo et al. 2002). (Loo, Bartlett et al. 2005)

Underexpression of mutant ABC transporters due to defective folding and trafficking to the cell surface as in the cystic fibrosis conductance regulator (CFTR) and the sulfonylurea receptor (SUR1) cause cystic fibrosis (Riordan, Rommens et al. 1989; Cheng,

Gregory et al. 1990) and persistent hyperinsulinemic hypoglycemia (Dunne, Kane et al. 1997; Cartier, Conti et al. 2001). (Loo, Bartlett et al. 2005)
Multispecific drug efflux pumps confer simultaneous resistance to several drugs (Holland and Blight 1999) and frequently render human disease intractable. MDR presents a major challenge to the treatment of disease and the development of novel therapeutics (Chang and Roth 2001).

In addition to its expression in cancer cells, P-gp is mainly localized in the apical membrane of epithelial cells in the body, to transport P-gp substrates that are translocated from the basolateral to the apical side of the epithelium. Furthermore, P-gp can be found in the blood-brain barrier, blood-testis barrier, blood-nerve barrier and in the placenta (fetal-maternal barrier) (Smit, Huisman et al. 1999).
P-gp reduces the intracellular concentrations of a wide range of drugs and xenobiotics (Bodor, Kelly et al. 2005). Drugs known to bind to P-gp include verapamil, vinblastine, daunorubicin, rhodamine and propafenone type compounds (Gottesman and Pastan 1993; Schmid, Ecker et al. 1999). It seems to play a key role in the protection of cells and in the development of resistance to anticancer agents. Inhibition of P-gp by low molecular weight compounds, which themselves are non-toxic, was reported over the past decade. A number of clinical studies has been initiated to reverse drug resistance by inhibiting drug efflux (reviewed in (Fojo and Bates 2003; Polgar and Bates 2005)). But all inhibitors of P-gp entering clinical studies so far have failed. Thus it is important to understand the molecular principles of drug recognition and transport, and the prediction of substrate properties of compounds has gained a lot of interest in the pharmaceutical industry (Ecker, Stockner et al. 2008).

2.4 Structure and molecular architecture of P-glycoprotein

A number of techniques can be used to derive a protein structure. These techniques including cryo-electron microscopy (cryo-EM), X-ray crystallography, nuclear magnetic resonance (NMR) spectroscopy, and bioinformatics-based approaches can help in elucidation of the functional mechanism of a protein.

2.4.1 Topology of P-glycoprotein

P-gp has the molecular architecture of an ABC protein, a core structure of four domains. It is a 170 kDa glycosylated plasma membrane protein and has 1280 amino acids which are organized as two homologous halves joined by a linker region of approximately 60 amino acid residues (Chen, Chin et al. 1986). Each half begins with an amino-terminal hydrophobic transmembrane domain (TMD) containing six transmembrane (TM) segments followed by a carboxy-terminal hydrophilic nucleotide-binding domain (NBD). P-gp is made up of a single polypeptide containing all four domains in the order TMD-NBD-TMD-NBD from N- to C-terminus. The N- and C-terminus are considered to have arisen by gene duplication and are 43% identical (Chen, Chin et al. 1986; Raymond and Gros 1989). The two TMD-NBD halves have diverged during evolution. The TMD and NBD are coupled by a series of intracellular loops (ICL) which extend into the NBDs (O'Mara and Tieleman 2007). The two TMDs have been shown to be responsible and sufficient for solute recognition (Loo and Clarke 1999).

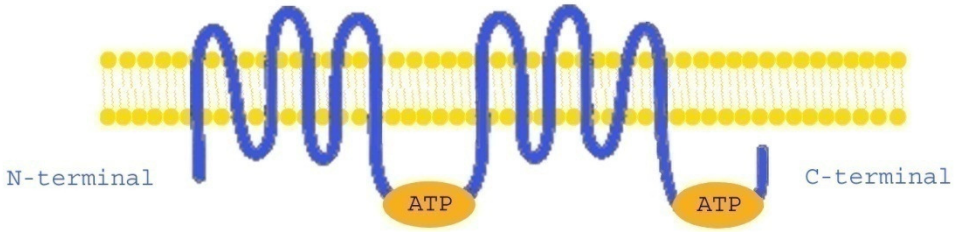

Figure 2.1: Topology of P-gp. P-gp has 12 transmembrane domains and two ATP-binding sites.

2.4.2 Low resolution structures of P-glycoprotein

At present no high-resolution structure of P-gp is available. The first three-dimensional structures for P-gp at low resolution obtained by cryo-electron-microscopy of two-dimensional crystals were performed by Rosenberg et al. (Rosenberg, Callaghan et al. 1997; Rosenberg, Mao et al. 2001; Rosenberg, Velarde et al. 2001; Rosenberg, Kamis et al. 2003; Rosenberg, Callaghan et al. 2005). The two-dimensional crystals were grown in the presence or absence of AMP-PNP, a non-hydrolysable analogue of ATP that is known to bind to the NBDs at the same site as ATP. Two-dimensional crystals of P-gp trapped at different steps of the transport cycle were correlated with functional changes. These data were interpreted to suggest that the transmembrane α–helices undergo dramatic conformational changes as a result of ATP binding, hydrolysis and substrate release. (Rosenberg, Kamis et al. 2003) The 8 Ångstrom (Å) resolution of the structure in

the presence of AMP-PNP was sufficiently high to confirm the existence of twelve transmembrane α–helices which span the membrane in two blocks of six. Five α–helices from each TMD exhibit a pseudo-2-fold symmetry, the sixth α–helices from each domain shows a less symmetrical relationship. The 8 Å resolution scan showed the same features already previously described in the three-dimensional structure of nucleotide-free P-gp: the transmembrane α–helices form a central pore, which is exposed at the extracellular face and closed at the intracellular face of the membrane. In contrast to the nucleotide-free P-gp structure, the transmembrane α–helices of the AMP-PNP-bound P-gp also enclose a central pore which is less closed at the intracellular face of the membrane and, additionally, is open to the lipid phase along one side with a gap appearing between two domains. This access from the lipid bilayer to the central pore might allow transport of lipophilic substrates from the membrane.

2.4.3 Protein homology models of P-glycoprotein

In the absence of high resolution structural data for P-gp, an alternative is to generate a protein homology model that provides a three-dimensional map of a protein. The availability of structures of a target protein at the atomic level is a critical factor for structure-based drug design. Protein homology models are based on the assumption of structural homology between a structurally resolved protein, the template and a protein of unknown conformation, the target. Sequence homology and an identical number of predicted transmembrane spanning helices are important for the selection of templates for modelling of membrane proteins (Ecker, Stockner et al. 2008). The quality of a homology model is determined by the accuracy of the sequence alignment between the protein of interest and the template protein, and the quality of the crystal structure used as the modelling template.

2.4.3.1 Available template crystal structures for P-glycoprotein

2.4.3.1.1 MsbA as template crystal structure

Several groups, including our own, have generated models based on the MsbA structures of *E. coli* and *V. cholerae* (Chang and Roth 2001; Chang 2003; Seigneuret and Garnier-Suillerot 2003; Stenham, Campbell et al. 2003; Pleban, Kopp et al. 2005; Reyes and Chang 2005), which were the only available structures at this time. MsbA, the lipid

A flippase found in Gram-negative bacteria, was the first structure of a full length ABC-transporter at 4.5 Å published in 2001 (Chang and Roth 2001). MsbA was crystallized as a homodimer of two monomers composed of an N-terminal TMD fused to a C-terminal NBD. It shows an identical number of TM-helices and the protein sequence is 36% and 32% identical to the N-terminal and C-terminal halves of human MDR1, respectively (Altschul, Gish et al. 1990). The crystal structure was obtained in the absence of substrate and nucleotide, showed an inverted V-shape and was later referred to as the open apo structure. Subsequently, MsbA from *V. cholerae* was resolved to 3.8 Å (Chang 2003). In this structure the NBDs were much closer. Again this structure was obtained in the absence of solutes and nucleotide and termed closed apo structure. Availability of these structures seemed to open a path for protein homology modelling of P-gp (Ecker, Stockner et al. 2008).
However, a homology model is an approximation of the structure and the exact positioning of the various domains may differ between template and target.

2.4.3.1.2 Sav1866 as template crystal structure

In September 2006 the crystal structure of a bacterial ABC transporter, Sav1866 from *Staphylococcus aureus*, was published (Dawson and Locher 2006). This first Sav1866 structure has been resolved to 3.0 Å. The Sav1866 structure, as MsbA, is a homodimeric ABC transporter that is homologous to P-gp. Sav1866 was crystallized in the presence of two adenosine diphosphate (ADP) molecules bound at the interface of the NBDs, the P-loops and the ABC signature motifs of opposing subunits. The NBDs of the Sav1866 homodimer are similar in structure to those of other ABC transporters (Dawson and Locher 2006). These domains show conserved ATP-binding and -hydolysis motifs at the shared interface in a head-to-tail arrangement (Schneider and Hunke 1998; Hopfner, Karcher et al. 2000; Smith, Karpowich et al. 2002). In 2007 the authors published the crystal structure of Sav1866 in complex with AMP-PNP (Dawson and Locher 2007). A comparison and superposition of both structures, the AMP-PNP-bound Sav1866 and the ADP-bound Sav1866, indicated that these structures are essentially identical and represent the ATP-bound state of the transporter. The apparently different structures of MsbA were indicated to be reconcilable with the Sav1866 when mirrored and under the assumption that the published topology of the MsbA structures was wrong. This consequently led to retraction of all three incorrect MsbA structures in the December 2006 issue of Science (Chang, Roth et al. 2006).

The overall architecture differs from the side-by-side arrangement of TMDs as observed for the ABC importers BtuCD (Locher, Lee et al. 2002), HI1470/1 (Pinkett, Lee et al. 2007), $ModB_2C_2$ (Hollenstein, Frei et al. 2007), and $MalFGK_2$ (Oldham, Khare et al. 2007). In ABC exporters the TMDs interact with the helical domains of the NBDs through coupling helices that are located in the loops between TM helices (Rees, Johnson et al. 2009). One intracellular loop of each TMD makes contact with the contralateral NBD. The coupling helices are domain swapped (Hollenstein, Dawson et al. 2007). The two subunits exhibit a considerable twist (Dawson and Locher 2006).
The transmembrane helices of Sav1866 diverge into two discrete 'wings' which point away from one another towards the cell exterior of the membrane, providing what might be thought of as an outward-facing conformation. Helices from both TMDs contribute to form each of these two 'wings'(Dawson and Locher 2006). The helix arrangement observed in Sav1866 is consistent, except for helices 6 and 12, with cross-linking studies which identified neighbouring TM helices in human P-gp (Dawson and Locher 2006). Helices 6 and 12 are positioned closer to each other than in the Sav1866 crystal structure (Stockner, de Vries et al. 2009). The arrangement of the 12 canonical transmembrane helices observed for Sav1866 is in agreement with the ABC exporter topology (Dawson and Locher 2006). Also, they are consistent with electron density maps of human P-gp and cross-linking restraints (Stenham, Campbell et al. 2003). The ATP-bound state of the NBDs, with the two nucleotide-binding domains in close contact, is likely to be coupled to the outward-facing conformation of the TMDs. In this conformation the helices line a central cavity, which is open to the cell exterior.

The three previously published structures from *Escherichia coli* (*E. coli*), *Vibrio cholerae* and *Salmonella typhimurium* were revised by the group of Chang. Now all models show the same topology as Sav1866 (Ward, Reyes et al. 2007).

2.4.4 Architecture of the transmembrane subunits

The crystal structures of five full ABC transporters have become available. Four of them are importers: The vitamin B_{12} transporter BtuCD from *E. coli*, the metal-chelate-type transporter HI1470/1 from *Haemophilus influenzae*, the molybdate transporter ModBC from *Archaeoglobus fulgidus* in complex with its binding protein (ModA), and the maltose transporter $MalFGK_2$ from *E. coli* in complex with the maltose-binding protein (MBP). ABC importers require a periplasmic or cell surface-associated substrate-

binding protein that captures the substrates with high affinity and delivers them to the external face of the transporter (Quiocho and Ledvina 1996). Only the binding protein, not the transporter, binds the substrate. In contrast, ABC exporters recruit their substrates directly from the cytoplasm or, in the case of very hydrophobic substrates, from the inner leaflet of the plasma membrane. After retraction of the incorrect MsbA structures, there are currently only two similar structures of ABC exporters, that of the multidrug transporter Sav1866 from *S. aureus* and that of the MsbA from *V. cholerae*.

The *E. coli* BtuCD protein mediates vitamin B_{12} uptake. The BtuCD and the HI1470/1 TMDs contain a total of 20 transmembrane α-helices (10 from each TMD) with the N and C termini located in the cytoplasm. This is in contrast to the 12 helices of P-gp. BtuCD shows a closed internal (cytoplasmic) gate which is formed by the intracellular loops between TM4 and TM5 of each BtuC subunit (Hollenstein, Dawson et al. 2007). In contrast, HI1470/1 consisting of two membrane-spanning HI1471 subunits and two nucleotide-binding HI1470 subunits reveals a closed external gate formed by the extracellular loops between TM5 and helix5a from each HI1471 subunit.

The structure of ModBC shows a closed gate near the external side of the membrane. Each ModB subunit crosses the membrane 6 times for a total of 12 transmembrane segments in the transporter (Hollenstein, Dawson et al. 2007). The structure of the $MalFGK_2$ shows five subunits: the two transmembrane subunits, MalF and MalG, composing eight and six TM helices, the two nucleotide-binding MalK subunits, and MBP.

The crystal structures of these transporters suggest at least two major states: an inward-facing conformation with the substrate translocation pathway open to the cytoplasm, and an outward-facing with the translocation pathway facing the opposite side of the membrane (Oldham, Khare et al. 2007). While ModBC and HI1470/1 reveal inward-facing conformations, BtuCD, MalFGK2 and Sav1866 adopt outward-facing states (Oldham, Khare et al. 2007).

2.4.5 Transmission interface

The NBD-TMD contact interface transmits critical conformational changes induced by binding and hydrolysis of ATP. These conformational changes are transmitted via non-covalent interactions at the share interfaces. The region of the NBD that interacts with the TMD primarily involves the L loops (EAA sequence) of the TMDs (Mourez, Hofnung et al. 1997; Locher, Lee et al. 2002), and the Q loops (Smith, Karpowich et al. 2002) and structurally diverse regions (Schmitt, Benabdelhak et al. 2003) of the NBDs,

that are in close proximity to each other and mediates the interactions between TMD and NBD.

2.5 Mechanisms of transport

There is no high-resolution crystal structure of a complete eukaryotic ABC exporter (complete structures of MalK and BtuCD have been published meanwhile). To gain a better understanding about domain-domain interactions in ABC transporters such as P-gp, it will be necessary to obtain crystal structures of the protein in different conformations (Loo and Clarke 2008). A number of isolated nucleotide binding domains (NBDs) of ABC-transporters has been crystallized and studied in detail (Karpowich, Martsinkevich et al. 2001; Schmitt and Tampe 2002; Procko, Ferrin-O'Connell et al. 2006; Sauna and Ambudkar 2007). But to understand binding of solutes to the TMDs and the transport process of multispecific drug efflux pumps remains a major scientific challenge. Drug binding to P-gp involves an induced-fit mechanism (Loo, Bartlett et al. 2003), such that binding of substrate or inhibitor may change the structure of P-gp and thus complicate the interpretation of crystallography studies.

In early studies of bacterial ABC transporters many different groups have published the link between substrate transport and ATP-binding and hydrolysis at the NBDs (Hobson, Weatherwax et al. 1984; Higgins, Hiles et al. 1985; Bishop, Agbayani et al. 1989; Mimmack, Gallagher et al. 1989; Panagiotidis, Reyes et al. 1993).

2.5.1 How is the transport process powered?

The mechanism how transport is mediated is very complex.

Binding of ATP flips the ABC transporters into an outward-facing conformation, whereas dissociation of the hydrolysis products ADP and phosphate returns them to an inward-facing conformation (reviewed in (Dawson, Hollenstein et al. 2007)). Conformational changes in the NBDs, induced by binding and hydrolysis of ATP along the dimer interface are coupled to conformational changes in the TMDs that then mediate transport of substrate.

2.5.2 Motor domains NBDs

The motor domains of ABC transporters, the NBDs, are between 200 and 300 amino acids in length and contain a number of conserved motifs (Schneider and Hunke 1998; Dawson, Hollenstein et al. 2007). The Walker A motif has a consensus sequence of GxxGxGKST, where x represents any amino acid; the Walker B motif consists of four hydrophobic amino acids followed by two negatively charged residues, aspartate and glutamate (Walker, Saraste et al. 1982). The Walker A motif binds the phosphate groups of the nucleotide. The aspartate residue of the Walker B motif coordinates the Mg^{2+} ion through H_2O (Karpowich, Martsinkevich et al. 2001; Yuan, Blecker et al. 2001; Verdon, Albers et al. 2003) and the glutamate residue of the Walker B motif binds to the attacking water and the Mg^{2+} ion (Moody, Millen et al. 2002; Smith, Karpowich et al. 2002). The ABC signature motif also contacts the nucleotide, but only in the ATP-bound state, and the Q-loop is in the contact interface with the TMD. Both, the general fold and the arrangement of the NBDs are conserved. The NBDs present these motifs at the shared interface. The arrangement of the NBDs is called head-to-tail or Rad50-like after the structure of the Rad50 protein in which it was first visualized (Hopfner, Karcher et al. 2000). They face each other across a dimer with the following orientation: two composite ATP binding sites are formed between the P-loop (Walker A motif) of one NBD and the LSGGQ motif (C-sequence) of the other and vice versa (Jones and George 1999). A number of isolated NBDs or subunits have been crystallized (Diederichs, Diez et al. 2000; Hopfner, Karcher et al. 2000; Gaudet and Wiley 2001; Karpowich, Martsinkevich et al. 2001; Yuan, Blecker et al. 2001; Smith, Karpowich et al. 2002; Chen, Lu et al. 2003; Lu, Westbrooks et al. 2005) since the first structure, the HisP protein from *Salmonella typhimurium* (Hung, Wang et al. 1998) was published. Many soluble ABCs have solute-independent ATPase activity when isolated from their cognate TM domains (Liu, Liu et al. 1999; Karpowich, Martsinkevich et al. 2001), proposing that ATP interacts primarily with the NBDs. The structures of the ATP-bound state of isolated NBDs which include both importers and exporters have been reported.

2.5.3 How are solutes transported

P-gp transports substrates which passively diffuse across the lipid bilayer and enter the cytoplasm.

Various distinct mechanisms have been proposed in the literature for coupling of drug transport to ATP hydrolysis.

Early studies of the mammalian multidrug resistance P-gp by Alan Senior's group defined the biochemistry of the ATPase cycle and proposed the alternating catalytic site model with drug transport linked to relaxation of a high-energy NBD conformation generated by ATP hydrolysis (Senior, al-Shawi et al. 1995). In addition, these studies showed that the two catalytic sites are both required for transport function (Figure 2.2).

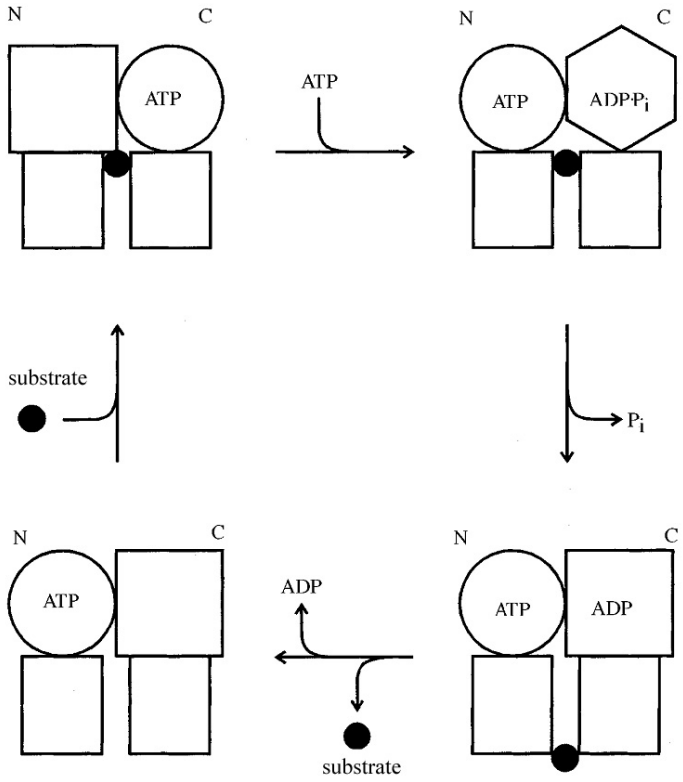

Figure 2.2: Alternating catalytic sites cycle of ATP hydrolysis by P-gp (adapted from (Senior, al-Shawi et al. 1995)). Rectangels represent the two TMDs. Circels, squares and hexagon represent different conformations of the N- and C-catalytic sites of NBD1 and NBD2. ATP binding at the N-site allows ATP hydrolysis at the C-site.

Subsequently, several related models for transport appeared (Senior and Gadsby 1997; Nikaido and Ames 1999; van Veen, Margolles et al. 2000; Sauna and Ambudkar 2001) for other transporters. These models assumed that the two NBDs which hydrolyze ATP, thus supplying the energy for translocation, operate alternately and may therefore be coupled to distinct steps in the transport cycle (Higgins and Linton 2004).

The recent availability of structural data in combination with biochemical and genetic studies of several ABC transporters have led to the ATP-switch model of function (Higgins and Linton 2004; Linton and Higgins 2007).

2.5.4 The catalytic cycle of P-gp - The ATP-switch model

The ATP-switch model involves communication via conformational changes in both directions, between the NBDs and TMDs (Higgins and Linton 2004). This model suggests a switch between two principal conformations of the NBDs:

- formation of a closed dimer formed by binding two ATP molecules at the dimer interface, and
- dissociation of the closed dimer to an open dimer facilitated by ATP hydrolysis and release of Pi and ADP.

Switching between the open and closed conformations of the dimer induces conformational changes in the TMDs necessary for transport of substrate across the membrane (Higgins and Linton 2004).

The model consists of four steps (see also (Higgins and Linton 2004)) (Figure 2.3):

Step one: Substrate binding to P-gp

The basal state of P-gp has low affinity for ATP, and the NBDs are in the open dimer configuration. The binding site for the transport substrate on the TMDs is accessible from the cytoplasmic face of the membrane. Transport substrate binding to its high-affinity binding site(s) on the TMDs of P-gp initiates the transport cycle. There are several studies which appear to show that this is the first step in the transport cycle. Petronilli et al. (Petronilli and Ames 1991) and Davidson et al. (Davidson, Shuman et al. 1992) generated mutant proteins of bacterial ABC NBDs HisP and MalK in which the ATPase activity of the transporter is uncoupled from periplasmic protein binding, leading to futile cycles of ATP hydrolysis.

Binding of the transport substrate induces a conformational change which is transmitted to the NBDs to initiate the ATP catalysis cycle. Several studies have shown substrate-induced conformational changes in the NBDs of P-gp (Liu and Sharom 1996; Sonveaux, Vigano et al. 1999), TAP (Neumann, Abele et al. 2002), MRP1 (Manciu, Chang et al. 2003), and the bacterial histidine (Kreimer, Chai et al. 2000) and maltose permeases (Mannering, Sharma et al. 2001).

Step two: ATP binding to P-gp

The second step in the transport cycle, the ATP binding, provides the energy input required for translocation of the drug from the inner leaflet of the membrane to the outside

of the cell. ATP binding induces closed NBD dimer formation and a major conformational change in the TMDs to initiate translocation.

Martin and colleagues used radioligand-binding techniques to characterize vinblastine interaction sites on P-gp and determine how drug binding site parameters are altered during a catalytic cycle of P-gp (Martin, Berridge et al. 2000; Martin, Berridge et al. 2000; Martin, Higgins et al. 2001). The authors showed that the binding capacity for vinblastine on P-gp decreased when the protein was incubated with the non-hydrolyzable ATP analogues AMP-PNP (Martin, Higgins et al. 2001) and ATP-γ-S (Martin, Berridge et al. 2000). These data suggest that ATP binding, in the absence of ATP hydrolysis, causes the initial shift to a low-affinity conformation of the drug binding site. Studies by van Veen et al. showed the presence of two vinblastine binding sites in the bacterial LmrA transporter, a homolog of P-gp: A low-affinity binding site exposed at the extracellular (outside) surface of the membrane and a high-affinity binding site exposed at the intracellular (inside) surface of the membrane (van Veen, Margolles et al. 2000). Only the low-affinity binding site is accessible for vinblastine in the ADP/vanadate-trapped LmrA protein which corresponds to a posthydrolysis situation. These data suggest that ATP binding or hydrolysis provides the conformational change by which the transport substrate is translocated to the outside of the cell.

Step three: ATP hydolysis

ATP hydrolysis, the trigger is unknown, initiates the transition of the NBD closed dimer to the open dimer and returns the transporter to its basal state (Higgins and Linton 2004). Many groups used the technique of vanadate trapping with 8-azido-ATP or 8-azido-ADP to obtain a posthydrolytic transition state when studying the catalytic sites of P-gp (Urbatsch, Sankaran et al. 1995; Urbatsch, Sankaran et al. 1995; Sharma and Davidson 2000; Payen, Gao et al. 2003; Urbatsch, Tyndall et al. 2003). The ATPase activity is inhibited by vanadate.

Step four: Restore P-gp to the basal state

Pi and then ADP are released and the protein is ready to initiate another transport cycle.

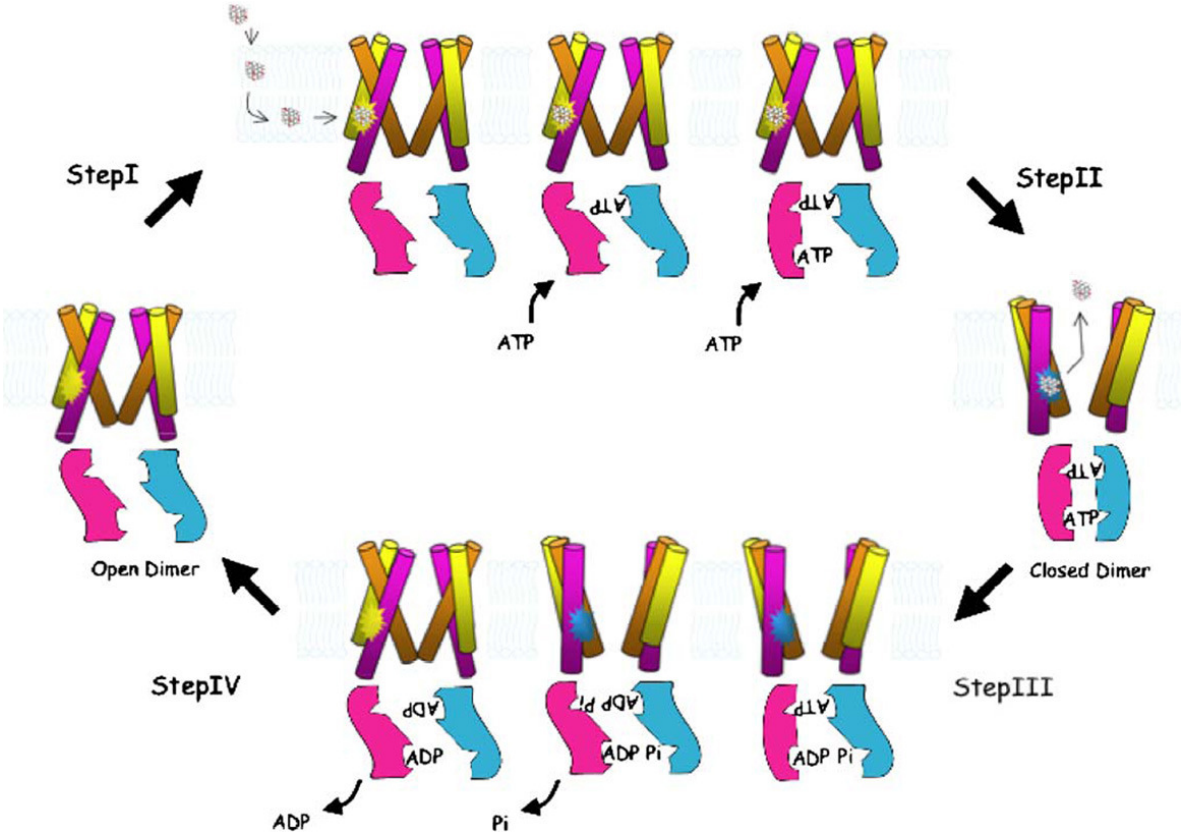

Figure 2.3: The ATP-switch model for the transport cycle of vinblastine by P-gp (adapted from (Linton and Higgins 2007)).

2.5.5 Binding of solutes to TMDs

2.5.5.1 Photolabelling of P-gp with substrate analogues

In our group photolabelling of P-gp has been used in combination with high resolution mass spectrometry to identify helices involved in binding of propafenone analogues (Pleban, Kopp et al. 2005). Six photoaffinity ligands of different mass related to the compound propafenone were used to photolabel P-gp by irradiation at a wavelength of 340-360nm. These compounds have previously been shown to be P-gp substrates and inhibitors (Chiba, Ecker et al. 1996; Schmid, Ecker et al. 1999). After irradiation, P-gp was purified by SDS-polyacrylamide gel electrophoresis and proteolytically degraded by chymotrypsin digestion. Ligand-labeled peptides were identified by matrix-assisted laser desorption/ionization time-of-flight (MALDI-TOF) mass spectrometry. The mass spectrum shows masses corresponding to component peptide fragments with covalently bound ligand, which can be identified and aligned. Peptide fragments which are covalently modified by the photoligand shift from their original position in the mass spectrum to an *m/z* position, which is increased by the ligand mass (Ecker, Pleban et al.

2004). The photoaffinity labelling allowed the identification of four TM helices, TMs 3, 5, 8 and 11, indicating that these four TM segments are involved in the substrate-binding event (Pleban, Kopp et al. 2005). These helices are located at the TMD/TMD interfaces. The highest labelling scores were observed for residues M197 in TM3 and F951 in TM11, and A311 in TM5 and T769 in TM8 for the TM 5/8 interface (Figure 2.4). In addition, methionine residues which have been reported to show a preferred reaction with benzophenone-type ligands (Rihakova, Deraet et al. 2002) are shown as red crosses. A number of methionine residues were not labeled and thus inaccessible for the photoligands (Pleban, Kopp et al. 2005). The ability of benzophenones to react with aliphatic residues was reported by Dorman et al. (Dorman and Prestwich 2000).

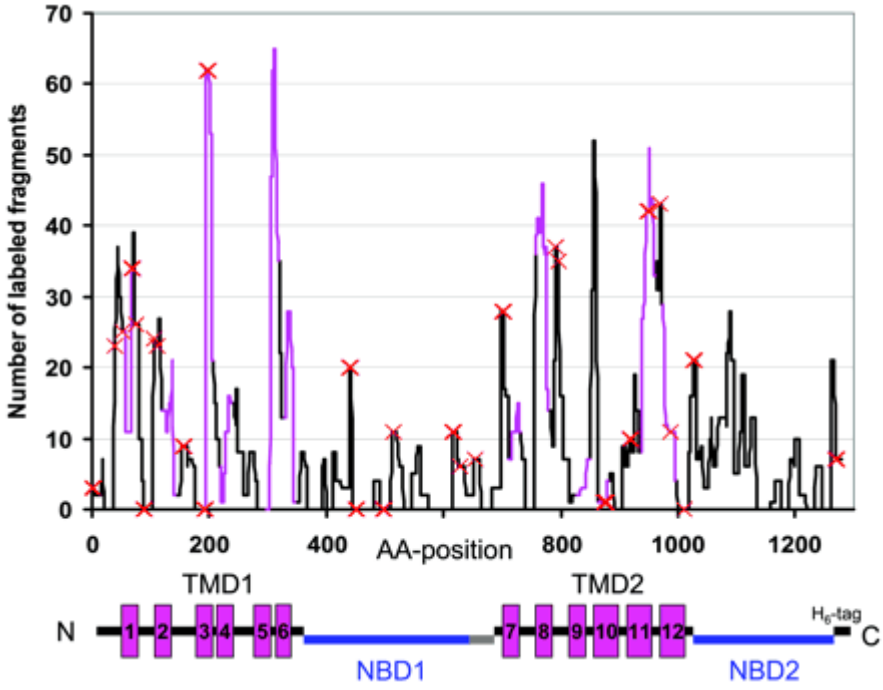

Figure 2.4 Frequency distribution analysis of photolabeling (adapted from (Pleban, Kopp et al. 2005)). The number of labeled fragments in which each particular amino acid residue in the primary sequence of P-gp is found is plotted as a function of this amino acid position. Predicted TM segments are shown in magenta, and the remainder of the sequence is in black. For easier orientation, a schematic representation is shown below the graph. TMDs 1 and 2 represent the N-terminal and C-terminal transmembrane domains, and the motor domains NBD1 and NBD2 are shown in blue. The linker region is indicated in gray, and the C-terminal hexa-His tag is depicted in black. The positions of methionine residues are highlighted by red symbols (x). The highest labeling is observed for putative TMs 3, 5, 8, and 11. In addition, the loop region connecting TMs 9 and 10 (extracellular loop 5) has a high labeling score.

In our group a protein homology model of P-gp was generated to allow projection of labelling data on a 3 dimensional model of the protein using the crystal structure of *V. cholerae* MsbA as template (Pleban, Kopp et al. 2005). A side and top view of the ho-

mology model of P-gp is shown in Figure 2.5. At this time the crystal structure of MsbA was the only available template structure.

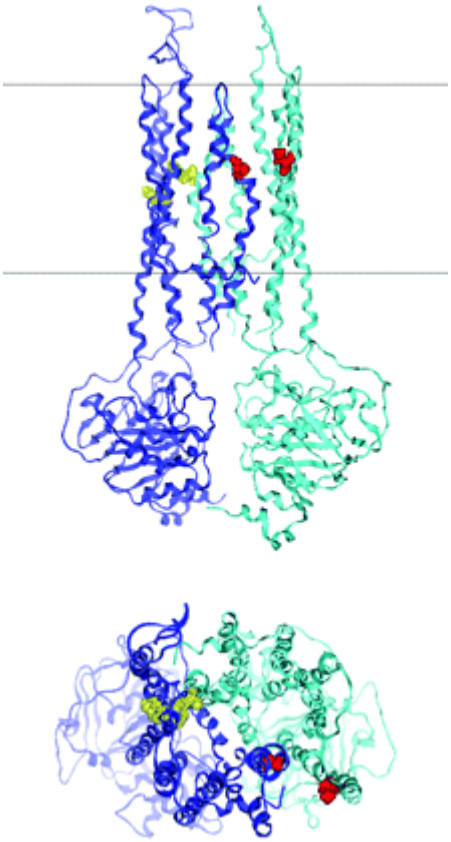

Figure 2.5 Side and top view of a P-gp homology model based on the V. cholerae MsbA structure (adapted from (Pleban, Kopp et al. 2005)). The N-terminal half of P-gp is depicted in dark blue, the C-terminal half is in cyan. Residues with the highest labelling are shown in yellow and red. Met197 in TM3 and Phe951 in TM11 are depicted in yellow. These residues are located on different halves of P-gp and thus, helices 3 and 11 contribute to one of the two TMD/TMD interfaces. Ala311 in TM5 and Thr769 in TM8 are depicted in red and are located at the other TMD/TMD interface.

These studies suggested the existence of two pseudosymmetric binding pockets at the two TMD/TMD interfaces.

2.6 Objectives of the thesis

An important goal in understanding the mechanism of drug transport has been to identify the locations of the drug-binding sites of P-gp. Presently, the location of the drug binding sites of multispecific drug efflux transporters is undefined because of the lack of high resolution structures of ABC-transporters with bound substrate. Thus, alternative approaches are needed to provide insight into the structure and function of P-gp.

The aim of this project was the identification and characterization of TMD1/TMD2 contact interface residues, which are important for transport of solutes. Functional assays were performed with P-gp mutants, in which the TMD1/TMD2 contact interface residues were mutated to residues other than cysteine by site directed mutagenesis based on overlap extension polymerase chain reaction (OE-PCR). The mutational concept was guided by photoaffinity labelling, availability of protein homology models, in-silico importance prediction of residues by real valued evolutionary trace (JMB 2003) and data-driven docking results (JACS 2004, HADDOCK) based on previous site-directed mutagenesis data. Thus, hypothesis driven generation of P-gp mutants with amino acid residues that will be tolerated in the protein to obtain a high number of correctly targeted and functional transporters was performed.
Another aspect of this project was correction of protein folding in mutants by pharmacological chaperones. Mutations often result in folding abnormalities, which lead to the newly synthesized protein being retained at the endoplasmic reticulum (ER) by the ER quality control machinery.

Objective 1: Identification of amino acid residues in the protein, which are important for transport. TMD1/TMD2 contact interface residues were mutated to residues other than cysteine.
A large number of functionally important P-gp residues within the TMDs have previously been identified by systematic site directed mutagenesis experiments in both human and mouse P-gp. The group of David Clarke exchanged every single residue in predicted transmembrane segments of human P-gp to cysteine by using a site directed mutagenesis approach. The protein contains only seven endogenous cysteine residues, all of them were mutated to alanine (Loo and Clarke 1995) resulting in an active cysteine-less P-gp. Residues that line TMD1/TMD2 contact interfaces have been identified to impair function when mutated to cysteines and reacted with cysteine reactive substrate molecules. A large number of those residues are known to participate in drug transport as demonstrated by mutagenesis and solute cross-linking experiments (Loo and Clarke 2005).

Objective 2: Influence of pharmacological chaperones on protein folding.
Many mutants do not correctly traffic to the plasma membrane. Proteins which are unable to adopt a stable conformation because of a specific mutation or aberrant glycosy-

lation are trapped in the ER (Welch and Brown 1996). These proteins are targeted to a degradative pathway. Different chaperones interact with unfolded or misfolded proteins to allow the protein to pass the secretory pathway (Brown, Hong-Brown et al. 1996).
Two glutamine residues (Q132 and Q773) of P-gp are located at the domain interfaces. It was considered possible that these glutamine residues if mutated to other amino acids cause the protein to be retained in the ER. The mutant protein would then be degraded rapidly. P-gp has been reported to be a good model system for the study of folding defects and action of pharmacological chaperones. It is possible to monitor cell surface expression of the transporter using a P-gp-specific antibody and flow cytometry.

2.6.1 Rational selection of residues

Why glutamine residues? Is it rational to mutate the glutamine residues at the position 132 and 773?
The glutamine residues are:

a. highly conserved

b. located at the interfaces

c. predicted by in-silico docking to contribute highest energy to interaction with propafenone analogues

d. located in the vicinity of amino acids showing high labelling with photoaffinity ligands

Alignments of the N- and C-terminal half of P-gp
Sequence alignments of the amino- and carboxy-terminal half of P-gp indicate two conserved glutamine (Q) residues in positions 132 and 773 (shown in Figure 2.6). Q773 is the only residue in helix 8 other than G763 that is conserved between helix 2 and helix 8.

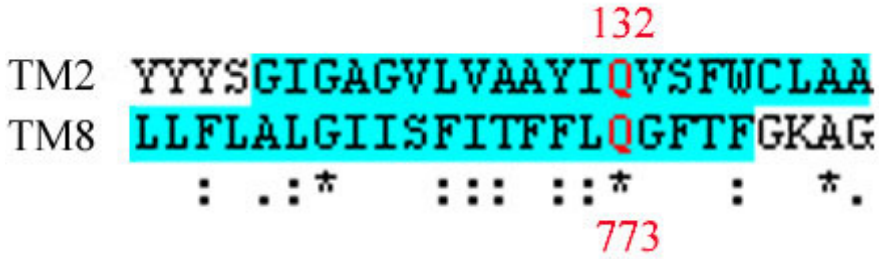

Figure 2.6: Partial sequence alignments of TMs 2 and 8 of the N- and C-terminal half of P-gp. The transmembrane segments are highlighted in turquoise. Glutamine residues at positions 132 and 773 are shown in red.

Position of the glutamine resisdues at each of the TMD/TMD interfaces

Position of the glutamine residues Q132 and Q773 at each of the TMD/TMD interfaces are shown in Figure 2.7.

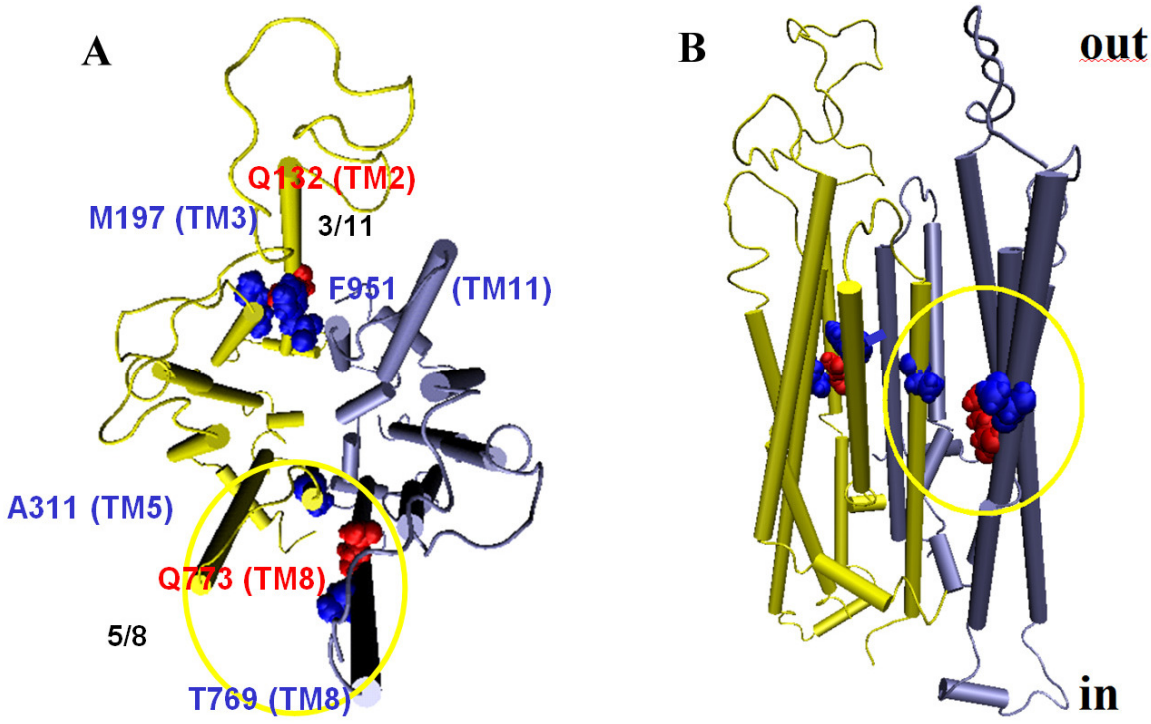

Figure 2.7: Top view (A) and side view (B) of the P-gp model (generated in our group with VMD 1.85). TMDs are only shown (NBDs omitted). The N-terminal half of P-gp is depicted in yellow, the C-terminal half is in grey. Residues M197 (TM3), A311 (TM5), T769 (TM8), and F951 (TM11) have been shown to be highly accessible for photoaffinity ligands. Gludamine residues Q132 (TM2) and Q773 (TM8) are shown in red. The TM5/TM8 interface is highlighted by a yellow circle.

Data-driven docking of propafenones to each of the interfaces

To gain additional insights into the binding mechanism of drugs to P-gp, computational docking was used to generate structural models. High Ambiguity Driven DOCKing (HADDOCK) was initially developed as a protein-protein docking tool (Dominguez, Boelens et al. 2003). HADDOCK has been used in a large number of studies, including protein-protein docking (van Dijk, de Vries et al. 2005; van Dijk, Fushman et al. 2005; Volkov, Ferrari et al. 2005; de Vries, van Dijk et al. 2006), protein-peptide docking (Tzakos, Fuchs et al. 2004; Denisov, Chen et al. 2006), protein-DNA docking (van Dijk, van Dijk et al. 2006), protein-RNA docking (Volpon, D'Orso et al. 2005) and protein-ligand docking (Schieborr, Vogtherr et al. 2005). The data-driven docking program HADDOCK, developed and performed by the group of Alexandre Bonvin, was used to study binding of propafenone analogues to P-gp. HADDOCK distinguishes between active and passive residues. Information derived from photoaffinity labelling and site

directed mutagenesis is complemented by data-driven docking. Protein-ligand contact profiles identified two glutamine residues, Q132 in TM2 and Q773 in TM8 adopting identical positions in sequence alignments of the amino- and carboxy-terminal half of P-gp, at each of the interfaces as privileged interaction partners.

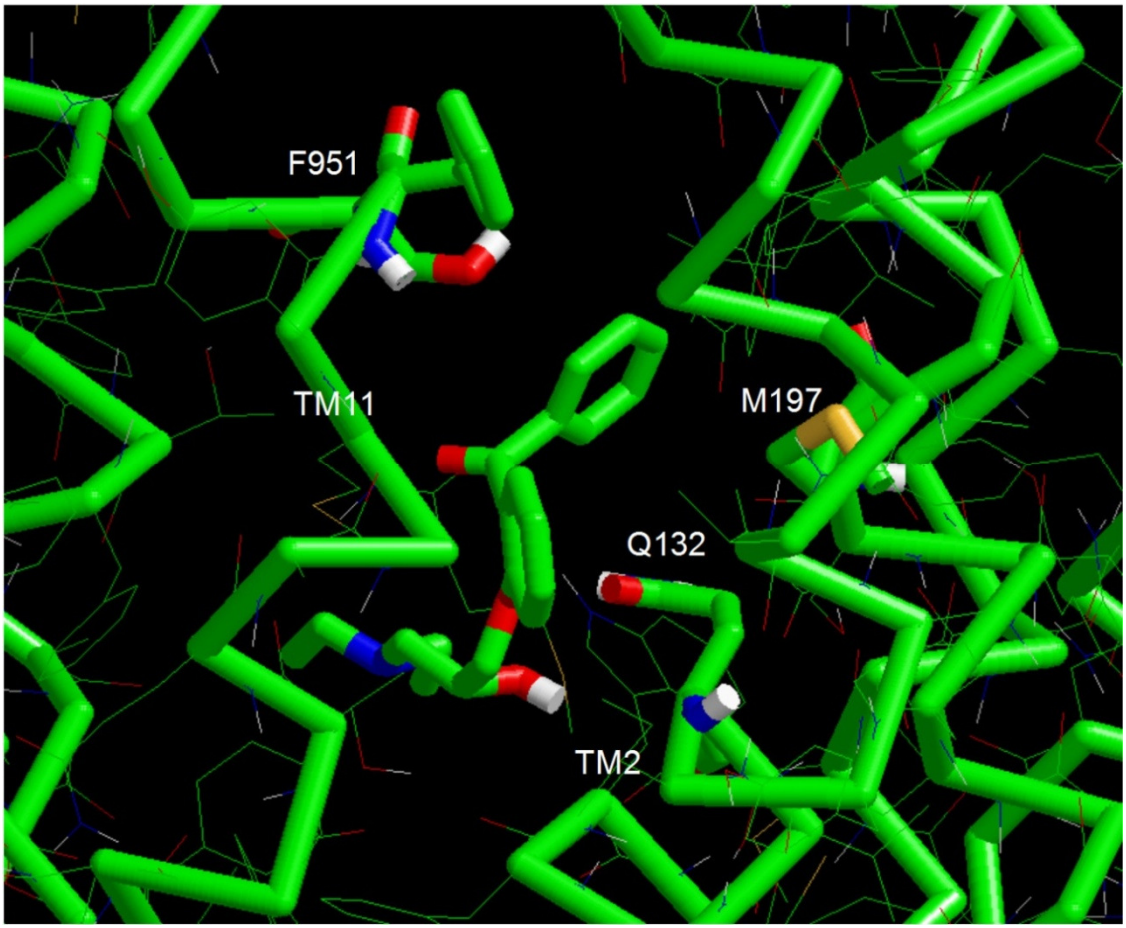

Figure 2.8: TM 3/11 interface (generated by Sjoerd de Vries in Dr. Alexandre M.J.J. Bonvin's group at Utrecht University): One pose of the most highly ranked cluster is shown. H-bonding contacts with Q132 in TM2 are predicted. The most highly accessible residues for propafenone photoligands (residues M197 in TM3 and F951 in TM11) are in close proximity of the ligand, though a bias for these residues is not introduced during the docking procedure.

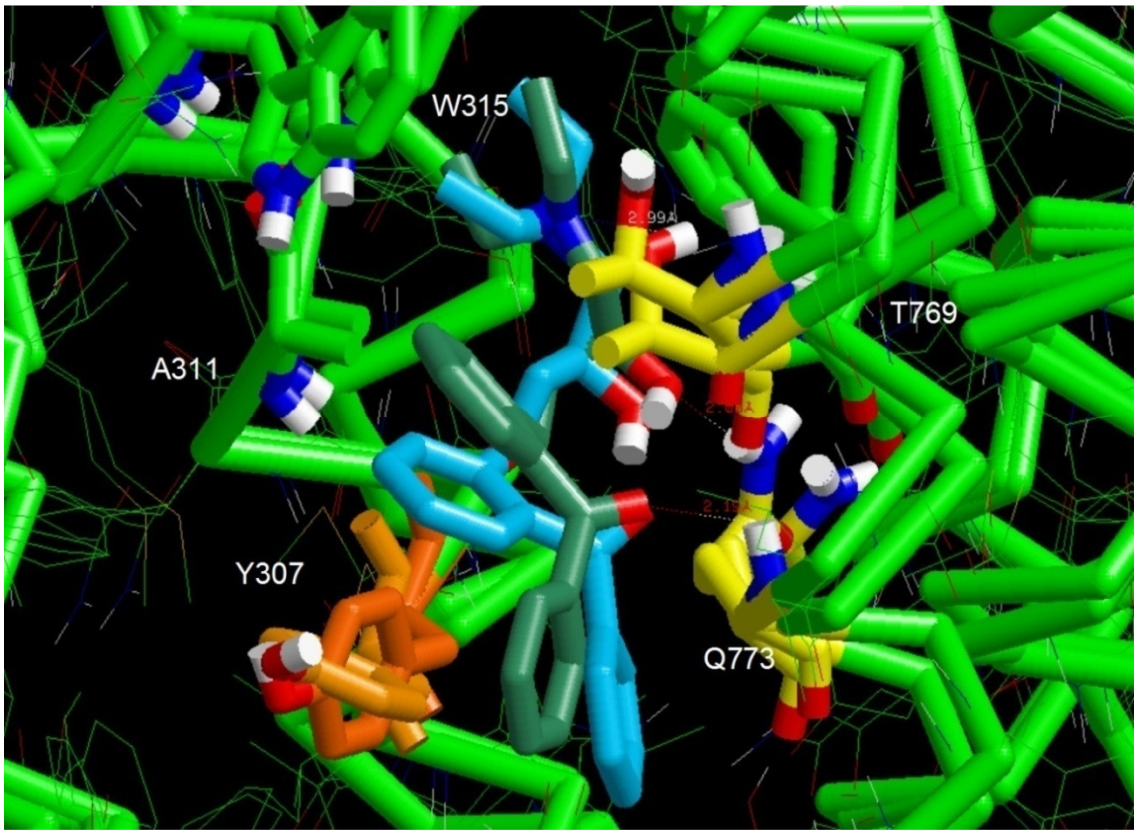

Figure 2.9: TM 5/8 interface (generated by Sjoerd de Vries in Dr. Alexandre M.J.J. Bonvin's group at Utrecht University): Two individual poses of the most highly ranked cluster are shown. The movements occurring during the flexible refinement stage of docking are illustrated by different backbone and rotamer positions. The two ligands are shown in different coloring. In both poses the ligand makes two H-bonding contacts with residue Q773 in TM8 and an aromatic stacking interaction with residue Y307 in TM5. The photolabelled residues A311 in TM5 and T769 in TM8 are again in close proximity of the ligand.

Determination of sequence variation

Evolutionary variation in both, Q132 and Q773, positions is low as indicated by multiple sequence alignments of P-gp sequences of different species using real valued evolutionary trace (rvET) (Mihalek, Res et al. 2004) (http://mammoth.bcm.tmc.edu). Generation of mutants was guided by the mutational space explored by nature.

The central objective of this work was to study the functional biology of P-glycoprotein by combining site directed mutagenesis and direct transport assays. The influence of the mutations on function was measured by drug accumulation assays in whole cells.

3 Materials and methods

3.1 Chemicals and reagents

10mM dNTP Mix (Fermentas, Cat. No. R0191)

2mM dNTP Mix (Fermentas, Cat. No. R0241)

Ampicillin (Sigma, Cat. No. A9518)

C219 (Eubio, Austria, Cat. No. ALX 801002)

Goat anti-mouse Ig FITC (BectonDickinson, Cat. No. 349031)

Gateway® LR ClonaseTM Enzyme Mix (Invitrogen, 20 reactions Cat. No. 11791-019)

GenEluteTM Plasmid Miniprep Kit (Sigma, Cat. No. PLN350)

GFX PCR DNA and Gel Band Purification Kit (Amersham Biosciences, Cat. No. 27-9602-01)

Gentamicin (Invitrogen, Cat. No. 15750-060)

HiSpeed® Plasmid Midi Kit (QIAGEN, Cat. No. 12643)

Isopropyl-ß-thiogalactopyranoside (IPTG) (Invitrogen, Cat. No. 15529-019)

Hygromycin B (Invitrogen, Cat. No. 10687-010)

IgG2a (BectonDickinson, Cat. No. 340394)

iScriptTMcDNA Synthesis Kit (BioRad, 25 reaction kit Cat. No. 170-8890)

Kanamycin (Gibco, Cat. No. 11815-024)

LipofectamineTM 2000 (Invitrogen, Cat. No. 11668-027)

MRK 16, monoclonal antibody to P-glycoprotein, (Alexis Biochemicals, Cat. No. 801-008-C150)

PageRulerTM Prestained Protein Ladder (Fermentas, Cat. No. SM0679)

Platinum Taq polymerase (5units/µl) (Invitrogen, Cat. No. 10966-018)

Pfu DNA Polymerase, native and 10x PCR Buffer with MgSO4 (Fermentas, Cat. No. EP0571)

Rapid DNA Ligation Kit (Fermentas, Cat. No. K1422) containing T4 DNA Ligase (5u/µl), 5x Rapid Ligation Buffer and water (nuclease-free)

Restriction endonucleases (Fermentas): *Bam*HI (Cat. No. ER0051)
SalI (Cat. No. ER0641)
XbaI (Cat. No. ER0685)
XhoI (Cat. No. ER0691)
*Eco*RI (Cat. No. ER0271)

Rhodamine 123 (Sigma, Cat. No. R8004)

Tetracycline (Sigma, Cat. No. T3258)

TRIzol® Reagent (Invitrogen, Cat. No. 15596-026)

X-Gal (Sigma, Cat. No. B9146)

3.2 Solutions

Solutions were made using de-ionised or ultra-pure water.

Sterilisation was carried out by autoclaving at 125°C for 20 minutes, or by filtration using a 0.2 μm filter (Millipore, SLGS03355).

3.3 Chemical structures of compounds

The following chemicals were used in this work:

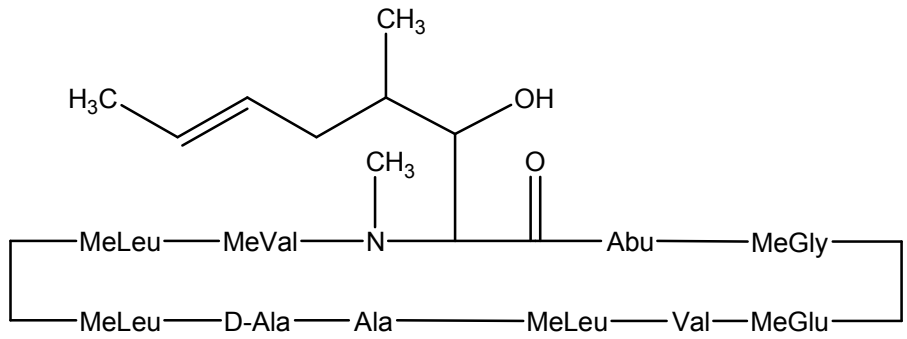

Figure 3.1: Structure of Cyclosporin A. Formula: $C_{62}H_{111}N_{11}O_{12}$; Molecular Weight: 1202.61

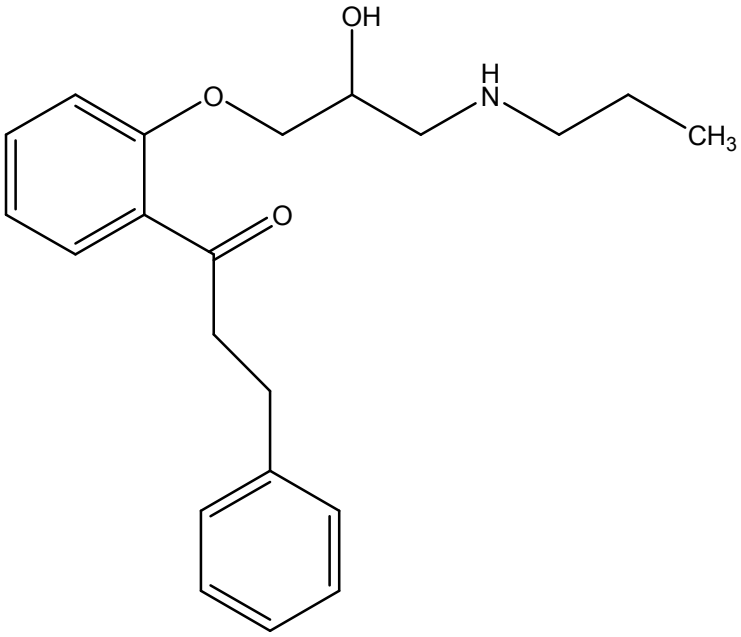

Figure 3.2: Structure of GPV01. Formula: $C_{21}H_{27}NO_3$; Molecular Weight: 341.44

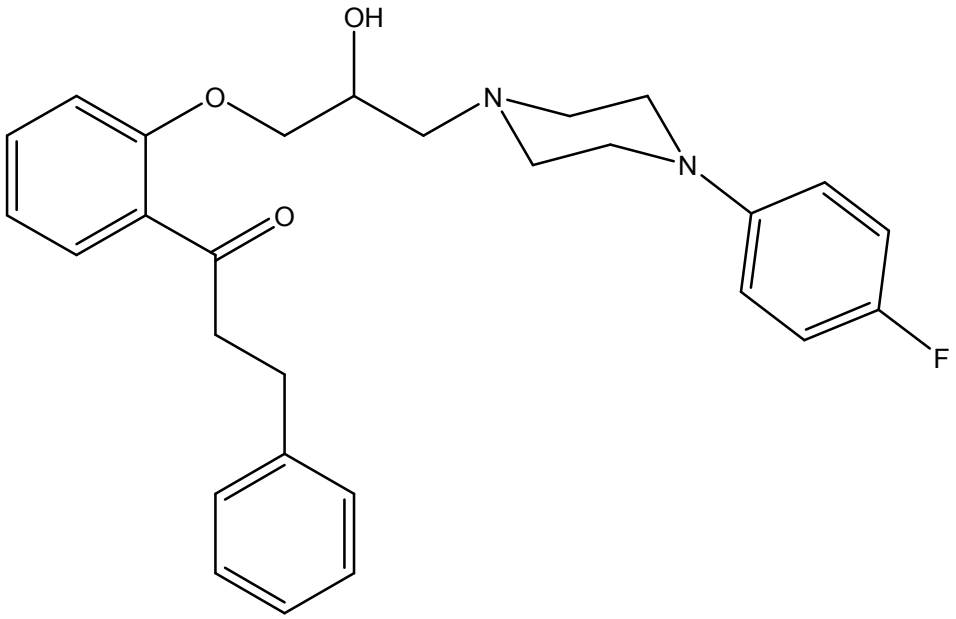

Figure 3.3: Structure of GPV31. Formula: $C_{28}H_{31}FN_2O_3$; Molecular Weight: 462.56

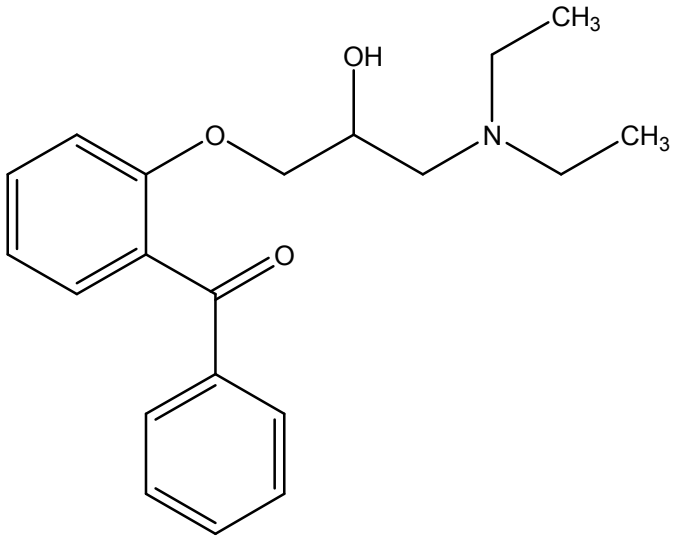

Figure 3.4: Structure of GPV51. Formula: $C_{20}H_{25}NO_3$; Molecular Weight: 327.42

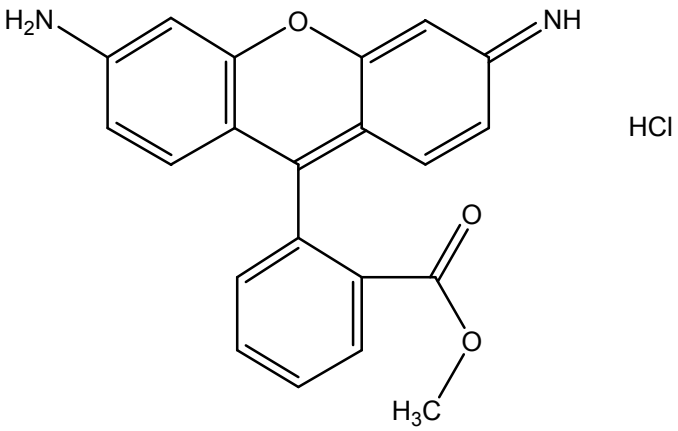

Figure 3.5: Structure of rhodamine 123. Formula: C21H17ClN2O3; Molecular Weight: 380.82

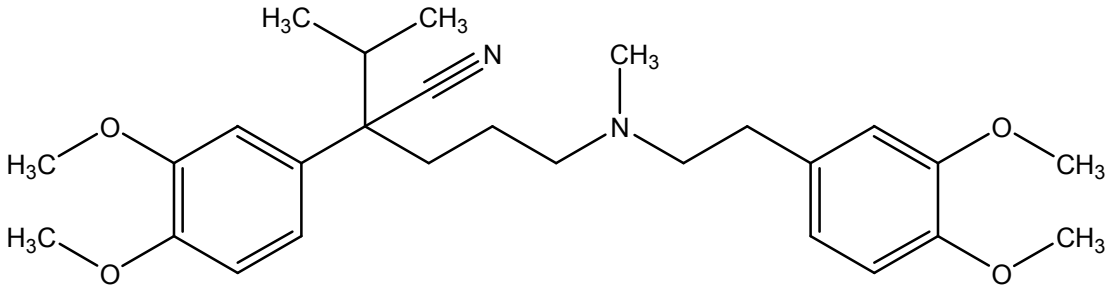

Figure 3.6: Structure of verapamil. Formula: $C_{27}H_{38}N_2O_4$; Molecular Weight: 454.6.

GPV01, GPV31 and GPV51 are propafenone analogues which were synthesized according to published procedures (Chiba, Burghofer et al. 1995; Chiba, Ecker et al. 1996). Stock solutions were prepared in pure DMSO and the final DMSO concentration did not exceed 0.2% (v/v).

3.4 Microbiology

3.4.1 Bacterial strains

One shot® TOP10, one shot® DB3.1, one shot® *ccd*B Survival T1 Phage-Resistant cells and MAX efficiency® DH10Bac™ chemically competent *E. coli* cells were supplied by Invitrogen.

Library Efficiency® DB3.1™ Chemically Competent *E. coli* Cells (Cat. No. 11782-018)
Genotype
F- *gyr*A463 *end*A1 Δ(*sr*1-*rec*A) *mrc*B *mrr hsd*S20(r_B^-, m_B^-) *sup*E44 *ara*14 *gal*K2 *lac*Y1 *pro*A2 *rps*L20(Sm^r) *xyl*5 Δ*leu mtl*1

One Shot® TOP10 Chemically Competent *E. coli* Cells (Cat. No. C4040-03)
Genotype
F- *mrc*A Δ(*mrr-hsd*RMS-*mc*rBC) Φ80*lac*ZΔM15 Δ*lac*X74 *rec*A1 *ara*D139 Δ(*ara-leu*)7697 *gal*U *gal*K *rps*L (Str^R) *end*A1 *nup*G

One shot® *ccd*B Survival T1 Phage-Resistant Chemically Competent *E. coli* Cells (Cat. No. C7510-03)
Genotype
F- *mrc*A Δ(*mrr-hsd*RMS-*mcr*BC) Φ80*lac*ZΔM15 Δ*lac*X74 *rec*A1 *ara* Δ139 Δ(*ar*a, *leu*)7697 *gal*U galK *rps*L (Str^R) *end*A1 *nup*G *ton*A::P_{trc}-*ccd*A

MAX Efficiency® DH10Bac™ Chemically Competent *E. coli* Cells (Cat. No. 10361-012)
Genotype
F- *mcr*A Δ(*mrr-hsd*RMS-*mcr*BC) Φ80*lac*ZΔM15 Δ*lac*X74 *rec*A1 *end*A1 *ara*D139 Δ(*ar*a,
leu)7697 *gal*U galK λ- *rps*L *nup*G/bMON14272/pMON7124

The DB3.1 *E. coli* strain contains a gyrase mutation (gyrA643) that renders it resistant to CcdB effects and can support the propagation of plasmids containing the control of cell death (*ccd)*B gene (Bernard and Couturier 1992; Miki, Park et al. 1992; Bernard, Kezdy et al. 1993). The *ccd*B Survival T1 Phage-Resistant *E. coli* cells are also resistant to the CddB effects.

3.4.2 Bacterial culture medium, culture and storage

Lysogeny broth (LB)-Bouillon:	Peptone from casein 10 g/l, yeast extract 5.0 g/l, sodium chloride 10 g/l (MERCK, Darmstadt, Germany, Cat. No. 1.10285.0500); stored at room temperature
LB agar:	Peptone from casein 10 g/l, yeast extract 5.0 g/l, sodium chloride 10.0 g/l, Agar-agar 12.0 g/l (MERCK, Darmstadt, Germany, Cat. No. 1.10283.0500); stored at room temperature
S.O.C. medium:	2% tryptone, 0.5% yeast extract, 10 mM NaCl, 2.5 mM KCl, 10 mM $MgCl_2$, 10 mM $MgSO_4$, 20 mM glucose (Invitrogen, Cat. No. 15544-034); stored at room temperature

Selection media:
Solid or liquid growth media were supplemented with kanamycin to a final concentration of 50µg/ml kanamycin or with ampicillin to a final concentration of 100µg/ml or with kanamycin (50 µg/ml), gentamicin (7 µg/ml), tetracycline (10 µg/ml), X-Gal (100 µg/ml) and IPTG (40 µg/ml).

LB agar plates containing the appropriate antibiotic to select for the vector were stored at 4°C for approximately 2 weeks, liquid selection media were always prepared fresh.
Bacteria were grown in liquid media with shaking (300rpm), or on plates in an incubator, at 37°C. For long-term storage bacteria were frozen at -80°C in a mixture of 850 µl LB medium and 150 µl glycerol.

3.5 Moleculare Biology

3.5.1 Plasmids

All plasmids used in this study were purchased from Invitogen.

Product	Amount	Catalog no.
pEF5/FRT/V5-DEST Gateway™Vector	6 µg	V6020-20
pENTR™4	10 µg	11818-010
pDEST™8	6 µg	11804-010
pOG44	20 µg	V6005-20
pENTR™/SD/D-TOPO® Cloning Kit	20 reactions	K2420-20

The entry vector, pENTR4 and both destination vectors, pEF5/FRT/V5-DEST and pDEST8, are components of the Gateway® Technology system (Invitrogen). The Gateway® Technology cloning method is based on the site-specific recombination properties of the bacteriophage lambda (Landy 1989) (Invitrogen 2003). The site-specific recombination properties of this bacteriophage provide a rapid and efficient way of moving the coding sequence into multiple vector systems in a directional and specific way for functional analysis and protein expression (Hartley, Temple et al. 2000). The lambda site-specific recombination system facilitates integration of the lambda genome into the *E. coli* chromosome and switches between the lytic and lysogenic pathways (Invitrogen 2003). The components of the lambda recombination system are modified to improve the specificity and efficiency of the system (Bushman, Thompson et al. 1985; Invitrogen 2003).

The pENTR4 vector contains a multiple cloning site, *rrnB* transcription termination sequences preventing basal expression of the PCR product in *E. coli*, the kanamycin resistance gene for selection in *E. coli*, the pUC origin for high-copy replication and maintenance of the plasmid in *E. coli*, and a Kozak consensus sequence for efficient translation initiation in eukaryotic systems (Invitrogen 2004). In addition, the pENTR4 vector has attachment (*att)* L sites (100 bps) and is used to clone restriction fragments, which do not contain *att* sites to generate entry clones. A *ccdB* gene is located between the two *att*L sites for negative selection (Invitrogen 2004). Before cloning, the pENTR4 vector must be digested on each site of the *ccdB* gene for removing the *ccdB* gene. The *att* sites, *att*L1 and *att*L2, allow site-specific recombination of the entry clone with a

destination vector (pEF5). The destination vector contains *att*R sites (125 bps), *att*R1 and *att*R2, and recombines with the entry clone in a LR reaction to generate an expression clone containing *att*B sites (25 bps). Therefore, *att*L1 sites react only with *att*R1 sites and *att*L2 sites react only with *att*R2 sites (Invitrogen 2003). The recombination reaction is mediated by the LR Clonase™ Enzyme Mix (Invitrogen, 20 reactions, Cat. No. 11791-019). The LR Clonase Enzyme Mix is a mixture of enzymes that bind to specific sequences (*att* sites), bring together the target sites, cleave them, and covalently attach the DNA using a lytic pathway (Invitrogen 2003). The lytic pathway is catalyzed by bacteriophage lambda Integrase (Int) and Excisionase (Xis) proteins, and the E. coli Integration Host Factor (HIF) protein (Invitrogen 2003).

LR recombination reaction:

Component	Sample
Entry clone (100-300 ng/reaction)	0.5-2 µl
Destination vector (300 ng/reaction)	2 µl
5x LR Clonase Reaction Buffer	2 µl
TE buffer (10 mM Tris-HCl, pH 8.0, 1 mM EDTA	To 8 µl

2 µl of the LR Clonase Enzyme Mix were added to each sample which was then vortexed briefly. The LR recombination reaction was incubated for 1 hour at 25°C. After incubation 1 µl Proteinase K was added and the samples reincubated for 10 minutes at 37°C. Then 2 µl of each reaction were transformed into 50 µl of One Shot TOP10 Chemically Competent Cells in an Eppendorf tube and incubated 30 minutes on ice. The cells were heat-shocked by incubating at 42°C for 30 seconds and placed on ice for approximately 2 minutes. After cooling, 250 µl S.O.C. medium was added and the tubes were incubated at 37°C for 1 hour at 300 rpm in a shaking thermoblock (Eppendorf Thermomixer comfort). Finally, the cells were spread on LB plates containing 100 µg/ml Ampicillin and incubated overnight at 37°C. The generated clones were screened by size exclusion and restriction enzyme digestion.

The first cloning experiments were done using the pENTR/SD/D-TOPO vector to clone PCR products containing no *att* sites to generate entry clones. The forward primer has to be designed in a manner that allows the ATG initiation codon of the PCR product to directly follow the CACC sequence being the prerequisite for directional cloning (Invi-

trogen 2006). These 4 nucleotides pair with the overhang sequence GTGG in each pENTR TOPO vector (Invitrogen 2006). Mixing the PCR product and pENTR TOPO vector starts the TOPO Cloning Reaction resulting in an entry clone. Unfortunately, the insert always proofed to be either too short or in the reverse orientation.

The pEF5 destination vector contains the following components (see also (Invitrogen 2002)):

- human EF-1alpha promoter for high-level expression of mammalian cells
- T7 promoter
- two recombination sites, attR1 and attR2
- chloramphenicol resistance gene located between the two *att*R sites for counterselection
- ccdB gene between the two *att*R sites
- bovine growth hormone (BGH) polyadenylation sequence for proper termination and processing of the recombinant transcript
- FLP Recombination Target (FRT) for Flp recombinase-mediated integration of the vector into Flp-In™ host cell line
- hygromycin resistance gene that lacks a promoter and an ATG initiation codon, therefore transfection of the pEF5 vector alone into mammalian host cells will not confer hygromycin resistance to the cells
- pUC origin
- the ampicillin (*bla*) resistance gene for selection in *E. coli*
- SV40 early polyadenylation signal for efficient transcription termination and polyadenylation of mRNA

The pEF5 vector allows high-level, constitutive expression of a coding sequence in a variety of mammalian hosts using the Flp-In™ system.

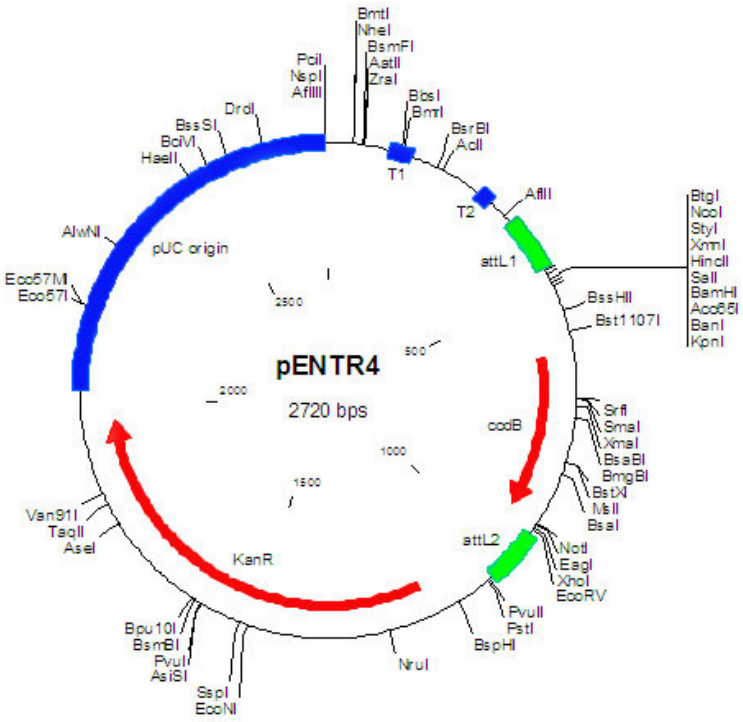

Figure 3.7: The map of the pENTR4 vector. Enzymes with unique restriction sites are shown, enzymes with two or more restriction sites are not shown. KanR: Kanamycin resistance gene, T1: *rrnB* T1 transcription termination sequence, T2: *rrnB* T2 transcription termination sequence

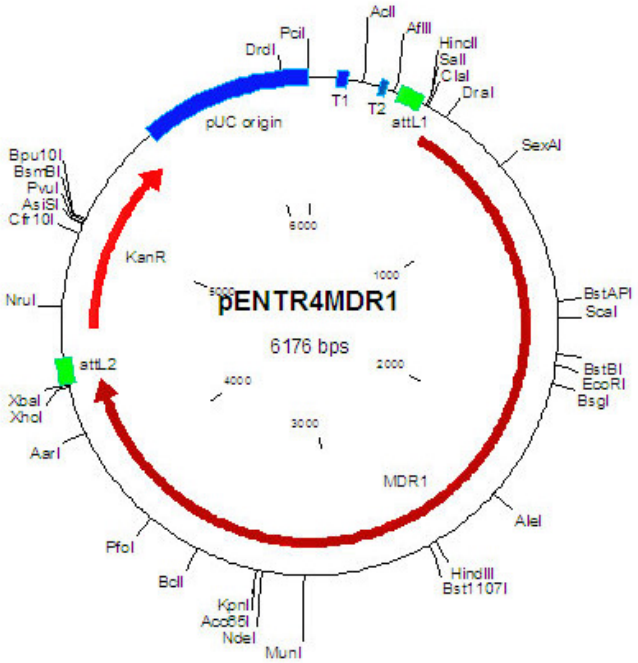

Figure 3.8: The map of the pENTR4MDR1 vector. Enzymes with unique restriction sites are shown, enzymes with two or more restriction sites are not shown. KanR: Kanamycin resistance gene, T1: *rrnB* T1 transcription termination sequence, T2: *rrnB* T2 transcription termination sequence

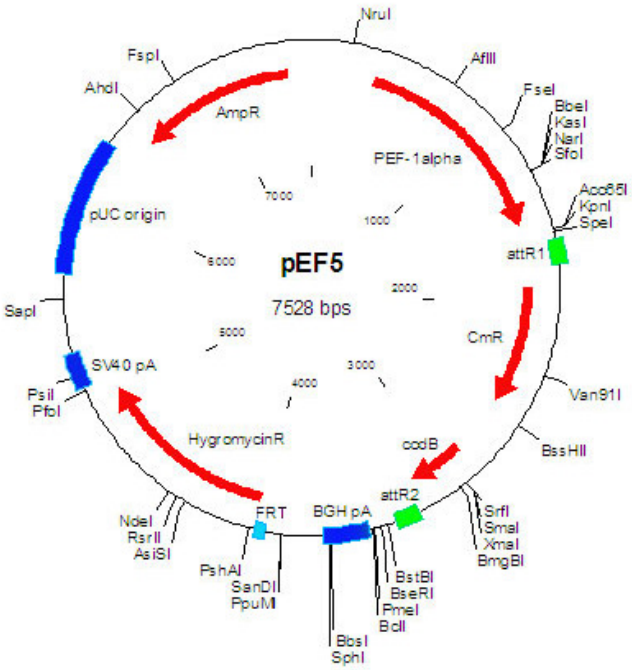

Figure 3.9: The map of the pEF5 vector. Enzymes with unique restriction sites are shown, enzymes with two or more restriction sites are not shown. AmpR: Ampicillin resistance gene, BGH pA: Bovine growth hormone polyadenylation sequence, CmR: Chloramphenicol resistance gene, FRT: FLP Recombination Target site, HygromycinR: Hygromycin resistance gene, PEF-1 alpha: EF-1alpha promoter, SV40 pA: SV40 early polyadenylation signal

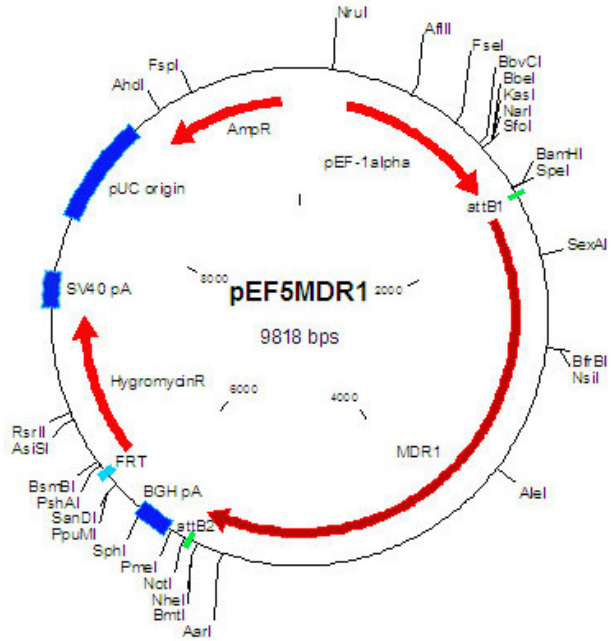

Figure 3.10: The map of the pEF5MDR1 vector. Enzymes with unique restriction sites are shown, enzymes with two or more restriction sites are not shown. AmpR: Ampicillin resistance gene, BGH pA: Bovine growth hormone polyadenylation sequence, FRT: FLP Recombination Target site, HygromycinR: Hygromycin resistance gene, PEF-1 alpha: EF-1alpha promoter, SV40 pA: SV40 early polyadenylation signal

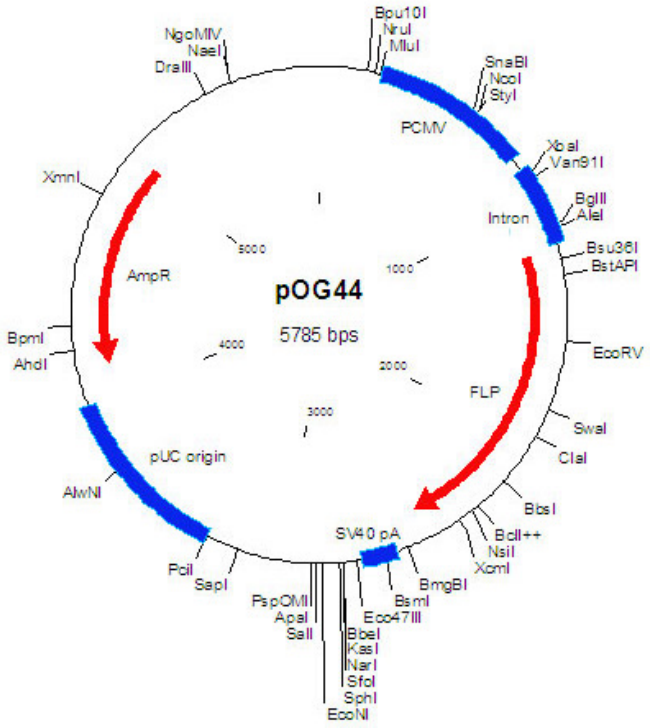

Figure 3.11: The map of the pOG44 vector. Enzymes with unique restriction sites are shown, enzymes with two or more restriction sites are not shown. Amp: Ampicillin resistance gene, P_{CMV}: human cytomegalovirus immediate-early enhancer/promoter, SV40 pA: SV40 late polyadenylation signal

The pDEST^{TM}8 vector has the following features (see also (Invitrogen 2004):

- Polyhedrin gene promoter from *Autographa californica* multi nuclear polyhedrosis virus (AcMNPV) for high-level expression of the gene of interest (Possee and Howard 1987).
- Mini-Tn7 elements for site-specific transposition into the bacmid DNA propagated in *E. coli* (Luckow, Lee et al. 1993).
- Two recombinates sites, attR1 and attR2
- Chloramphenicol resistance gene located between the two *att*R sites for counterselection
- ccdB gene between the two *att*R sites
- The ampicillin (*bla*) resistance gene for selection in *E. coli*
- The gentamicin resistance gene for selection of transformants containing recombinant bacmid DNA
- SV40 early polyadenylation signal for efficient transcription termination and polyadenylation of mRNA
- pUC origin

With the pDEST8 vector the gene of interest can be moved into a bac-to-bac baculovirus expression system. The Bac-to-Bac baculovirus expression system is a rapid and efficient method to generate recombinant baculoviruses based on the site-specific transposition properties of the Tn7 transposon (Luckow, Lee et al. 1993) (Invitrogen 2004). The DH10Bac^{TM} *E. coli* host strain contains a baculovirus shuttle vector (bacmid) and a helper plasmid and allows generation of a recombinant baculovirus for high-level expression of the gene of interest in insect cells (Invitrogen 2004). The baculovirus shuttle vector propagates in the DH10Bac *E. coli* as a large plasmid which confers resistance to kanamycin and can complement a *lac*Z deletion present on the chromosome to form colonies which are blue (Lac^{+}) in the presence of X-gal and the inducer IPTG (Invitrogen 2004). The helper plasmid encodes the transposase and confers resistance to tetracycline.

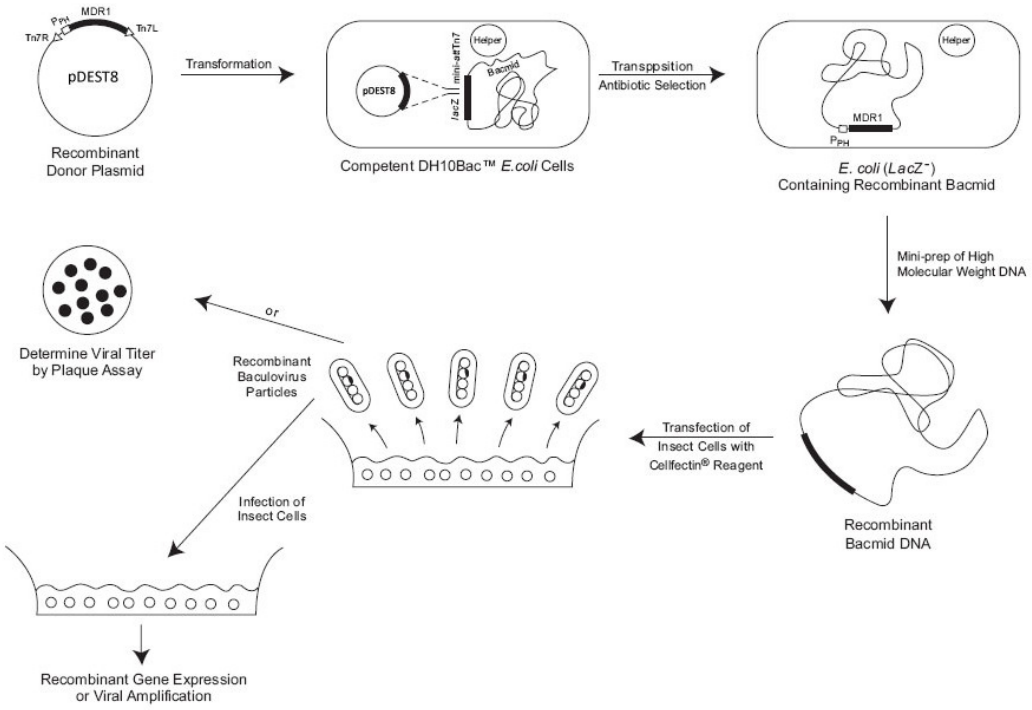

Figure 3.12: Generation of recombinant baculovirus and gene (MDR1) expression using the bac-to-bac baculovirus expression system (adapted from (Invitrogen 2009)).

1 ng of each pDEST8 construct was transformed into 50 µl of MAX Eficiency DH10Bac Chemically Competent Cells in an Eppendorf tube and incubated for 30 minutes on ice. The cells were heat-shocked by incubating at 42°C for 30 seconds and placed on ice for approximately 2 minutes. After cooling, 900 µl S.O.C. medium were added and the tubes were incubated at 37°C for 4 hours at 300 rpm in a shaking ther-

moblock (Eppendorf thermomixer comfort). Finally, the cells were spread on LB plates containing 50 µg/ml kanamycin, 7 µg/ml gentamicin, 10 µg/ml tetracycline, 100 µg/ml X-gal, and 40 µg/ml IPTG. The plates were incubated for 48 hours at 37°C. White colonies were picked for analysis because insertions of the mini-Tn7 into the mini-*att*Tn7 attachment site on the bacmid disrupt the expression of the LacZα peptide (blue/white selection). The bacmid was then isolated and purified.

Analyzing recombinant bacmid DNA by PCR:
PCR analysis was performed to verify the presence of the *MDR1* gene in the recombinant bacmid. The bacmid contains M13 forward and M13 reverse priming sites flanking the mini-*att*Tn7 site (Invitrogen 2009).

Reaction mix per sample:

Recombinant bacmid DNA (100 ng)	0.5-1 µl
10X PCR Buffer	2.5 µl
10 mM dNTP Mix	0.5 µl
50 mM $MgCl_2$	0.75µl
Primer_for (10 µM stock)	1 µl
Primer_rev (10 µM stock)	1 µl
ddH_2O	18-18.5 µl
Platinum Taq polymerase (5 units/µl)	0.25 µl
Total Volume	25 µl

Primer	**Nucleotide sequence (5' → 3')**
M13_for	5'-GTTTTCCCAGTCACGAC-3'
M13_rev	5'-CAGGAAACAGCTATGAC -3'
MDR1Hind_for	5'-GCCCAAGACAGAAAGCTTAGTACC-3'
MDR1Hind_rev	5'-GGTACTAAGCTTTCTGTCTTGGGC-3'
MDR1Q132R_for	5'-GCTGCTTACATTCGTGTTTCATTTTG-3'
MDR1Q132R_rev	5'-CAAAATGAAACACGAATGTAAGCAGC-3'
MDR1Q773R_for	5'-CATTTTTCCTTCGAGGTTTCACATTTG-3'
MDR1Q773R_rev	5'-CATTTTTCCTTCGAGGTTTCACATTTG-3'

Table 3.1: Oligonucleotides used for analyzing recombinant bacmid DNA.

The thermal cycling conditions were as following:

Step	Temperature, °C	Time, min	Number of Cycles
Initial Denaturation	93	3	1
Denaturation	94	0.75	
Annealing	55	0.75	35
Extension	72	5	
Final Extension	72	7	1

If transposition was successful, bands with the following sizes should be visible on the agarose gel:

Primerpair	bps (approximately)	Template
M13_for ; M13_rev	6278	G185V; G185V-Q132R; G185V-Q773R; G185V-Q132R/Q773R
M13_for; MDR1Hind_rev	3800	G185V; G185V-Q773R; G185V-Q132R/Q773R
MDR1Hind_for; M13_rev	2640	G185V; G185V-Q132R; G185V-Q132R/Q773R
MDR1Q132R_for; MDR1Hind_rev	1671	G185V; G185V-Q132R
MDR1Q132R_for; M13_rev	4285	G185V-Q132R
MDR1Q132R_for; MDR1Q773R_rev	1951	G185V-Q132R/Q773R
M13_for; MDR1Q132R_rev	2155	G185V-Q132R; G185V-Q132R/Q773R
MDR1Q773R_for ; M13_rev	2353	G185V-Q773R; G185V-Q132R/Q773R
M13_for; MDR1Q773R_rev	4077	G185V-Q773R
MDR1Hind_for; MDR1Q773R_rev	304	G185V-Q773R

Table 3.2: PCR was performed to verify the presence of the mutated MDR1 gene in the recombinant bacmid. The table shows the primerpairs, expected PCR products and templates which were used to amplify the mutated MDR1.

After this procedure, the recombinant bacmids, containing P-gp mutants, were ready to transfect insect cells to produce recombinant baculovirus.

3.5.2 Preparation of plasmid DNA

3.5.2.1 Small-scale plasmid DNA preparation

The GenElute™ Plasmid Miniprep Kit was used to generate small-scale plasmid DNA preparations as described by the manufacturer (Sigma-Aldrich 2006). The protocol is based on a modified alkine-SDS lysis procedure, which was first described by Birnboim and Doly (Birnboim and Doly 1979). All steps were carried out at room temperature. 1.5 ml bacterial cells from a 5 ml overnight recombinant *E. coli* culture were harvested by centrifugation for 1 minute at 14,000 rpm in an Eppendorf 5415C centrifuge (Eppendorf, Germany). The supernatant was discarded and the cell pellet was completely resuspended in 200 µl Resuspension Solution (50 mM Tris-HCl pH 8.0, 10 mM EDTA, 100 µg/ml RNase A). Resuspended cells were lysed by adding 200 µl Lysis Solution (2 mM NaOH, 1% SDS), mixed by gentle inversion and incubated for 5 minutes. The alkaline lysis procedure denatures plasmid DNA. After 5 minutes, 350 µl Neutralization/Binding Solution (3.0 M Potassium acetate pH 5.5) was added and the tube gently inverted causing the precipitation of cell debris, proteins, lipids, SDS, and chromosomal DNA as a cloudy, viscous precipitate. The lysate was then centrifuged for 10 minutes at 14,000 rpm. For maximized binding of DNA to the membrane, GenElute Miniprep Binding Columns were prepared by adding 500 µl Column Preparation Solution (750 mM NaCl, 50 mM MOPS, 15% ethanol, 0.15% TritonX-100, pH 7.0) and centrifuged for 1 minute by 14,000 rpm. The flow-through liquid was discarded and the cleared lysate was transferred to the prepared column and centrifuged for 1 minute at 14,000 rpm. As before, the flow-through liquid was discarded and the columns were washed with 750 µl wash solution (1.0 M NaCl, 50 mM MOPS, 15% ethanol, pH 8.5) to remove contaminants followed by centrifugation for 1 minute at 14,000 rpm. The eluted wash solution was discarded and the columns were centrifuged as before to remove excess ethanol. After centrifugation, the column was transferred to a fresh collection tube and plasmid DNA was eluted by adding 50 µl ddH_2O to the column followed by centrifugation for 1 minute at 14,000 rpm. Plasmid DNA was now ready for immediate use in restriction enzyme digestion or storage at -20 °C.

3.5.2.2 Large-scale plasmid DNA preparation

Large-scale plasmid DNA preparations were generated using the HiSpeed® Plasmid Midi Kit as described by the manufacturer (QIAGEN 2005). It is a similar protocol as

the GenElute™ Plasmid Miniprep Kit. Bacterial cells from 50 ml of an overnight culture were harvested by centrifugation at 3,500 rpm for 30 minutes at 4 °C in an Eppendorf 5403 centrifuge (Eppendorf, Germany). The cell pellet was resuspended in 6 ml Resuspension Buffer (50 mM Tris-HCl pH 8.0; 10 mM EDTA; 100 µg/ml RNase A) and 6 µl LyseBlue, a color indicator which provides visual identification of optimum buffer mixing. Then 6 ml Lysis Buffer (200 mM NaOH, 1% SDS) were added, and the content of the tube mixed by inversion followed by 5 minutes incubation at room temperature. The cell suspension was homogeneously blue after addition of Lysis Buffer. After incubation 6 ml Neutralization Buffer (3.0 M Potassium acetate pH 5.5) were added to the lysate and mixed by inversion. A white precipitate containing cell debris, proteins and genomic DNA became visible. The lysate was transferred into the barrel of the QIAfilter Cartridge which was capped and incubated for 10 minutes at room temperature. During the incubation, a HiSpeed Midi Tip was equilibrated by adding 4 ml Equilibration Buffer (750 mM NaCl, 50 mM MOPS, 15% isopropanol, 0.15% TritonX-100, pH 7.0). The column was allowed to empty by gravity flow. After incubation, the cap from the QIAfilter outlet nozzle was removed, and the plunger was gently inserted into the QIAfilter Cartridge and the lysate was filtered into the previously equilibrated HiSpeed Midi Tip. The cleared lysate was allowed to enter the resin by gravity flow. The HiSpeed Midi Tip was washed with 20 ml Wash Buffer (1.0 M NaCl, 50 mM MOPS, 15% isopropanol, pH 7.0) and the DNA was eluted with 5 ml Elution Buffer (1.25 M NaCl, 50 mM MOPS, 15% isopropanol, pH 8.5). The DNA was precipitated by adding 3.5 ml isopropanol to the eluted DNA, followed by mixing and incubatoin for 5 minutes at room temperature. During the incubation, the plunger from a 20 ml syringe was removed and the QIAprecipitator Midi Module was attached onto the outlet nozzle. The elute/isopropanol mixture was then transferred into the 20 ml syringe, the plunger was inserted and the mixture was filtered through the QIAprecipitator using constant pressure. The QIAprecipitator was removed from the syringe, the plunger was pulled out, the QIAprecipitator, reattached to the syringe and 2 ml 70% ethanol was added to the syringe. The DNA was washed by inserting the plunger and pressing the ethanol through the QIAprecipitator using constant pressure. The last step was repeated twice without ethanol to dry the membrane by pressing air through the QIAprecipitator. The outlet nozzle of the QIAprecipitator was dried with absorbent paper to prevent ethanol carryover. The same procedure was used to elute DNA by pressing 500 µl ddH_2O through the QIAprecipitator. (all: (QIAGEN 2005))

The size, quality and recovery of DNA were determined by quantitative analysis on an 1.6% agarose gel (1.6% agarose, 0.25 µg/ml ethidium bromide, in TAE buffer). 1 µl of DNA was mixed with 9 µl ddH_20 and 1 µl loading buffer (0.25% bromophenol blue, 0.25% xylene cyanol, 30% glycerol, in ddH_20), loaded into sample wells and electrophoresed at 50 V. The recovery of DNA was compared with 10 µl MassRuler DNA LadderMix (Fermentas, Cat. No. SM0403). The DNA was visualised using UV screen and images were recorded.

Plasmid DNA was now ready for immediate use in restriction enzyme digestion, cloning, PCR, transfection and sequencing or storage at -20 °C.

3.6 Generation of P-gp construct

A full-length human MDRl cDNA coding for human P-gp with 6 tandem histidine residues at its carboxy-terminus (P-gpHis6), a gift from Suresh V. Ambudkar (Maryland, USA), was cloned as a *BamH*I to *Xho*I fragment into a pENTR4 vector to give pENTR4MDR1H6. The plasmid was linearized at the *Bam*HI site and then blunt-ended with the Klenow fragment of DNA polymerase I disrupting the open reading frame with a second initiation codon. Nevertheless, there was a second Kozak sequence that is necessary for efficient initiation of translation in eukaryotic cells at the *Nco*I restriction site. A Kozak sequence contains the ATG initiation codon, a A or G at position -3 and a G at position +4 (CCATGG). The *Nco*I restriction site is the first restriction site in the multiple cloning site of the pENTR4 vector. Unfortunately, MDR1 cDNA contains this enzyme site too, and another restriction site was used for cloning generating a second initiation codon. As a precaution, a fragment of the pENTR4 vector containing an A to T mutation disrupting the initiation codon was created and introduced into the pENTR4 vector (CCTTGG) by site-directed mutagenesis based on overlap extension polymerase chain reaction (OE-PCR). Then the pENTR4 vector was cut with *Sal*I and *Xba*I and the *MDR*1 cDNA was subcloned as a *Sal*I to *Xba*I fragment into the vector. Finally, the pENTR4MDR1H6 vector was used as template for generation of P-gp mutants by OE-PCR. To generate a pENTR4 vector without the *ccdB* gene as a control, the entry vector was digested on each site of the *ccdB* gene with the double cutter *Eco*RI and recircularized.

3.7 Generation of P-gp mutants

Using site-directed mutagenesis based on OE-PCR mutated residues or nucleotides were introduced into the *MDR*1H6 gene. All construct sequences were ascertained by DNA sequencing (performed by IBL, Austria).

3.7.1 Overlap extension PCR

Overlap extension PCR was developed by Higuchi *et al.* (Higuchi, Krummel et al. 1988) and by Ho and colleagues (Ho, Hunt et al. 1989) almost simultaneously. Outside primers, mutagenic complementary oligodeoxyribo-nucleotide (oligo) middle primers and the polymerase chain reaction (PCR) were used to generate two DNA fragments with overlapping ends and intended mutations, both of which were introduced by two mutagenic middle primers. These fragments were combined in a subsequent 'fusion' reaction in which the overlapping ends annealed, allowing the 3' overlap of each strand to serve as a primer for the 3' extension of the complementary strand (Ho, Hunt et al. 1989). The resulting fusion product was amplified further by PCR using two outside primers. Specific alterations in the nucleotide (nt) sequence were introduced by incorporating nucleotide changes into the overlapping oligo primers (Opitz, Jenkins et al. 1998). The human MDR1H6 DNA was used as the template DNA for the overlap extension PCR technique for generation of the P-gp mutants. The primers were designed with the software package Clone Manager v.8.0 (SciEd Software NC, USA). All four primers (outside_for, outside_rev, mutagenic_for and mutagenic_rev) were used for the first round of PCR. The second round of PCR using primers outside_for and outside_rev resulted in a fusion product that was purified. The cDNA was then restriction digested and subcloned into the the pENTR4 vector. The resulting DNA fragment was sequenced.

Amino acid change	Primer out-side_for	Primer mutage-nic_for	Primer mutage-nic_rev	Primer out-side_rev
Q132A	NcoImut_for	MDR1Q132A_for	MDR1Q132A_rev	Hind_rev
Q132E	NcoImut_for	MDR1Q132E_for	MDR1Q132E_rev	Hind_rev
Q132R	NcoImut_for	MDR1Q132R_for	MDR1Q132R_rev	Hind_rev
Q773A	Hind_for	MDR1Q773A_for	MDR1Q773A_rev	MDR1blunt_rev
Q773E	Hind_for	MDR1Q773E_for	MDR1Q773E_rev	MDR1blunt_rev
Q773R	Hind_for	MDR1Q773R_for	MDR1Q773R_rev	MDR1blunt_rev
G185V	NcoImut_for	MDR1G185V_for	MDR1G185V_rev	Hind_rev

Table 3.3: Primer for site-directed mutagenesis of P-gp using overlap extension PCR

Primer	Nucleotide sequence (5' → 3')
MDR1Q132A_for	5′-CTGCTTACATT**GCG**GTTTCATTTTGG-3′
MDR1Q132A_rev	5′-CCAAAATGAAAC**CGC**AATGTAAGCAG-3′
MDR1Q132E_for	5′-GGTTGCTGCTTACATT**GAA**GTTTCATTTTG-3′
MDR1Q132E_rev	5′-CAAAATGAAAC**TTC**AATGTAAGCAGCAACC-3′
MDR1Q132R_for	5′-GCTGCTTACATT**CGT**GTTTCATTTTG-3′
MDR1Q132R_rev	5′-CAAAATGAAAC**ACG**AATGTAAGCAGC-3′
MDR1Q773A_for	5′-CATTTTTCCTT**GCG**GGTTTCACATTTGGC-3′
MDR1Q773A_rev	5′-GCCAAATGTGAAACC**CGC**AAGGAAAAATG-3′
MDR1Q773E_for	5′-CATTTTTCCTT**GAA**GGTTTCACATTTG-3′
MDR1Q773E_rev	5′-CAAATGTGAAACC**TTC**AAGGAAAAATG-3′
MDR1Q773R_for	5′-CATTTTTCCTT**CGA**GGTTTCACATTTG-3′
MDR1Q773R_rev	5′-CATTTTTCCTT**CGA**GGTTTCACATTTG-3′
MDR1G185V_for	5′-GATTAATGAA**GTT**ATTGGTGACAAAATTGG-3′
MDR1G185V_rev	5′-CCAATTTTGTCACCAAT**AAC**TTCATTAATC-3′
NcoImut_for	5′-CAGGCTCCACCTTGGGAACC-3′
Hind_for	5′-GCCCAAGACAGAAAGCTTAGTACC-3′
Hind_rev	5′-GGTACTAAGCTTTCTGTCTTGGGC-3′
MDR1blunt_rev	5′-ACAAATTGATAAGCAATGCTTTC-3′
NcoImut_rev	5′-GGTTCCCAAGGTGGAGCCTG-3′

Table 3.4: Oligonucleotides used for site-directed mutagenesis to generate P-gp mutants. Nucleotides in bold and underline indicate the mutagenic nucleotides which differ from the wild-type sequence. Underlined nucleotides indicate the mutagenic nucleotides which disrupted the *Nco*I restriction site in the pENTR4 vector.

Two rounds of PCR were necessary to generate mutations in the desired position of the *MDR1* gene. MDR1 cDNA was divided into two halves, an N-terminal and a C-terminal half, resulting in an approximately 2000 bps long PCR product for each half. Q132 and

G185 were located in the N-terminal, and Q773 in the C-terminal half. The following protocol was used:

First round of PCR:

Plasmid pENTR4MDR1H6 (~5 ng) was used as the template for generation of pENTR4MDR1H6G185V. Two outside primers and two mutagenic middle primers (each containing mutated nucleotides) were used to generate PCR products 1 and 2 in separate reactions. The primers were designed in such a way that an overlap region in the two PCR fragments would be created. DNA polymerase Pfu (Fermentas, Cat. No. EP0572) was used to reduce the chance of getting undesired mutations during the PCR.

Reaction mix per sample:

ddH_2O	16.75 µl
10x Buffer	2.5 µl
2 mM dNTP each	2.5 µl
Template: pentry vector	1µl
DNA polymerase Pfu	0.25 µl
Primer_for (10 µM stock)	1 µl
Primer_rev (10 µM stock)	1 µl
Total volume	25 µl

The thermal cycling conditions were as following:

Step	Temperature, °C	Time, min	Number of Cycles
Initial Denaturation	95	2	1
Denaturation	95	0.5	
Annealing	45	0.5	5
Extension	72	4	
Denaturation	95	0.5	
Annealing	50	0.5	25
Extension	72	4	
Final Extension	72	5	1

The first round PCR products were isolated by agarose gel electrophoresis. Gel fragments were visualised using a UV screen, excised with a scalpel and purified using GFX^{TM} PCR DNA and gel band purification kit (Amersham Biosciences, 27-9602-01).

Second round of PCR:

Purified PCR products 1 and 2 served as templates and were mixed in an equal volume. The two outside primers were used to amplify the full-length *MDR*1 product. Pfu DNA polymerase was used for 30 cycles of amplification.

Reaction mix per sample:

ddH_2O	16.75 µl
10x Buffer	2.5 µl
2 mM dNTP each	2.5 µl
Template: Mixture of PCR product 1 and 2 (equal volume)	1µl
DNA polymerase Pfu	0.25 µl
Primer_for	1 µl
Primer_rev	1 µl
Total volume	25 µl

The above PCR conditions were modified slightly:

Step	Temperature, °C	Time, min	Number of Cycles
Initial Denaturation	95	2	1
Denaturation	95	0.5	
Annealing	50	0.5	30
Extension	72	4	
Final Extension	72	5	1

The final products were cut with *Sal*I (Fermentas, Cat. No. ER0641) and *Hind*III (Fermentas, Cat. No. ER0501) or HindIII and *Xba*I (Fermentas, Cat. No. ER0682) restriction enzymes, and the approximately 2.0-kbp fragments containing the half-length MDR1 gene were subcloned into *Sal*I-*Hind*III-pENTR4MDR1H6 or *Hind*III-*Xho*I-pENTR4MDR1H6 to create mutant versions of pENTR4MDR1H6. The ligation was carried out with the Rapid DNA Ligation Kit from Fermentas (Cat. No. K1422) containing the T4 DNA Ligase (5u/µl), 5x Rapid Ligation Buffer and water (nuclease-free).
Reaction mix per sample:

Insert	X µl
Vector	X µl
ddH_2O	Up to 19
5x Rapid Ligation Buffer	4 µl
T4 DNA Ligase (5u)	1 µl
Total volume	20 µl

5 µl of the ligation mixture were used for transformation 50 µl One Shot TOP10 Chemically Competent Cells as before. The cells were spread onto LB agar plates with 50 µg/ml kanamycin and incubated overnight at 37°C.

3.7.2 Purification of DNA from solution or gel bands

For purifying PCR products, restriction fragments and plasmid DNA, the GFX PCR DNA and Gel Band Purification Kit was used as described by the manufacturer (AmershamBiosciences 2005). All steps were carried out at room temperature.
Purification from solution:

The GFX column was placed in a collection tube and 500 µl capture buffer, containing acetate and chaotrope, were added to the GFX column. The DNA solution (up to 100 µl) was transferred to the GFX column, mixed thoroughly by pipetting the sample up and down (4-6 times) causing denaturation of proteins and then centrifuged for 30 seconds in an Eppendorf 5415C centrifuge (Eppendorf, Germany) at 14,000 rpm. Then the sample was passed through the GFX column to capture the DNA onto the glass fiber matrix. The flow-through was discarded and the GFX column was placed back inside the collection tube. Then the matrix-bound DNA was washed with 500 µl wash buffer (10 mM Tris-HCl pH 8.0, 1 mM EDTA, in 80% ethanol) to remove salts and other contaminants and centrifuged for 30 seconds at 14,000 rpm. After centrifugation, the GFX column was transferred to a fresh 1.5 ml eppendorf tube and the DNA eluted by adding 50 µl ddH_2O. After 1 minute incubation, the purified DNA was recovered by centrifugation for 1 minute at 14,000 rpm. (all: (AmershamBiosciences 2005)**)**

Purification from gel bands:
The gel slice of agarose containing the DNA band to be purified was carefully excised using a scalpel and a UV light box and was then cut into smaller pieces. The pieces were transferred to a preweighted empty 1.5 ml eppendorf tube. The eppendorf tube containing the agarose slice was weighed again to determine the approximate volume of the gel slice. For each 10 mg of gel slice 10 µl Capture Buffer were added. The tube was closed, mixed by vortexing and incubated at 60 °C for 15 minutes or until the gel was completely melted. During incubation, the GFX column was placed in a collection tube. After the agarose was completely dissolved, the eppendorf tube was briefly centrifuged to collect the sample at the bottom of the tube and the sample was transferred to the GFX column. After 1 minute incubation, the GFX column was centrifuged for 30 seconds. Further steps were the same as before in the "purification from solution". (all: (AmershamBiosciences 2005))

3.8 Agarose gel electrophoresis

DNA fragments were separated by agarose gel electrophoresis (1.6% agarose, 0.25 µg/ml ethidium bromide, in TAE). Samples were mixed with 10% of the loading buffer volume, loaded into sample wells, and electrophoresed at constant 50 V. The electrophoresis chamber was filled with 1xTAE containing 0.25 µg/ml ethidium bromide. One

lane on each gel was loaded with 10 µl Mass Ruler DNA Ladder Mix (Fermentas, Cat. No. SM0403). The DNA was visualised using a UV screen and images were recorded.

10x TAE:	400 mM Tris base
	10 mM EDTA
	1.14% Acetic acid
	Stored at 4°C
Loading buffer:	0.25% bromophenol blue
	0.25% xylene cyanol
	30% glycerol
	Stored at room temperature

Ethidium bromide solution: 0.5 mg/ml in ddH_2O, stored at room temperature

3.9 Mammalian tissue culture

Dulbecco's Modified Eagle's Medium (DMEM) (Cat. No. 12800-116), 0.25% Trypsin-EDTA (Cat. No. 25200), Lipofectamine 2000 (Cat. No. 11668027), Donor Bovine Serum (DBS) (16030-074), Zeocin (Cat. No. R250-01) and Hygromycin B (Cat. No. 10687-010) were purchased from Invitrogen.

Human HEK 293 (FlpIn-293) cells and mouse NIH 3T3 fibroblasts (Flp-In-3T3), supplied by Invitrogen, were grown as monolayers in a T75 tissue culture flask (VWR, Cat. No. 734-2167) and maintained by regular passage in DMEM supplemented with 4.5 g/l glucose, 2 mM L-glutamine, 1 mM sodium pyruvat and 10% DBS (vol/vol) under 5% CO_2 at 37°C with a water vapour-saturated atmosphere.

All manipulations were performed in a sterile environment with sterile plastics and glassware.

3.10 Generation of stable mammalian expression cell lines

Cell lines and reagents were supplied from Invitrogen.

Cell Line	Amount	Catalog No.
Flp-In-293	3 x 10^6 cells, frozen	R750-07
Flp-In-3T3	3 x 10^6 cells, frozen	R761-07

Reagent	Catalog No.
Zeocin™	R250-01
Hygromycin B	10687-010

Stable mammalian expression cell lines were generated using the Flp-In™ system described by the manufacturer (Invitrogen 2002). With the Flp-In system it is possible to integrate and express a gene of interest in mammalian Flp-In cells at a specific genomic location (Invitrogen 2002). The Flp-In cell lines from Invitogen stably express the *lac*Z-Zeocin™ fusion gene whose expression is controlled by the SV40 early promoter and contain a Flp Recombination Target (FRT) site which has been inserted just downstream of the ATG initiation codon of the *lac*Z-Zeocin™ fusion gene. The FRT site serves as the binding and cleavage site for the Flp recombinase (Invitrogen 2002). Flp-In cell lines are Zeocin-resistant. An expression vector containing the gene of interest is then integrated into the genome via Flp recombinase-mediated DNA recombination at the FRT site (O'Gorman, Fox et al. 1991) (Invitrogen 2002). Expression of the gene is controlled by the human CMV promoter. Another component of the Flp-In System is the pOG44 plasmid which constitutively expresses the Flp recombinase (Broach and Hicks 1980; Broach, Guarascio et al. 1982; Buchholz, Ringrose et al. 1996) under the control of the human CMV promoter. (Invitrogen 2002)

The pOG44 plasmid and the pEF5MDR1 vector were cotransfected into the Flp-In-3T3 host cell line. Upon cotransfection, the Flp recombinase expressed from pOG44 mediated a homologous recombination event between the FRT sites (integrated into the genome and on pEF5MDR1) such that the pEF5MDR1 construct was inserted into the genome at the integrated FRT site (Invitrogen 2002). Insertion of pEF5MDR1 into the genome at the FRT site brings the SV40 promoter and the ATG initiation codon (from pFRT/lacZeo) into proximity and frame with the hygromycin resistance gene (from pEF5MDR1 lacking the promoter and the ATG initiation codon), and inactivates the

lacZ-Zeocin fusion gene (Invitrogen 2002). Thus, stable Flp-In expression cell lines could be selected for hygromycin resistance, Zeocin sensitivity, lack of β-galactosidase activity, and expression of the P-gp protein (Invitrogen 2002).

3.10.1 Stable cell transfection using Lipofectamine 2000

Human HEK 293 cells and mouse NIH 3T3 fibroblasts (Flp-In-3T3) were cultured in DMEM supplemented with 4.5 g/l glucose, 2mM L-glutamine, 1mM sodium pyruvat and 10% DBS at 37°C in 5% CO_2. The cells were grown in presence of 100 µg/ml Zeocin. One day prior to transfection, the cells were seeded onto six-well plates (Greiner bio one, Cat. No. 657160) in aliquots of 1 x 10^6 per well in the corresponding medium containing 10% DBS (1 ml medium/well) without Zeocin. After 24 hours, the growth medium of the cells was replaced with serum-/antibiotic-free medium (Opti-MEM) and the cells were treated with 2 µg/ml Lipofectamine 2000 complex in the corresponding Opti-MEM serum-/antibiotic-free medium (Invitrogen, Cat. No. 31985-047) according to the manufacturer's instructions (Invitrogen 2006) for 2 hours at 37°C. The cells were stably transfected in 6-well plates with pEF5 vector (Invitrogen) or pEF5 vector containing the human MDR1 gene. After 2 hours 2% donor bovine serum was added into the Opti-MEM. After 24 hours the cells were trypsinized and passaged at a 1:10 dilution into a T25 flask with fresh growth medium (DMEM containing 10% donor bovine serum). The following day the cells were selected with 200 µg/ml hygromycin B (Invitrogen, Cat. No. 10687-010). Nontransfected cells were killed by hygromycin B. The medium containing hygromycin B was exchanged every 3 to 4 days.

3.10.1.1 Expression of mutants

Human HEK 293 cells and mouse NIH 3T3 fibroblasts were transfected with the mutated *MDR1* cDNAs as described before. P-gp processing mutants expressed functional P-gp when they were kept in the presence of drug substrates or modulators of P-gp that correct the folding defect. To test for the effect of compounds on expression of P-gp processing mutants, cells were grown for 24h in Dulbecco's modification of Eagle'smedium (DMEM) with 10% (v/v) donor bovine serum at 37 °C in a 5% CO_2 incubator in the presence of 10 µM cyclosporin A (CsA). CsA is a substrate of P-gp and acts like a powerful chemical chaperone promoting maturation of P-gp (Loo and Clarke 1997). Other compounds used as pharmacological chaperones were 50 µM verapamil

and 50 µM GP51. Compounds were prepared as 500 X stocks in DMSO. Control cells were incubated in the presence of 0.2% (v/v) DMSO. Cells were harvested and prepared for the MRK16 staining.

3.11 Western blot analysis

3.11.1 Preparation of protein samples for SDS-Polyacrylamide gel electrophoresis (SDS-PAGE)

Cells were seeded onto 6-well plates in aliquots of 1 x 10^6 cells per well in the corresponding DMEM medium containing 10% DBS (2 ml medium/well) and in the presence of 10 µM CsA. Control cells were incubated in the presence of 0.2% (v/v) DMSO. After 24 hours, the cells were washed three times with ice-cold PBS and lysed directly in the wells by adding 60 µl of lysis buffer containing 1% of a protease inhibitor cocktail (Sigma, Cat. No. P8340) and incubated for 10 minutes. All steps were carried out on ice. After incubation, the cells were removed with a rubber policeman, transferred in an Eppendorf tube, broken with an ultrasonic stick for 2 seconds and incubated for 1 hour on ice. The samples were stored overnight at -20°C.

PBS:	137 mM NaCl
	2.7 mM KCl
	1.5 mM KH_2PO_4
	8.1 mM $Na_2HPO_4.12H_2O$
	Adjust to pH 7.4
Lysis buffer (prepared fresh):	62.5 mM Tris base, pH 6,8
	8 M urea
	20 mM EDTA
	20 mM EGTA
	10% Glycerol
	1% SDS

After 24 hours, the samples were thawed and centrifuged for 10 minutes at 14,000 rpm at 4°C. The supernatants were transferred into fresh Eppendorf tubes and vortexed.

3.11.2 Protein determination using Bradford protein assay

The Bradford protein assay (Bio-Rad, Cat. No. 500-0006) is a dye-binding assay. The absorbance maximum for an acidic solution of Coomassie Brilliant Blue G-250 dye shifts from 465 nm to 595 nm when binding to proteins occurs (BioRad 1994). Protein concentration was determined using the Bradford protein microassay by absorbance at 595 nm. A protein standard curve was made using bovine serum albumin (BSA) (Sigma, Cat. No. A4503) with concentrations of 0, 1, 2, 4, 6, 8, 10, 15 and 20 µg/ml.

BSA-Standard:

Standard	**BSA (100 µg/ml)**	**ddH_2O**	**Bio-Rad-Reagent**
0 µg/ml	0 µl	400 µl	100 µl
1 µg/ml	5 µl	395 µl	100 µl
2 µg/ml	10 µl	390 µl	100 µl
4 µg/ml	20 µl	380 µl	100 µl
6 µg/ml	30 µl	370 µl	100 µl
8 µg/ml	40 µl	360 µl	100 µl
10 µg/ml	50 µl	350 µl	100 µl
15 µg/ml	75 µl	325 µl	100 µl
20 µg/ml	100 µl	300 µl	100 µl

Samples:

Sample	**ddH_2O**	**Bio-Rad-Reagent**
2,5 µl	397,5 µl	100 µl

3.11.3 SDS-PAGE

Proteins were separated by electropheresis through vertical 0.75 mm thick polyacrylamide gels (0.1% SDS, 8% acrylamide). The samples were diluted and made up to 10 µl with PBS to equal protein amounts. Then equal amounts of protein were mixed with the 4x sample buffer in a 3:1 ratio and incubated for 30 minutes at 40°C in a water bath to denature the proteins. After cooling down, the samples were loaded onto the gel.

4x sample buffer:	50% Glycerol
	24% 0.5 M Tris-HCl (pH 6.8)
	21% ddH_2O
	8% (w/v) SDS
	A dash of bromophenol blue
	5% 2-Mercaptoethanol
	Prepared just before use
10x running buffer:	250 mM Tris base
	1.92 M Glycine
	1% SDS
	Stored at room temperature

Polyacrylamide gel: per gel (0.75 mm thickness)

Stacking gel (4% acrylamide):

Reagent	Volume
ddH_2O	1.54 ml
30% Acrylamid:Bis-acrylamide mix (29.2:0.8)	340 µl
3 M Tris-HCl, pH 8.45; 0.3% SDS	620 µl
10% APS	20 µl
TEMED	2 µl
Total volume	2.522 ml

Separating gel (8% acrylamide)

Reagent	Volume
ddH_2O	2.4 ml
30% Acrylamide:Bis-acrylamide mix (29.2:0.8)	1.6 ml
3 M Tris-HCl, pH 8.45/0.3% SDS	2 ml
10% APS	30 µl
TEMED	3 µl
Total volume	6.33 ml

10% Ammonium Persulfate (APS) (Sigma, Cat. No. 248614): aliquots were stored at -20°C

10% SDS: stored at room temperature

3 M Tris-HCl, pH 8.45; 0.3% SDS: 3 M Tris-HCl
0.3% SDS
Adjust to pH 8.45
Stored at room temperature

The solutions were prepared in 50 ml Falcon tubes. The polymerisation of the separating gel was initiated by the addition of N,N,N′,N′-teteramethylethane-1,2-diamine (TEMED) (Sigma, Cat. No. T9281) and filled in a Bio-Rad Mini Protean II gel cassette. Each gel was immediately overlaid with a thin layer of 30% isopropanol. After polymerisation, the overlay was removed and the gel surface was rinsed with ddH_2O. TEMED was added to the stacking gel to initiate polymerisation and was overlaid onto the separating gel. A 15-well comb was inserted. After polymerisation, the gel cassettes were put into the electrophoresis chamber according to the manufacturer's instructions. The chamber was filled with 1x running buffer and after removing the comb, the wells were rinsed with 1x running buffer prior to loading samples. One lane was loaded onto each gel with 2 µl Page Ruler Prestained Protein Ladder (Fermentas, Cat. No. SM0671) to enable the subsequent determination of protein molecular weights. Slots without any protein sample were filled with sample buffer. Electrophoresis was performed at constant 180V for 80 minutes at 4°C.

3.11.4 Detection of proteins by Western blotting

Proteins, separated by SDS-PAGE, were then electroblotted onto nitrocellulose membranes (Bio-Rad, Cat. No. 162-0115) using a Bio-Rad Mini Blotting apparatus, according to the manufacturer's instructions. Membrane, sponges and 3MM filter paper were prepared by soaking in western transfer buffer for 1 minute. The transfer components were put together as followed:

White side of the cassette (facing positive electrode)
Sponge
Filter paper
Nitrocellulose membrane
Gel
Filter paper
Sponge
Black side of the cassette (facing negative electrode)

Air bubbles between gel and nitrocellulose membrane were removed by rolling a glass eprouvette over the filter paper. The sandwich was assembled together with an ice block for cooling the buffer into the blotting apparatus. Electroblotting was carried out in transfer buffer at 0.4 A (0.06 A/ gel) for 45 minutes at 4°C.

Transfer buffer: 25 mM Tris base
192 mM Glycin
20% Methanol
1% SDS
Stored at 4°C and used again several times

3.11.4.1 Detection of proteins by Ponceau S

Total protein visualisation was carried out using the Ponceau S (Sigma, Cat. No. 78376) staining, immediately after SDS-PAGE to ensure complete transfer of proteins. The nitrocellulose membrane was placed in the Ponceau S solution for 5 minutes at room temperature. After visualisation of the proteins, the membrane was washed in ddH_2O at room temperature for 5 minutes to destain the gel.

Ponceau S:	1% Ponceau
	30% Trichloracetic acid
	30% Sulfosalicylic acid

3.11.4.2 Immunodetection

10x TBS:	200 mM Tris base
	1.45 M NaCl
	Adjust to pH7.4
Washing buffer (TBS-T):	1x TBS buffer
	0.1% Tween 20
Bloking solution:	5% (w/v) nonfat dry milk in TBS-T
	Prepared just before use

Primary antibody:
Primary antibodies were attenuated in blocking solution at the recommended dilution. A dash of NaN_3 was added to each antibody solution to avoid contamination. The primary antibodies were used again for several times and stored at 4°C.
The P-gp specific monoclonal antibody C219 was obtained from Eubio, Austria (Cat. No. ALX801-002) and diluted 1:250 in 1% BSA in TBS-T.
Anti-ß-Actin (Sigma, Cat. No. A2228) was diluted 1:5000 in 3% BSA in TBS-T.

Secondary antibody:
The secondary antibody goat anti-mouse IgG-HRP conjugate (Bio-Rad, Cat. No. 170-6516) was diluted 1:10000 in blocking solution.

After Ponceau S destaining, the membrane was cut according to the protein sizes. One membrane could be used to detect up proteins with different sizes: the upper part for P-gp (170 kDa) and the lower part for ß-Actin loading control (42 kDa) detection. The membranes were washed with TBS-T for 10 minutes and treated with 5% nonfat dry milk in TBS-T overnight at 4°C on a belly dancer for blocking. On the next day the membranes were washed three times for 5 minutes with washing buffer and incubated with primary antibody for 1 hour at room temperature on the belly dancer. After 1 hour,

the antibodies were removed and stored in the fridge until next use. Subsequently, the blots were washed three times with TBS-T for 10 minutes on the belly dancer and incubated for 1 hour at room temperature with a secondary antibody with shaking on the belly dancer. After incubation, the secondary antibody was discarded and the membranes were washed three times as before. Finally, antibody labelled proteins were visualized with ChemiGlow^{TM} West (Alpha Innotech Corporation, CA, USA). The ChemiGlow West working solution was prepared prior to use by mixing the Luminol/Enhancer Solution and the Stable Peroxidase Solution in equal volumes. The membranes were incubated for 5 minutes at room temperature and wrapped in plastic wrap. For detection a CCD camera in the ChemiImager^{TM} 4400 (Biozym) was used. Quantification was performed using the AlphaEaseFC software.

3.11.5 Determination of *MDR*1 gene expression levels by real -time quantitative RT-PCR

Real-time reverse transcription (RT) - PCR was used to assess the influence of cyclosporine A (CsA) on an mRNA level. Cells incubated with DMSO served as control.

3.11.5.1 Isolation of total RNA from cells

Total cellular RNA was isolated with TRIzol reagent (Invitrogen, Cat. No. 15596-026) as recommended by the manufacturer (Invitrogen 2007). One day prior to homogenization, the cells were seeded onto 6 cm diameter tissue culture dishes (Greiner Bio-One, Germany, Cat. No. 628160) in aliquots of 1x 10^6 per culture dish in the corresponding medium containing 10% DBS (5 ml medium/dish) and in the presence of 10 µM CsA. Control cells were incubated in the presence of 0.2% (v/v) DMSO. After 24 hours, the cells were washed and lysed directly in the culture dish by adding 800 µl of TRIzol reagent. The cell lysate was passed several times through a pipette, incubated for 1 minute at room temperature to permit the complete dissociation of nucleoprotein complexes and transferred to an eppendorf vial. The samples were stored at -80°C until RNA isolation.

The homogenized samples were briefly vortexed and centrifuged for 10 minutes at 12,000 rpm at 4 °C. For phase separation, 150 µl of chloroform were added per 800 µl of TRIzol reagent, shaked by hand for 15 seconds and incubated at room temperature for 5 minutes. The samples were centrifuged at 12,000 x g for 10 minutes at 4°C. The

mixture separated into a lower red, phenol-chloroform phase, an interphase, and a colorless upper aqueous phase containing the RNA. The aqueous phase (~400 µl) was transferred to a fresh tube, mixed with 400 µl isopropyl alcohol and incubated at room temperature for 10 minutes. After centrifugation at 12,000 x g for 10 minutes at 4°C, the supernatant was removed and the RNA pellet washed with 750 µl of 70% ethanol. The samples were mixed by vortexing and centrifuged at 7,500 x g for 5 minutes at 4°C. After the washing step, the RNA pellet was dried (air-dry) for approximately 10 minutes and dissolved in 50 µl diethylpyrocarbonate (DEPC)/DNase by passing the solution a few times through a pipette tip. To remove remaining DNA contamination 1-2 u of Turbo^{TM} DNase from Ambion was added to each sample and incubated for 15 minutes at 37 °C. The the samples were incubated for 10 minutes at 85 °C to inactivate the enzyme.

RNA concentration was determined by absorbance at 260 nm.

$E_{260nm} \times (\text{dilution})^{-1} \times e^{-1} = \text{concentration } \mu g/ml$

$e^{-1} = 40$ for single stranded RNA

To ensure equal loading and integrity of the RNA, 2 µg RNA were diluted in 5 µl RNA sample buffer containing ethidium bromide and run on MOPS/EDTA agarose gels. The amount of loaded RNA was controlled by visualisation on an UV screen.

3.11.5.2 RNA separation on MOPS/EDTA agarose gels

10x MOPS/EDTA:

MOPS	200 mM
Na-acetate	50 mM
EDTA	10 mM
Adjust to pH 7.0	

RNA sample buffer:

Formamide	15 ml
10x MOPS	3 ml
37% Formaldehyde	4.8 ml
RNase free H_2O	2 ml
Glycerol	2 ml
10% (w/v) Bromophenol blue	1.6 ml
Optional: 5 µl ethidium bromide (1 mg/ml)	
Storage at -20 °C	

MOPS/EDTA gel (1.2%):

Total volume	50 ml
Agarose	0.6 g
H_20	42.5 ml
10x MOPS	5 ml
37% Formaldehyde	2.5 ml

The RNA samples supplemented with sample buffer were heated up to 65 °C for 3 minutes causing the resolution of secondary structures in the RNA. Then the RNA samples were cooled on ice and loaded on a 1.2% MOPS/EDTA gel.

3.11.5.3 Reverse transcription

For cDNA synthesis, 1 µg of total RNA was reverse transcribed with an iScript cDNA synthesis kit (Bio-Rad, Cat. No. 170-8890) containing a mixture of oligo d(T) primers and random hexamer nucleotides.

Reaction mix per sample:

5x iScript reaction mix	4 µl
iScript reverse transcriptase	1 µl
Nuclease free H_2O	X µl
RNA template 1 µg of total RNA	X µl
Total volume	20 µl

Reaction condition:

Temperature, °C	Time, min
25	5
42	30
85	5
4	∞

3.11.5.4 SYBER green real-time PCR analysis

SYBER green real-time PCRs were performed with 0.5 µl of the RT reaction mixture by the iCycler iQ system (Bio-Rad) and Taq DNA Polymerase (recombinant) from Fermentas (Cat. No. EP0402) to quantify PCR assays. Reactions were performed in doublets. The RT reaction product was amplified in a 25 µl reaction with the *MDR*1 specific forward and reverse primer. The samples were heated to 95°C for 3 minutes and then amplified for 40 cycles consisting of 95°C for 20 seconds, 60°C for 25 seconds and 72°C for 25 seconds. The mouse hypoxanthine-guanine phosphoribosyltransferase (HPRT) housekeeping gene was amplified as a control and used to normalise mRNA levels between different samples.

Reaction mix per sample:

10x Taq buffer	2.5 µl
10 mM dNTP each	0.5 µl
25 mM $MgCl_2$	2.5 µl
TaqDNA polymerase (5U/µl)	0.2 µl
Primer F (10 pmol/µl)	0.25 µl
Primer R (10 pmol/µl)	0.25 µl
FITC Flourescein Calibration Dye (1 µM)	0.9375 µl
10x Syber Green (Bio-Rad)	1 µl
DEPC	11.8625 µl
Template	5.0 µl
Total volume	25.0 µl

Real-time PCR reaction:

Temperature, °C	**Time**	**Number of Cycles**
95	3 min	
95	20 sec	40x
AT	25 sec	
72	25 sec	
95	MC	
60		
20	∞	

MC: melting curve

AT: annealing temperature

RT-HPRT primer:

Primer	**Nucleotide sequence (5' → 3')**
RT-HPRT_for	GCTGGTGAAAAGGACCTCT
RT-HPRT_rev	CACAGGACTAGAACACCTGC

AT: 59°C

RT-MDR1 primer:

Primer	Nucleotide sequence (5' → 3')
RT-MDR1_for	CGAAGAGTGGGCACAAACCAG
RT-MDR1_rev	GTGGTGGCAAACAATACAGGTTCC

AT: 60°C

3.12 P-gp surface expression

3.12.1 P-gp surface expression for efflux studies

For the efflux assay, wild-type and mutant P-gp surface expression levels were compared and determined by a flow cytometer (FACSCalibur, BectonDickinson). Cells were trypsinized and counted, 200,000 cells were washed once with PBS and incubated with 50 µl MRK16 anti-P-glycoprotein primary antibody in PBS (10 µg/ml) at room temperature for 30 minutes. The rest of the cells was used for the rhodamine 123 efflux assay. After the incubation period, the cells were washed twice with PBS and treated with 50 µl Goat Anti-mouse IgG FITC (GAM Ig FITC) (BectonDickinson) in PBS. Cells were protected from light and incubated 30 minutes on ice. After the incubation period, cells were washed again twice with PBS and then resuspended in 200 µl PBS. The binding of the FITC-labeled P-gp antibody was analyzed with a flow cytometer (FACSCalibur, Becton Dickinson). Fluorescence was measured by counting 5,000 events with an excitation wavelenght of 488 nm.

3.12.2 P-gp surface expression increase using pharmacological chaperones

Mutations of amino acids are responsible for reduced levels or absence of functional proteins at a required location. These mutant proteins, synthesized in the endoplasmic reticulum, are defective in folding and trafficking (processing mutants).

The expression of P-gp and P-gp mutants in HEK 293 and NIH 3T3 cells was proven by surface protein expression analysis using the selective monoclonal antibody MRK16 and the FITC-labelled second antibody used in flow cytometry analysis. We tried different compounds as pharmacological chaperones, for example CsA, verapamil and GPV51. GPV51 is a propafenone which was designed in our group. The cells were pretreated for 24 hours with 10 µM CsA, 50 µM verapamil and 50 µM GPV51. After 24 hours the cells were trypsinized and counted for MRK16 staining. The prodecure is the same as before.

3.13 Transport studies

3.13.1 Rhodamine 123 zero trans efflux studies

The rhodamine 123 efflux assay is a direct and accurate functional method to measure inhibition of P-gp mediated transmembrane transport (Chiba, Ecker et al. 1996; Chiba, Holzer et al. 1998). Rhodamine 123 is a fluorescent substrate for the P-glycoprotein efflux pump (Kang, Fisher et al. 2004).

NIH 3T3 cells (7.5 x 10^5 at 37°C or 1.5 x 10^6 at 28°C) of each respective stable cell line were seeded into 9.4 cm diameter tissue culture dishes (Greiner Bio-One, Germany, Cat. No. 633171) using the corresponding medium containing 10% DBS and in the absence of hygromycin B. The cells were incubated at 37°C or 28°C depending on the P-gp mutant. After 48 hours, the medium was removed by pipetting from the culture dish into the lid of the culture dish and the cells were trypsinized with 800 µl of trypsin (Gibco) for 2-3 min at room temperature. The reaction was stopped by addition of the medium from the lid back into the culture dish. Cells were transferred to a 50 ml Falcon tube, counted, and approximately 2 x 10^6 cells were pelleted for 6 minutes at 1,100 rpm at 4 °C in an Eppendorf 5403 Centrifuge (Eppendorf, Germany).

After centrifugation, the supernatant was removed through suction, and the cells were resuspended in 10 ml DMEM medium containing 10% DBS, 50 mM HEPES (Merck, Cat. No. 110110.0250) pH7.8 and rhodamine 123 (Rh123) (Sigma, Austria) at a final concentration of 0.2 µg/ml (0.53 µmol/L). The cell suspension was incubated for 30 minutes using a gently shaking water bath at 37 °C, resulting in a steady state of rhodamine 123 accumulation. After incubation, the tube was chilled on ice water and 9 ml of its content aliquoted and transferred to 9 FACS tubes (Becton Dickinson, Cat. No. 352052). These tubes were centrifuged for 6 minutes at 1,100 rpm at 4 °C in an Eppendorf 5415C Centrifuge (Eppendorf, Hamburg, Germany) and washed once with 1 ml ice cold DMEM medium to remove extracellular fluorochrome. The tubes were centrifuged and the supernatant removed as described before. The cell pellets were resuspended in 900 µl DMEM medium containing either no modulator or modulator at various concentrations ranging from 164 nM to 100 µM (1:2.5 serial dilutions) depending on solubility and the expected potency for the modifier. The DMEM medium was prewarmed at 37 °C in a water bath. The time dependent decrease in cellular mean fluorescence was determined in the presence of eight serial diluted concentrations (1:2.5) for the GPV01 modulator. After 90, 180, 270 and 360 seconds, aliquots (200 µl) of the incubation mixture were transferred to tubes containing an equal volume of ice-cold stop solution

(DMEM medium containing GPV31 at a final concentration of 10 µM). Samples were kept in an ice water bath until the measurement was performed within 1 hour with a Becton Dickinson FACSCalibur flow cytometer (Becton Dickinson, Vienna, Austria). Viable cells were gated on the basis of forward and side scatter (Chiba, Ecker et al. 1996). To determine the mean fluorescence values the excitation and emission wavelengths were 488 nm and 534 nm, respectively and five thousand gated events were accumulated (Chiba, Ecker et al. 1996).

3.13.2 Daunomycin steady state studies

HEK 293 cells were cultured in DMEM medium containing 10% DBS and in the absence of hygromycin B. Cells were trypsinized for 2-3 min at room temperature and the reaction was stopped by addition of DMEM medium containing 10% DBS. Cells were transferred to a 50 ml Falcon tube, counted, and approximately 2 x 10^6 cells were pelleted for 6 minutes at 1,100 rpm at 4 °C in an Eppendorf 5403 Centrifuge (Eppendorf, Germany).

After centrifugation, the supernatant was removed through suction, and the cells were resuspended in 10 ml DMEM medium containing 10% DBS, 50 mM HEPES, pH7.8 and daunomycin (Sigma-Aldrich, Cat. No. D8809) at a final concentration of 3 µM. 10 µl DMSO and different inhibitor concentrations were added to 990 µl aliquots of the mixture depending on the expected potency of the compounds. Tubes containing these aliquotes were incubated for 30 minutes using a gently shaking water bath at 37 °C. During this time every single tube was spun with a vortex for optimal agitation. After incubation the cells were chilled on ice, pelleted, washed once with 1 ml ice-cold DMEM medium containing 10% DBS. Cells were again pelleted and resuspended in 200 µl ice-cold stop solution (DMEM medium containing GPV31 at a final concentration of 5 µM). Samples were kept in an ice water bath until the measurement was performed. The prodecure is the same as before in section 3.13.1.

3.13.3 Cytotoxicity of rhodamine 123 in FlpIn NIH 3T3 cells

Cells (5 x 10^5) of each respective stable cell line were seeded into a 25-cm^2 tissue culture flask without hygromycin B. After 48 hours, the medium was removed by suction from the subconfluent tissue culture flask, washed with 5ml PBS and trypsinized with 1 ml of trypsin (Gibco) for 2-3 min (checked under microscope) at room temperature. The

reaction was stopped by addition of 13 ml DMEM/20%DBS and the cells were transferred to a 100 ml tissue culture glass flask with 56 ml of medium (this means 1:5 split from confluency). The cells were counted for 0 time points and seeded into 24 well plates (1 ml/well) in dupilcates for each day of a 3-day growth study. After 1 hour 1 ml of medium with varying concentrations of rhodamine 123 in ddH_2O and lacking DBS was added into each well, resulting in a 1:2 serial dilution of rhodmamine 123 ranging from 2.34 mM to 150 mM. The first well was left without rhodamine 123 addition. Every 24 hours after the initial seed, the cell number from each plate was determined with a Casy cell counter (Innovatis AG, Germany). The medium was removed from the 24-well plate by suction, washed with 1ml of PBS and trypsinized with 100µl of trypsin solution. The reaction was then stopped by addition of 120µl of medium and the total volume (220µl) was transferred to a count vial containing ~9.8ml of counter fluid and counted with a Casy cell counter to measure the number of surviving cells. During the study, the growth medium was not changed.

3.13.4 Determination of first order rate constant (FORC) and IC_{50} values of modulators

Rhodamine 123 zero trans efflux

Cells were loaded with fluorescent substrate and efflux was determined in absence and presence of different inhibitor concentrations. At time point zero the extracellular concentration of the fluorochrome was zero and the intracellular concentration was high as compared to the extracellular concentration during the whole experiment. The effluxed fluorescent substrate did not reenter to any significant extent. Initial efflux in the zero trans efflux experiments was calculated from the time dependent exponential decrease in mean fluorescence by nonlinear regression analysis using least squares. First order rate constants (V_{max}/K_m) were calculated for each experiment. Dose response curves of modifier concentrations were calculated as the independent variable versus first order rate constants and were fitted according to follow equation:

$$v = \frac{V_{max} - ME \times c^n}{(IC_{50}{}^n + c^n)}$$

v	first order rate constant as a function of modulator concentration
V_{max}	the initial rate of efflux observed in the cell line in the absence of a modulator
ME	modulator efficacy
c	the modifier concentration
n	Hill coefficient

IC_{50} values of modulators were calculated from the dose response curves of the first order rate constant versus the modifier concentration. The IC_{50} value is the concentration of the modulator yielding a half-maximal effect.

Daunomycin steady state

In contrast, the steady state protocol evaluates steady state levels of fluorochrome inside the cell at different concentrations of pump inhibitors. The extracellular concentration is higher than the intracellular concentration and the fluorescent substrate enters the cells by diffusion along the concentration gradient. Two processes occur simultaneously: the transporter pumps solutes to the extracellular side and a concentration gradient dependent diffusion of substrate occurs at the same time. Therefore, the steady state accumulation levels of fluorochrome are a function of the pump activity and of diffusion rates of the compounds.

In steady state experiments the mean fluorescence units of the starting inhibitor concentration were calculated with the following equation:

$$MFU_{c0} = \frac{MFU_{c0} + MFU_{cinf\,-c0} \times [S]^n}{(IC_{50}{}^n + [S]^n)}$$

MFU_{C0}	Mean fluorescence unit of starting inhibitor concentration
$MFU_{Cinf\,-\,C0}$	Mean fluorescence unit of inhibitor concentration after 30 minutes minus starting concentration

[S]	Substrate concentration
n	Hill coefficient

For comparing IC_{50} values of the steady state assay with those of the zero trans efflux experiment it was multiplied with the quotient C_0/C_{inf} (beginning concentration divided through end concentration) (Stein 1997).

3.13.5 Flow cytometer

Flow cytometry was performed using a FACSCalibur flow cytometer (Becton Dickinson, Vienna, Austria). FACS flow sheath fluid (Cat. No. 342003) and 5 ml polypropylene FACS tubes (Cat. No. 352052) were purchased from BDBiosciences.

Cells were cooled in an ice water bath and measured within 1 hour. Every tube after another was measured.

It is possible to measure straylight and fluorescent signals with a flow cytometer. An argon-ion laser detects the single cells by forward scattered light (FSC) which is a measure for cell size and side scattered light (SCC) which stands in relation to cell structure (granularity of cells). Cells were shown in a correlated two-parameter dot plot: FSC against SSC.

Cell data were evaluated after measurement, the viable population was differentiated from dead cells with an automatic attractor (BD-software package of BD flow cytometry). To determine the mean fluorescence values five thousand gated events were accumulated. The cell population could be more differentiated from other cells with a subattractor inside of the first gate.

4 Results

4.1 Motivation for selection of mutated residues

4.1.1 Which residues at the TMDs interfaces should be mutated?

The high resolution structure of the Sav1866 transporter has a twisted topology. Evidence for an analogous architecture of P-glycoprotein was presented by the group of Kenneth Linton in 2007 (Zolnerciks, Wooding et al. 2007). Using cross-linking analysis, the authors showed that the intracellular loop (ICL) 4 within TMD2 forms an interface with NBD1 of P-gp. In earlier studies by Loo and Clarke (Loo, Bartlett et al. 2004) and Stenham et al (Stenham, Campbell et al. 2003) in Linton's group cysteines were introduced into both the extracellular end of transmembrane segments 2 and 11. These data showed that transmembrane helix 2 is close to transmembrane helix 11. Likewise, transmembrane helix 5 was shown to be close to transmembrane helix 8 (Stenham, Campbell et al. 2003; Loo, Bartlett et al. 2004). The equivalent transmembrane helices in the Sav1866 structure, helices 2, 5' and 2', 5 of the monomers, corresponding to helices 5/8 and 2/11 in P-gp, form the contact interfaces between the two TMDs. In addition, site directed mutagenesis studies by the group of David Clarke indicated that residues lining these interfaces impair the ability of the transporter to function properly when mutated to cysteines (Loo and Clarke 2005). Most of these residues cannot be protected by substrates from reacting with MTS-coupled verapamil or rhodamine 123.

Alignments of the N- and C-terminal half of P-gp indicate two conserved glutamine residues which are predicted to be located in predicted transmembrane segments 2 and 8 (Figure 4.1). Q132 in the N-terminal half and Q773 in the C-terminal half align. These two residues are the only non-glycine residues which are conserved between TM helices 2 and 8 (Figure 4.1).

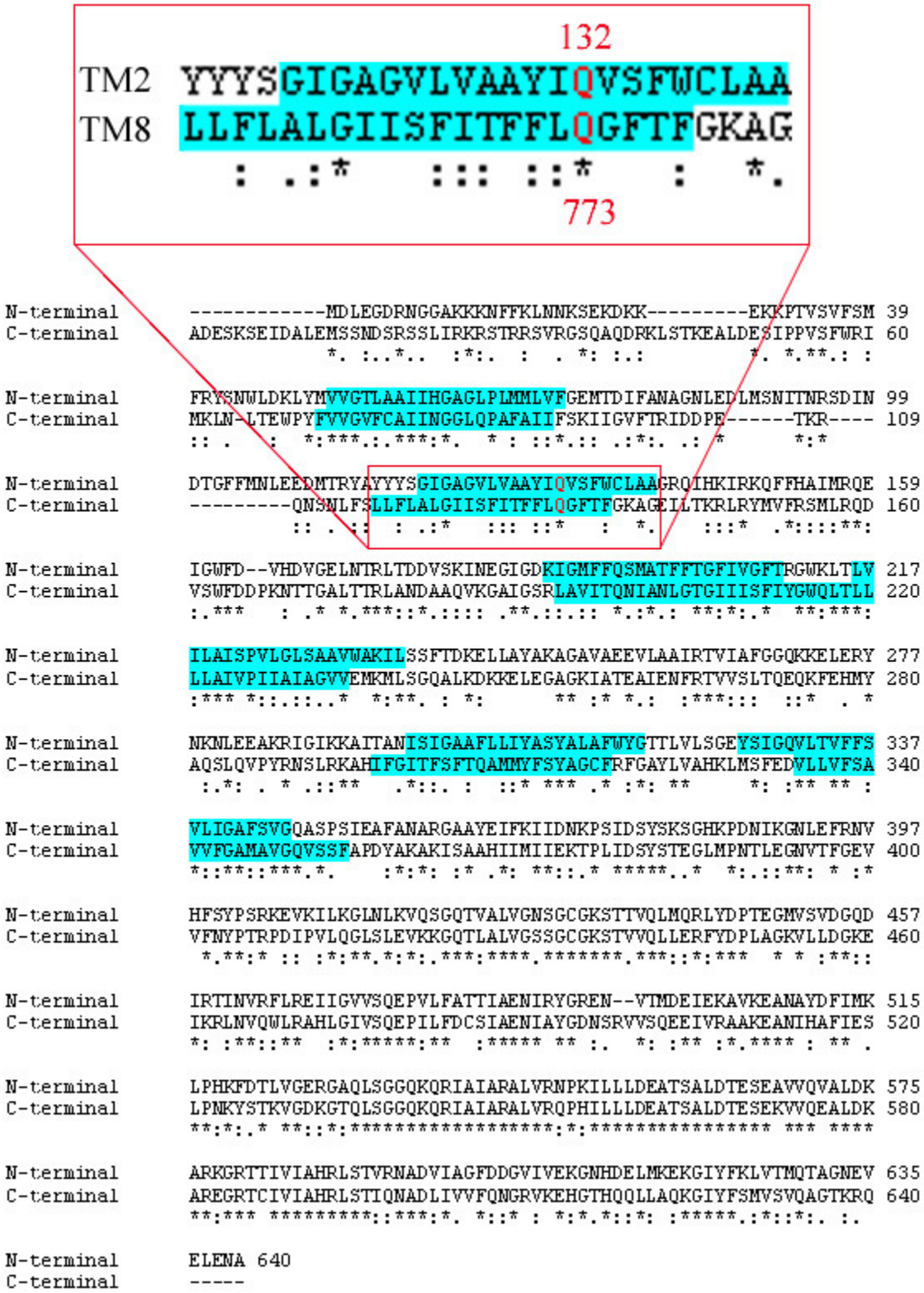

Figure 4.1: Sequence alignments of the N- and C-terminal half of P-gp using Clustal 2.0.8 multiple sequence alignment. The transmembrane segments are highlighted in turquoise. Glutamine residues which were mutated in this study are shown in red. For easier orientation, a partial sequence alignment of TMs 2 and 8 is shown above the alignment.

A total of 9 glutamine residues are found in predicted TM segments. Our homology model of P-gp suggests two of these glutamine residues to be located in between most highly photolabelled residues M197 and F951 (Q132) at the TM3/11 interface and A311 and T769 (Q773) at the TM5/8 interface. In addition, these residues are capable of forming H-bonds with solutes/inhibitors and are predicted in docking experiments to be involved in solute interaction.

4.1.2 Which mutants should be generated?

The next question was which mutants should be generated at the positions 132 and 773 to yield fully functional transporters?

To estimate the relative evolutionary pressure on residues in P-gp, our group used a method originally published in 2004 by Mihalek et al. (Mihalek, Res et al. 2004) . It is helpful to have an estimate of the relative importance of residues as a guide when a protein is intended to be mutated. When exploring the mutational space of nature a high number of correctly targeted and functional transporters is expected to be obtained. Determination of sequence variation which is based on multiple sequence alignments (MSAs) using the real valued evolutionary trace (rvET) was performed by Ivana Mihalek. The conservation patterns show that these two glutamine residues are not conserved among P-gps of all species. At least one of these glutamines, however is conserved in P-gps of species ranging from bacteria to humans. Glutamine residues are uncharged polar residues, which were replaced by nonpolar alanine residues, a positively charged arginine or a negatively charged glutamic acid, individually or in combination. MSAs indicated that a charge might be tolerated in this position of the protein. In this study, the influence of replacement of glutamine by positively or negatively charged or by uncharged amino acid residues was investigated in order to characterize their possible role in the transport process.

Importantly, a number of residues which had been identified as being critically involved in rhodamine 123 and verapamil binding, are located in vicinity of these residues in protein homology models of P-gp.

4.2 Generation of expression vectors

In this study the site directed mutagenesis experiments were guided by the mutational space explored and delineated by nature. We have created a series of constructs to be

able to express mutants of P-gp. Q123 and Q773 were mutated to glutamic acid, arginine and alanine, individually or in combination. Mutants were generated in the wt and in the G185V background in the entry vector using overlap extension PCR. After site directed mutagenesis, the pEF5 vector encoding for P-gp or P-gp mutants were generated via LR recombination reaction.

G185V background	Wildtype background
Q132A	Q132A
Q773A	Q773A
Q132A/Q773A	Q132A/Q773A
Q132E	
Q773E	Q773E
Q132E/Q773E	
Q132R	
Q773R	Q773R
Q132R/Q773R	

Table 4.1. Constructs of P-gp mutants.

It was expected that a replacement leads to altered substrate binding and transport, which can be analysed by efflux assays of diverse substrates.

4.3 Creation of stable cell lines expressing P-gp mutants

To determine potential effects of the expression of Q132 and Q773 mutants, we carried out stable transfection in FlpIn HEK 293 and mouse FlpIn NIH 3T3 cell lines expressing the wt or mutant form of P-gp by using the vector pEF5.

Expression and function of P-gp in FlpIn HEK 293 cells

Stable transfectants were obtained by selection in 200 μg/ml hygromycin B and surviving clones were screened by flow cytometry using the MRK16 antibody, which detects P-gp on the cell surface recognizing an external epitope. We started with the transfection of HEK 293 cells with the vectors pEF5MDR1H6G185V and pEF5 as control. The P-gp G185V mutant was first isolated from highly colchicine-resistant cell lines (Choi, Chen et al. 1988). Cells expressing G185V P-gp had a decreased rate of colchicine uptake when compared to cells with wild-type P-gp (Omote, Figler et al. 2004). It has

been shown that this mutation is responsible for high colchicine resistance. In addition, the G185V mutation near transmembrane domain 3 of human P-gp confers an increased resistance to etoposide and doxorubicin but a decreased resistance to vinblastine, Taxol and actinomycin D (Ruth, Stein et al. 2001).

To estimate the amount of non-specific binding of mouse monoclonal antibodies to human cell-surface antigens a mouse IgG2a antibody was used as fluorescence control. This antibody reacts specifically with keyhole limpet hemocyanin (KLH), an antigen not expressed on human cells or human cell lines (BectonDickinson). The P-gp overexpressing human T-lymphoblast cell line CCRF-CEM VCR 1000, provided by V. Gekeler (Byk Gulden, Konstanz, Germany), served as a positive control and mock transfected cells served as the negative control. The CCRFvcr 1000 cell line has been characterized previously (Gekeler, Weger et al. 1990; Gekeler, Frese et al. 1992; Chiba, Ecker et al. 1996). Using goat anti-mouse Ig FITC (GAM Ig FITC) resulting mean fluorescence units (MFU) were measured by flow cytometry (Figure 4.2: MRK16 and IgG2a staining. Red bars refer to cells incubated with MRK16 and blue bars to those incubated with IgG2a control antibody.).

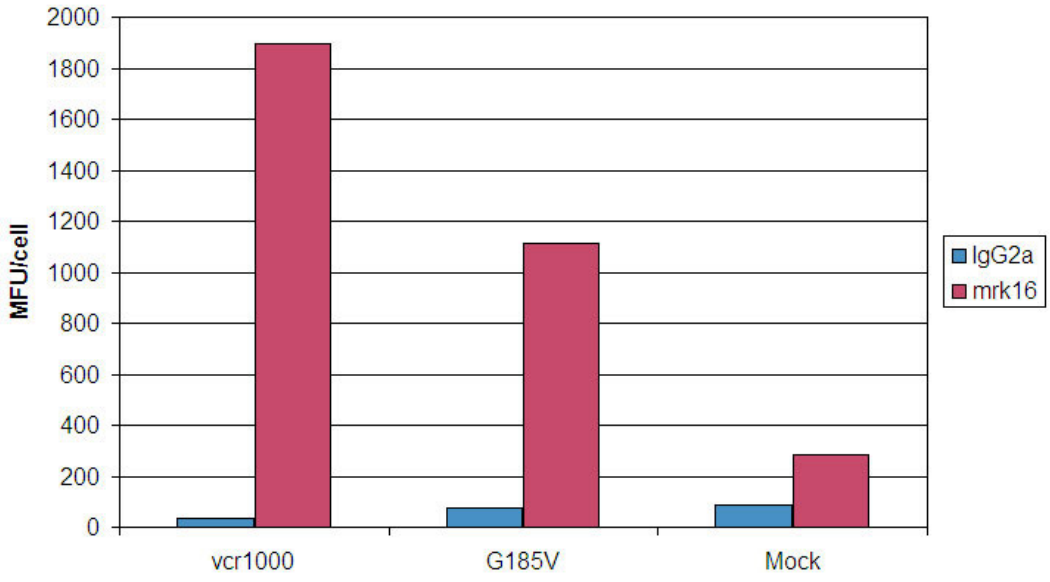

Figure 4.2: MRK16 and IgG2a staining. T-lymphoblast cell line CCRF-CEM VCR 1000 (vcr1000), HEK 293 cells transfected with G185V P-gp (G185V) and mock transfected HEK 293 cells (Mock) are shown. Red boxes are cells incubated with MRK16 and blue boxes are cells incubated with IgG2a as control.

To test the pump activity of the transfected cell lines, steady state experiments were performed. The pump activity of G185V P-gp was compared to mock transfected cells. In this protocol inhibitor and fluorochrome are added simultaneously and a steady state is reached after 30 minutes. In addition, inhibition of the pump increases intracellular

fluorochrome levels and therefore the pump activity. An example of such an experiment is given in Figure 4.3: Daunomycin steady state experiments with HEK 293 cells. By measuring cellular mean fluorescence units (MFU) in the absence and presence of 8 different concentrations of the propafenone analogue GPV31, IC_{50} values were calculated using a hyperbolic curve fit. Left: HEK 293 cells transfected with G185V P-gp. Right: Mock transfected HEK 293 cells. The IC_{50} value for G185V P-gp was 0.21 µM.

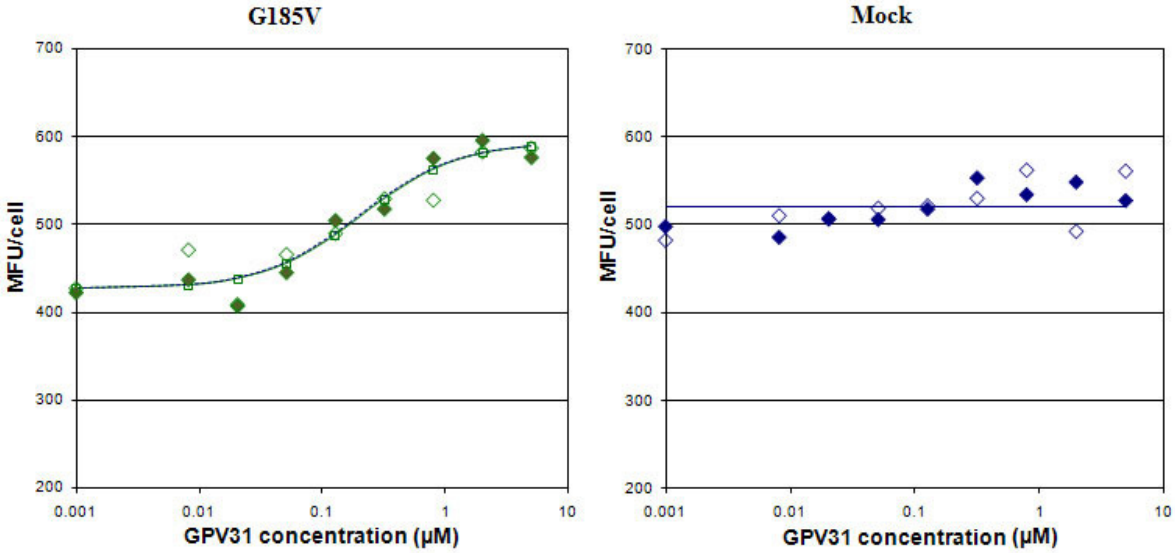

Figure 4.3: Daunomycin steady state experiments with HEK 293 cells. By measuring cellular mean fluorescence units (MFU) in the absence and presence of 8 different concentrations of the propafenone analogue GPV31, IC_{50} values were calculated using a hyperbolic curve fit. Left: HEK 293 cells transfected with G185V P-gp. Right: Mock transfected HEK 293 cells.

The P-gp clone positive for the G185V mutation was expanded for further study. We tested different compounds as inhibitors and compared the pump activity between G185V and mock transfected cells. The propafenone analogues which were used have different lipophilicity. Lipophilicity (calculated logP) is a main determinant for biologic activity of the compounds with respect to MDR inhibition (Chiba, Ecker et al. 1996; Schmid, Staudacher et al. 2003). LogP values of the compounds were calculated based on the incremental method described by Ghose et al. (Ghose and Crippen 1987). Highly lipophilic compounds have high potency ($1/IC_{50}$ values) because in the membrane, the site of pharmacological action, lipophilic compounds accumulate. IC_{50} values for G185V P-gp expressing HEK 293 cells were determined by daunomycin steady state experiments using different propafenone analogues. Results are summarized in Table 4.3. To compare IC_{50} values of the steady state assay with those of the zero trans efflux experiment they were multiplied with the quotient C_0/C_{inf} (accumulation at an inhibitor concentration of zero divided by accumulation rate at infinite concentration of inhibitor

(Stein 1997). In the example illustrated in Figure 4.3 the apparent IC_{50} value of the propafenone analogue GPV31 was 0.21 µM. To compare it with the IC_{50} value obtained in the zero trans efflux protocol it was multiplied by 0.718 (426.7 MFU/594.1 MFU). The corrected IC_{50} value was 0.15 µM. The rational for correction of IC_{50} values obtained in the steady state protocol is that any inhibition of the transporter results in an increase of the intracellular concentration of solute and thus an increased pump rate. This partially antagonizes the inhibition leading to observed IC_{50} which are higher than actual values. For the theory behind the correction term specified above the reader is referred to the work of Stein et al.

Modulator	logP	IC50 VCR 1000	IC50 HEK 293	log(1/ IC50) VCR 1000	log(1/ IC50) HEK 293
GPV01	3.39	0.33	1.27	0.48	-0.10
GPV02	3.62	0.91	2.25	0.04	-0.35
GPV05	3.67	0.59	0.45	0.23	0.35
GPV09	4.25	0.38	0.32	0.42	0.50
GPV12	2.07	14.30	284.68	-1.16	-2.45
GPV27	5.26	0.03	0.07	1.55	1.17
GPV31	4.93	0.08	0.15	1.08	0.83
GPV46	0.94	222.00	100.93	-2.35	-2.00
GPV48	2.94	2.48	3.37	-0.39	-0.53
GPV51	3.26	2.32	1.92	-0.37	-0.28
GPV57	2.54	3.67	6.59	-0.56	-0.82
GPV62	3.98	0.06	0.09	1.24	1.04
GPV90	4.3	0.37	2.77	0.44	-0.44
GPV163	4.52	1.74	2.57	-0.24	-0.41
GPV164	4.88	0.66	0.32	0.18	0.50
GPV181	6.16	0.80	0.43	0.10	0.37
GPV240	4.23	6.47	30.47	-0.81	-1.48
GPV317	3.62	0.24	0.26	0.62	0.59
GPV319	4.57	0.31	0.32	0.51	0.41
GPV323	1.73	1.96	8.03	-0.29	-0.90
GPV381	2.38	1.17	1.08	-0.07	-0.03
GPV570	3.4	29.50	43.25	-1.47	-1.64
GPV576	5.8	0.01	0.09	2.25	1.06
GPV703	5.59	0.09	0.16	1.07	0.80

Table 4.2: All used compounds listed with their calculated lipophilicity, IC_{50} values and log(1/IC_{50}) of G185V P-gp expressed in HEK 293 cells and wt-P-gp in CCRFvcr 1000 cells.

In a comparison of 24 compounds, the modulator log potency (log(1/IC_{50}) values) obtained in these steady state experiments of G185V P-gp HEK 293 cell line correlated well with those obtained in the daunomycin zero trans efflux studies performed in CCRFvcr 1000 cells (Figure 4.6).

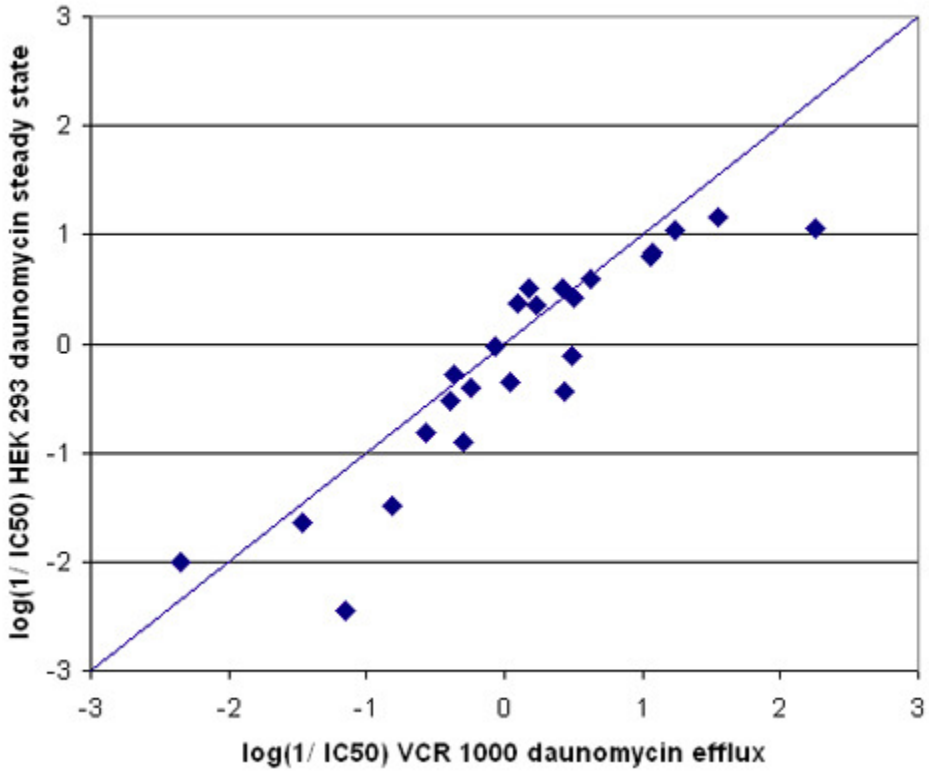

Figure 4.4: Correlation between log potency values obtained for HEK 293 cell containing G185V P-gp line in daunomycin steady state experiments and log potency values for the P-gp overexpressing human T-lymphoblast cell line CCRF-CEM VCR 1000 as determined by a zero trans efflux protocol. Results for a set of propafenone analogues are shown. The propafenone analogs are located close to the solid line which represents the ideal 1:1 correlation. Data points represent the mean of at least duplicate determinations.

Mock transfected cells served as negative control and the effect of propafenone ananlogues observed in these cells was negligible for most compounds. An important observation however, was that the mock transfected cells did sometimes show some pump activity because of endogenously expressed human wt P-gp. In the representative experiment for compound GPV31 shown in Figure 4.3, the highest loading level at the highest compound concentration was 600 MFU/cell for G185V P-gp and 550 MFU/cell for mock transfected cells. To overcome the human endogenous P-gp expression in HEK 293 cells, we switched to the NIH 3T3 mouse cell line which is also compatible with the Flp-In system but expressing very much lower endogenous P-gp levels.

Expression and functional characterization of P-gp in FlpIn3T3 cells

Mutated membrane proteins with impaired folding often fail to reach the plasma membrane (Loo, Bartlett et al. 2005). They are retained in an inactive form in the endoplasmic reticulum (ER) by the cell's quality control mechanism and are rapidly degraded (Pind, Riordan et al. 1994; Chen, Bartlett et al. 2000; Loo, Bartlett et al. 2005). In publi-

cations of Loo and Clarke a majority of mutants showed correct targeting to the plasma membrane in the presence of the pharmacological chaperone cyclosporine A (CsA). In order to correct the trafficking deficiency of mutant P-gp and study the transporter functionally, the P-gp mutants were grown in the presence of 10 µM CsA as previously suggested by Loo, Bartlett and Clarke. In fact, the P-gp expression level was higher in the presence of CsA which is shown in Figure 4.5 for the example of the G185V, G185V-Q132R/Q773R P-gp. We tested two different incubation times for 10 µM CsA. However, incubation for 24 hours could rescue the double R mutant and increase the expression level of G185V P-gp. The mock transfected cells only showed a small stimulation. After 48 hours, the effect diminished except for the double R mutant in which it was identical.

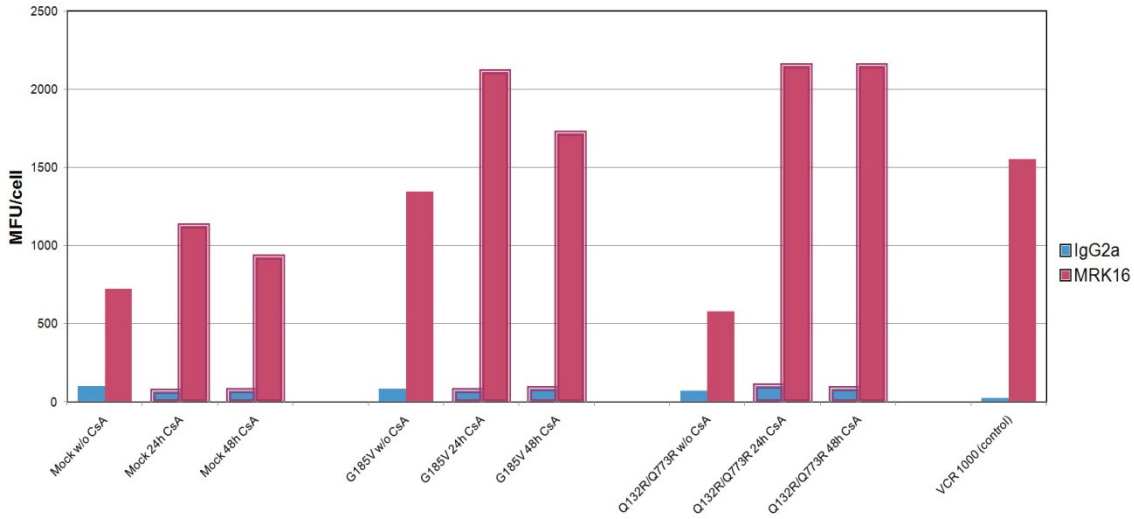

Figure 4.5: MRK16 and IgG2a staining. Red boxes are cells incubated with MRK16 and blue boxes are cells incubated with IgG2a as control.

4.4 Characterization of P-gp expression at the protein level

We investigated whether CsA could influence the P-gp expression level. For this purpose, we performed Western blot analysis with the specific monoclonal C219 antibody which recognizes a highly conserved amino acid sequence found in the nucleotide binding domain of P-gp. We observed a significant increase of all P-gp mutant proteins in NIH 3T3 cells, which were preincubated with 10 µM CsA for 24 hours at 37°C. Control cells were incubated with DMSO only. The C219 antibody also recognized the mouse P-gp but the difference between mock transfected cells was negligible (Figure 4.6).

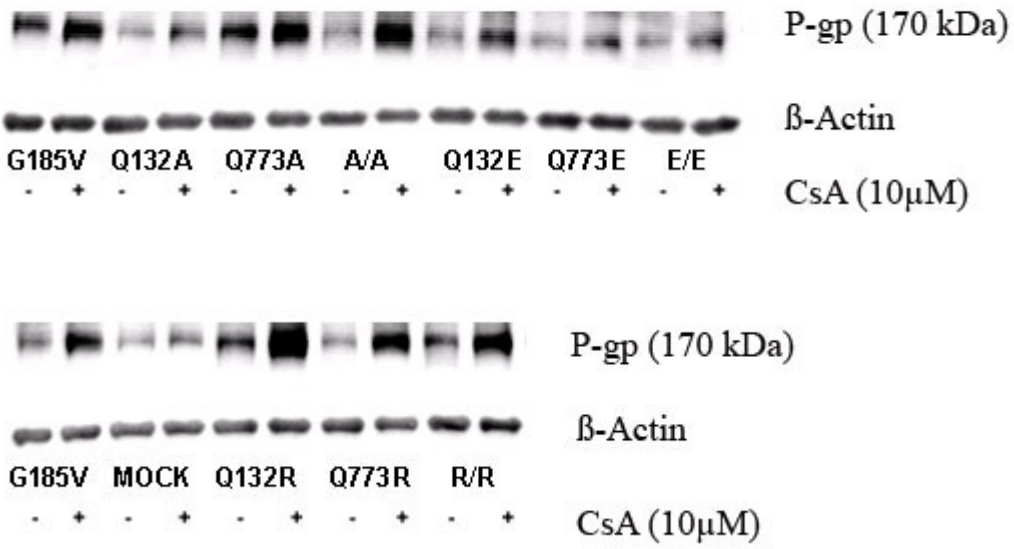

Figure 4.6: Effect of CsA on maturation of P-gp mutants. NIH3T3 cells expressing mutants were preincubated with 10 µM CsA (+) or DM SO only (-) for 24 hours at 37°C. Equivalent amounts of whole cell SDS extracts were then subjected to SDS-PAGE and Western blot analysis with the monoclonal anti-P-glycoprotein antibody C219. The positions of the mature form (170 kDa) of P-gp mutants are indicated.

4.5 Effect of CsA on mRNA level

SYBR green real-time reverse transcription PCR was used to asses the influence of CsA on mRNA level. The mouse hypoxanthine-guanine phosphoribosyltransferase (HPRT) gene was used to normalise mRNA levels between different samples. CsA had no effect on mRNA level (Figure 4.7).

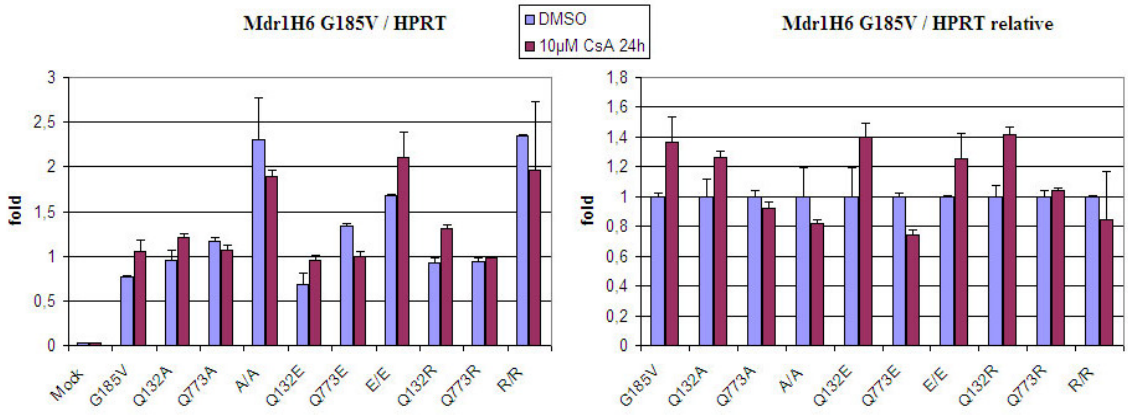

Figure 4.7: SYBR green real-time RT-PCR analysis of P-gp mutants. Total RNA isolated from P-gp mutants NIH 3T3 cells was reverse transcribed, and PCR was performed with primers specific for cDNA of the *MDR1* gene. Red boxes refer to cells incubated with 10 µM CsA for 24 hours and blue boxes refer to cells incubated with the solvent DMSO as control. Left: Gene expression levels were normalized to HPRT levels and shown as expression levels of P-gp mutants relative to those of the control. Right: Gene expression levels were normalized to HPRT levels and shown as expression levels of P-gp mutants relative to those of the control (arbitrarily set to 1).

4.6 Pharmacological chaperones

We tested whether mutations introduced in TM segments 2 and 8 (forming part of the drug binding pocket) inhibit maturation of the protein. The presence of P-gp and P-gp mutant protein in HEK 293 and NIH 3T3 cells was detected by surface protein expression analysis using the selective monoclonal antibody MRK16 and the goat anti mouse FITC-labelled secondary antibody. The fluorescence intensity of some P-gp mutants was comparable to the background fluorescence intensity, thus the level of P-gp expression was negligible. Pharmacological chaperones such as cyclosporin A and verapamil are predicted to promote maturation of P-gp processing mutants.

4.6.1 Surface expression of P-gp in FlpIn NIH 3T3 fibroblasts

We tried different compounds as pharmacological chaperones, for example CsA, verapamil and GPV51. These tests are useful, especially in terms of optimization of concentration of substrates. Thus, the first step was to compare various concentration of the propafenone analogue GPV51 for the efficiency in promoting maturation of P-gp. For this, cells were incubated in the absence or presence of 10 different concentrations ranging from 1.17 to 300 μM (1:2 serial dilution) of GPV51 for 24 hours to optimize the tolerable dosage of GPV51 to act as a pharmacological chaperone. Additionally, cyclosporin A at a concentration of 10 μM was used as a control. After a 24 hour incubation, the distribution pattern of the protein expression level was determined by immunocytochemical staining using the monoclonal antibody MRK16 as described above. Figure 4.50 - Figure 4.54 represent the mean of two independently performed experiments. The arginine mutants were tested due to the comparability of the G185V-Q773R and G185V-Q132R/Q773R mutants' expression levels to those of the mock transfected cells. The arginine mutants were compared to G185V P-gp and mock transfected cells.
All arginine mutants showed a higher expression in the presence of CsA and GPV51 compared to the control.

The G185V P-gp and Q132R, Q773R and Q132R/Q773R P-gp mutants in the G185V background showed a concentration-dependent increase in the expression level of P-gp (Figure 4.8 - Figure 4.11). However, the mock transfected cells showed a similar pattern (see Figure 4.12). Incubation of all R mutants in the presence of GPV51 gave a similar

pattern. The propafenone analogue GPV51 was able to increase the expression level of all R mutants to a small extent (shown in Figure 4.9 - Figure 4.11).

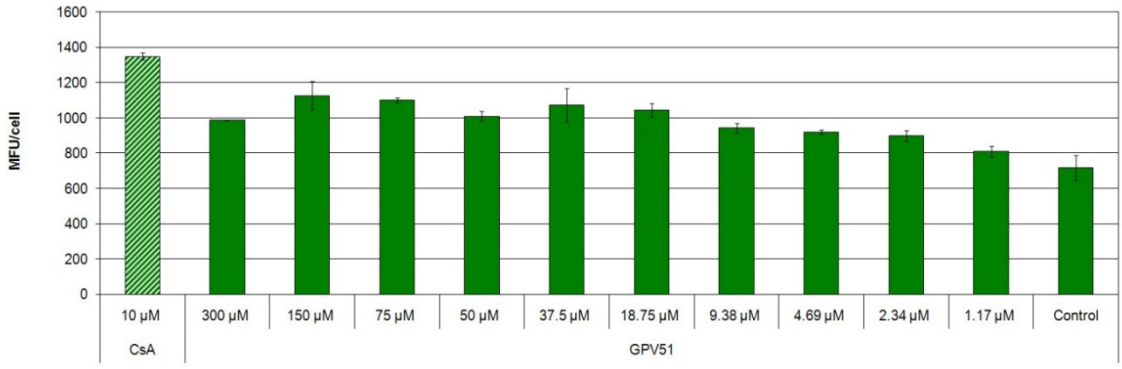

Figure 4.8: Distribution pattern of the protein expression level of G185V P-gp expressing NIH3T3 cells. In the absence and presence of 10 different concentrations of the propafenone analogue GPV51, the tolerable dosage was tested. Incubation with 10 µM CsA served as control.

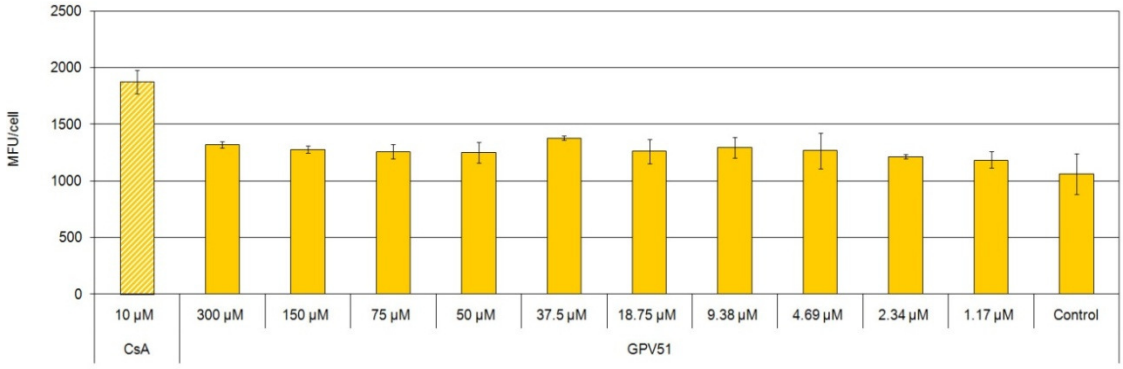

Figure 4.9: Distribution pattern of the protein expression level of G185V-Q132R P-gp expressing NIH3T3 cells. In the absence and presence of 10 different concentrations of the propafenone analogue GPV51, the tolerable dosage was tested. Incubation with 10 µM CsA served as control.

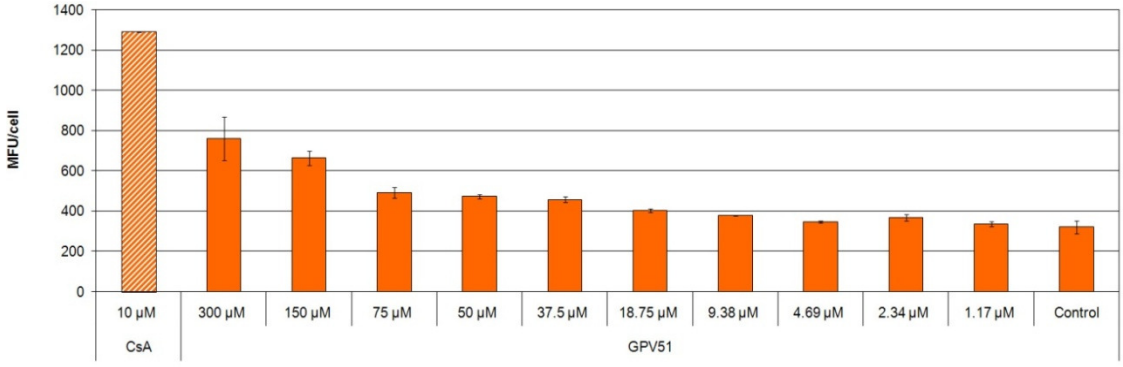

Figure 4.10: Distribution pattern of the protein expression level of G185V-Q773R P-gp expressing NIH3T3 cells. In the absence and presence of 10 different concentrations of the propafenone analogue GPV51, the tolerable dosage was tested. Incubation with 10 µM CsA served as control.

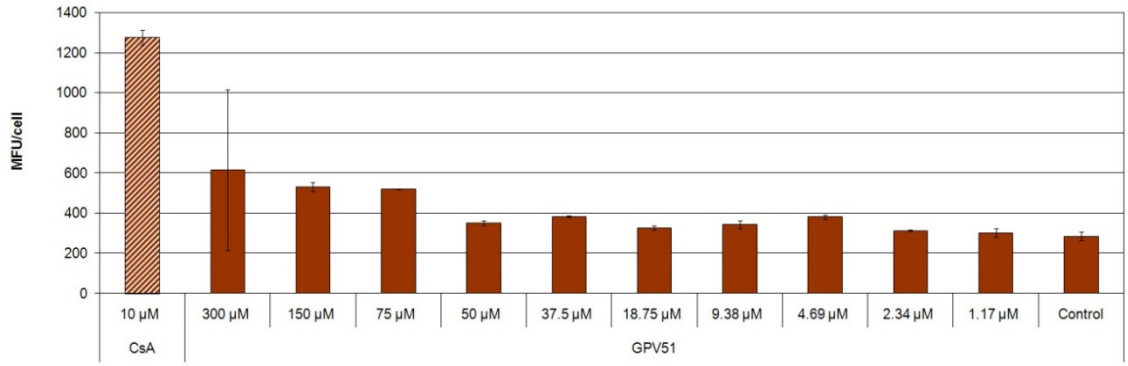

Figure 4.11: Distribution pattern of the protein expression level of G185V-Q132R/Q773R P-gp expressing NIH3T3 cells. In the absence and presence of 10 different concentrations of the propafenone analogue GPV51, the tolerable dosage was tested. Incubation with 10 µM CsA served as control.

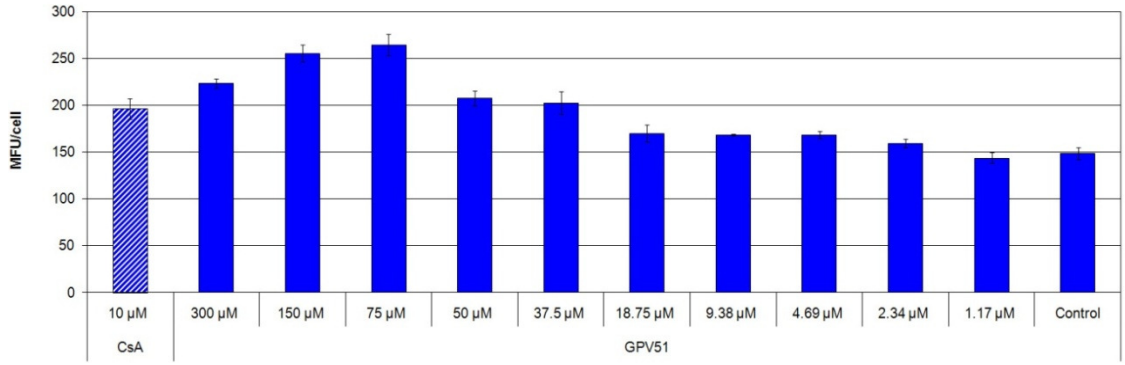

Figure 4.12: Distribution pattern of the protein expression level of mock transfected NIH3T3 cells. In the absence and presence of 10 different concentrations of the propafenone analogue GPV51, the tolerable dosage was tested. Incubation with 10 µM CsA served as control.

The expression levels of the G185V P-gp and G185V P-gps mutants are increased by a 24 hours pre-treatment with the pharmacological chaperone GPV51.

We used 50 µM GPV51 for further experiments due to the fact that a more than 20% increase in endogenous mouse P-gp expression ensued from administration of higher concentrations (shown in Figure 4.12: Control: 100%, 75 µM GPV51: 179%). At 150 and 300µM the effect was less pronounced than at 75µM.

For compounds such as cyclosporin A and verapamil which are predicted to promote maturation of P-gp processing mutants we used published concentrations: 10 µM cyclosporin A (CsA) and 50 µM verapamil (Vera).

The next step was to compare these compounds in their effect on P-gp mutants. The effect of CsA, verapamil and GPV51 on P-gp expression level was determined by immunocytochemical staining using the monoclonal antibody MRK16 as described above.

DMSO was required at a final concentration of 0.2% to prepare CsA and GPV51 stocks. Verapamil was prepared in water. Therefore 0.2% final concentration of DMSO was added to control cells and cells that were incubated with verapamil for 24 hours.

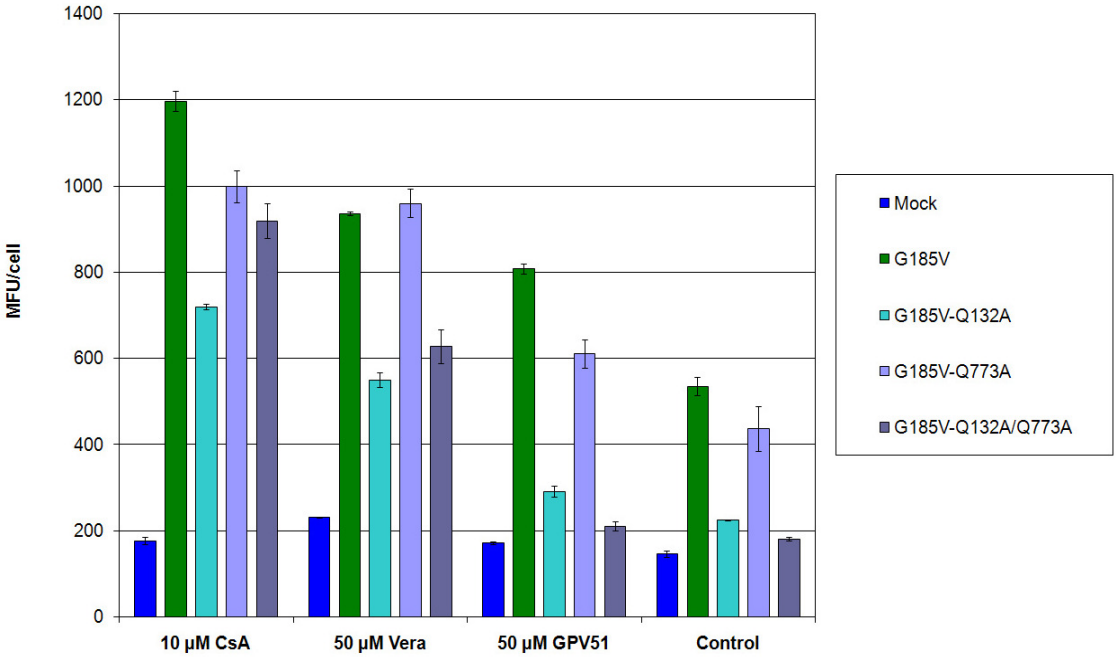

Figure 4.13: MRK16 staining of G185V P-gp, Q132A, Q773A and Q132A/Q773A P-gp mutants in the G185V background, and mock transfected NIH 3T3 cells. All cell lines were preincubated for 24 hours with 10 µM CsA, 50 µM Vera and 50 µM GPV51. Control cells were incubated with DMSO.

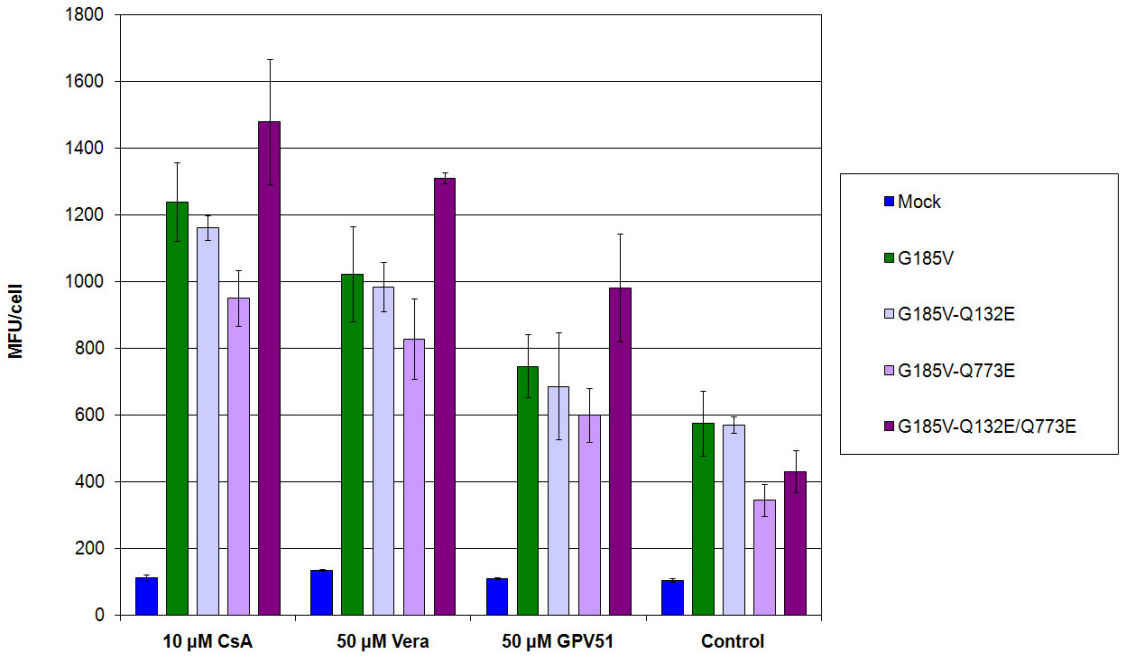

Figure 4.14: MRK16 staining of G185V P-gp, Q132E, Q773E and Q132E/Q773E P-gp mutants in G185V background, and mock transfected NIH 3T3 cells. All cell lines were preincubated for 24 hours with 10 µM CsA, 50 µM Vera and 50 µM GPV51. Control cells were incubated with DMSO.

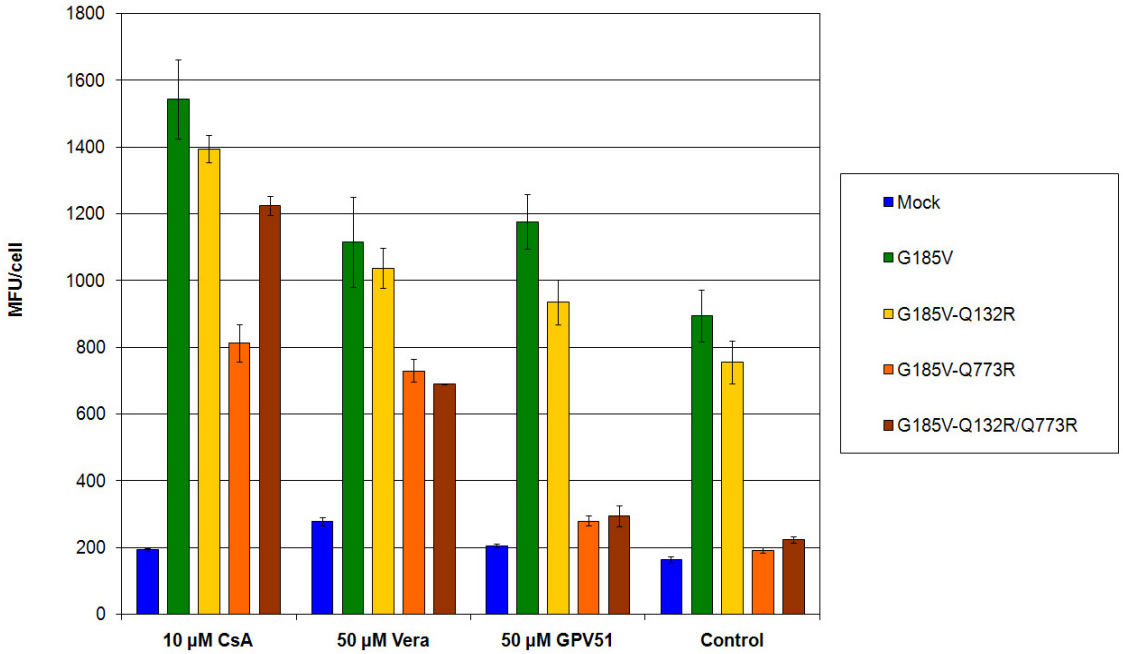

Figure 4.15: MRK16 staining of G185V P-gp, Q132R, Q773R and Q132R/Q773R P-gp mutants in G185V background, and mock transfected NIH 3T3 cells. All cell lines were preincubated for 24 hours with 10 µM CsA, 50 µM Vera and 50 µM GPV51. Control cells were incubated with DMSO.

The expression level of all mutants was increased by a 24 hours pre-incubation with CsA, verapamil and GPV51. The best effect was obtained with the chaperone CsA, followed by verapamil. The propafenone analogue GPV51 only was able to increase the expression level of all mutants to a small extent.

4.6.2 Surface expression of P-gp in FlpIn HEK 293 cells

The effect of CsA, verapamil and GPV51 on P-gp expression level also was tested in HEK 293 cells expressing G185V P-gp, G185V-Q773R and G185V-Q132R/Q773R mutants.

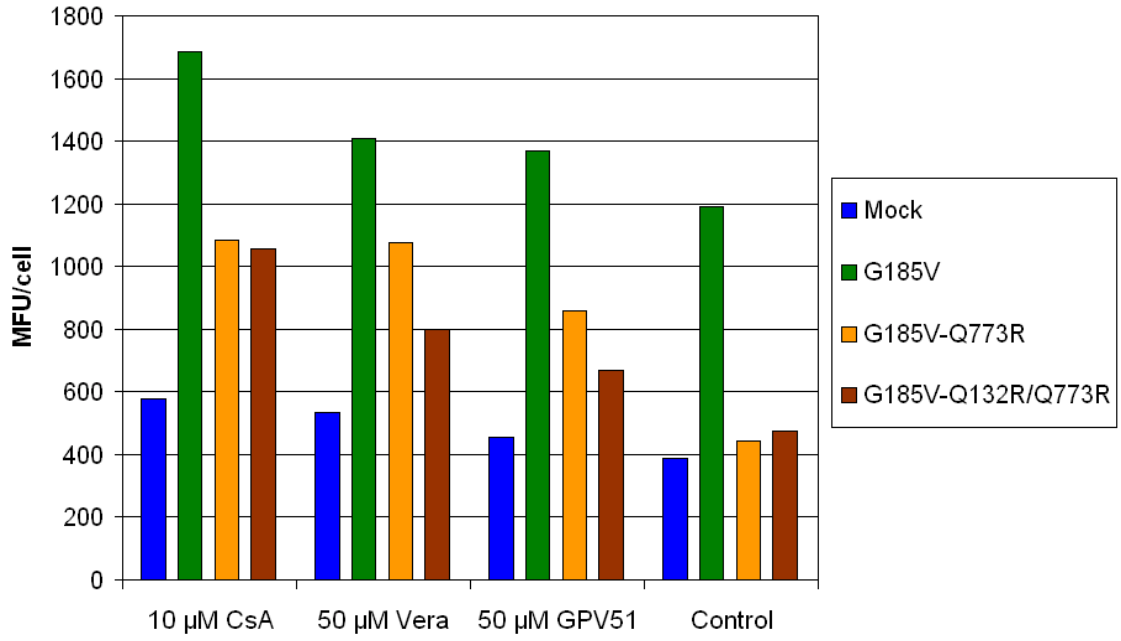

Figure 4.16: MRK16 staining of G185V P-gp, Q773R and Q132R/Q773R P-gp mutants in G185V background, and mock transfected HEK 293 cells. All cell lines were preincubated for 24 hours with 10 µM CsA, 50 µM Vera and 50 µM GPV51. Control cells were incubated with DMSO.

The mock transfected HEK 293 control cells showed a higher background expression compared to mock transfected NIH 3T3 control cells based on the human endogenous P-gp.

Apart from that, the expression pattern for the G185V P-gp, G185V-Q773R and double R mutant are similar in both human and mouse cell lines preincubated with CsA, verapamil and GPV51.

4.7 Cytotoxicity of rhodamine 123

The purpose of this experiment was to investigate the effect of rhodamine 123 on MDR and therefore the influence on cell growth in FlpIn NIH 3T3 transfected cell lines. The drug resistance of stable cells expressing MDR1 wild-type or MDR1 mutants was evaluated by measuring the cell viability after exposing them to a wide range of rhodamine 123 concentrations. The cells were incubated in the absence or presence of various concentrations ranging from 2.34 µM to 150 µM (1:2 serial dilutions) of rhodamine 123 for 24 hours, 48 hours and 72 hours. The cell number was determined with a Casy cell counter (Innovatis AG, Germany). At the beginning we compared G185V P-gp and wt P-gp. Mock transfected cells again served as negative control. All cytotoxicity experiments were performed in duplicate, using cells obtained from independent experiments. Experimental data are presented as the mean ± standard deviation (S.D.). The cells ex-

pressing G185V P-gp exhibit higher resistance to rhodamine 123, suggesting a gain of function phenotype (Figure 4.17 - Figure 4.19). The concentrations required for 50% cell death (half maximal effective concentration, IC_{50}) after 72 hours incubation for wt P-gp, G185V P-gp and mock transfected cells were 104 μM, 306.3 μM and 32.5 μM. Thus, G185V P-gp was of great interest for mutant characterization. We used this G185V "gain-of-function" mutation in all of the mutants in order to be able to study them functionally by flow cytometry using rhodamine 123 as a substrate.

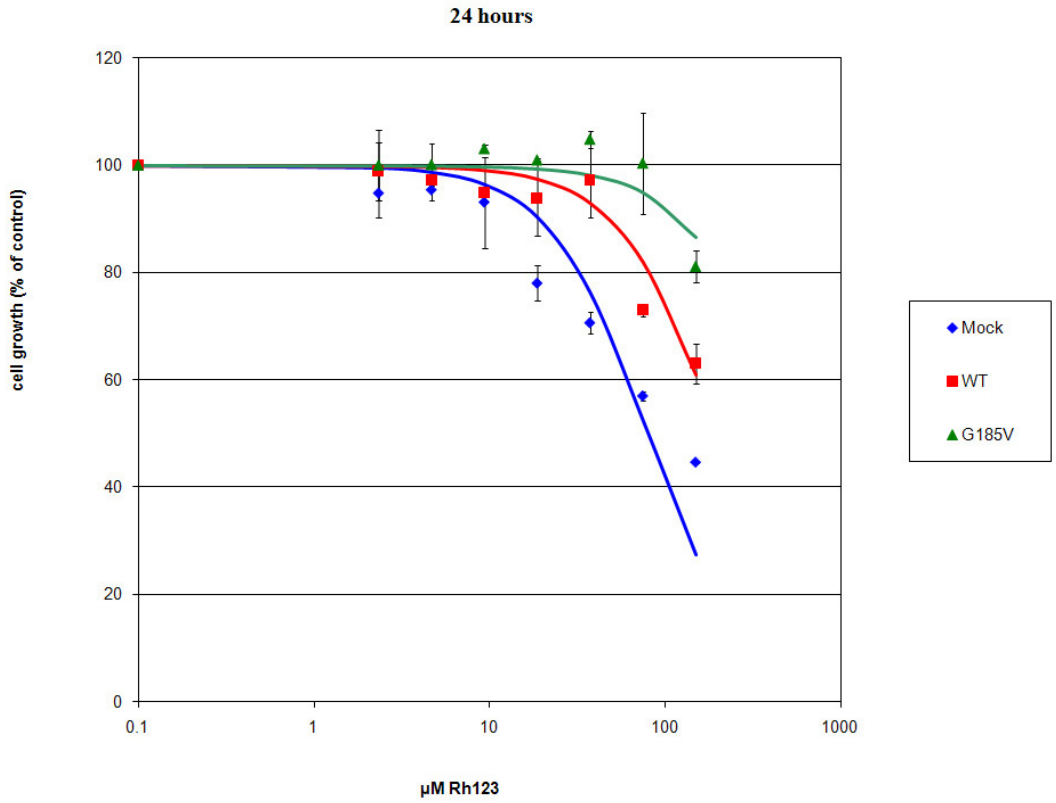

Figure 4.17: Cell growth as a percentage of control for G185V P-gp, wt P-gp and mock transfected NIH3T3 cells after 24 hours incubation with rhodamine 123 at 37°C. Each experiment was performed in duplicate.

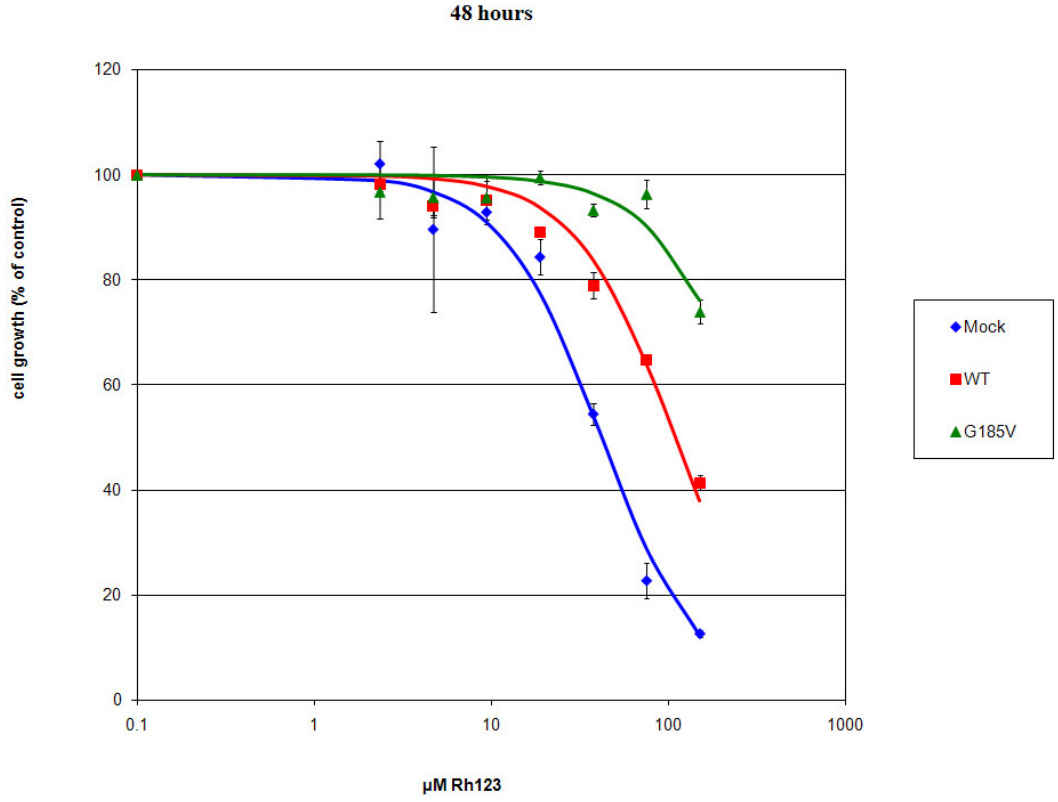

Figure 4.18: Cell growth expressed as a percentage of control for G185V P-gp, wt P-gp and mock transfected NIH3T3 cells after 48 hours incubation with rhodamine 123 at 37°C. Each experiment was performed in duplicate.

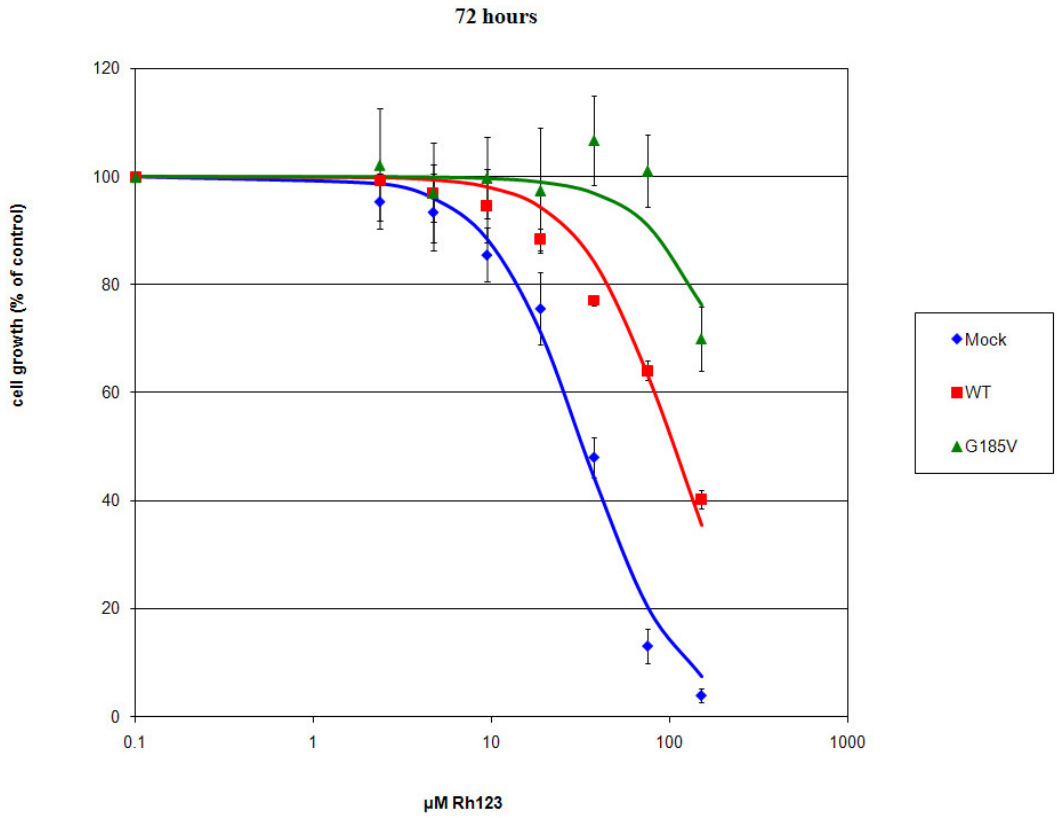

Figure 4.19: Cell growth expressed as percentage of control for G185V P-gp, wt P-gp and mock transfected NIH3T3 cells after 72 hours incubation with rhodamine 123 at 37°C. Each experiment was performed in duplicate.

All mutants were compared with G185V P-gp and mock transfected cells. Cell surface labelling of P-gp was carried out for all cell lines, in parallel with cytotoxicity experiments. These additional studies confirmed the expression of all A mutants (shown in Figure 4.20) and E mutants (shown in Figure 4.22). The R mutants showed a different expression pattern (shown in Figure 4.24). The Q773R and Q132R/Q773R had an expression level which was similar to that of mock transfected cells, i.e. did not show trafficking to the plasma membrane. The expression level was higher than in positive controls in Q132E, Q132R and Q773A mutants. Both Q773A and Q132E showed a small increase, but expression of the Q132R mutant was significantly increased.

As before, all cytotoxicity experiments were performed in duplicate using cells obtained from independent experiments with the same concentration of rhodamine 123. However, only the 72 hour time point is shown (Figure 4.21, Figure 4.23 andFigure 4.25). Experimental data are presented as the mean ± standard deviation (S.D.).

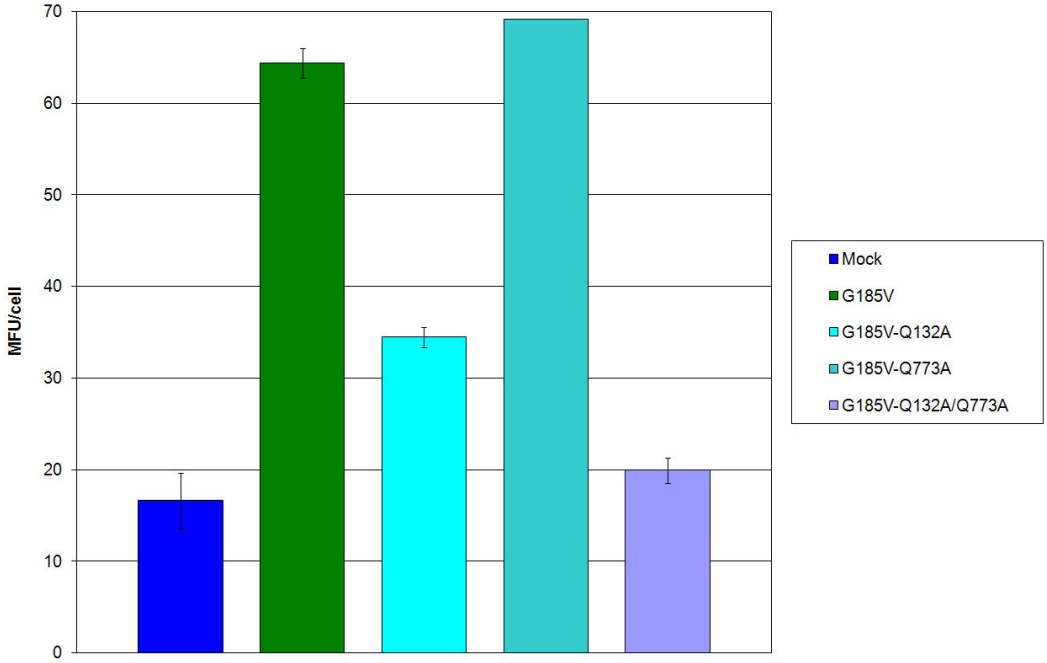

Figure 4.20: MRK16 staining of G185V P-gp, G185V A mutants and mock transfected cells. All mutants were expressed. Each experiment was performed in duplicate.

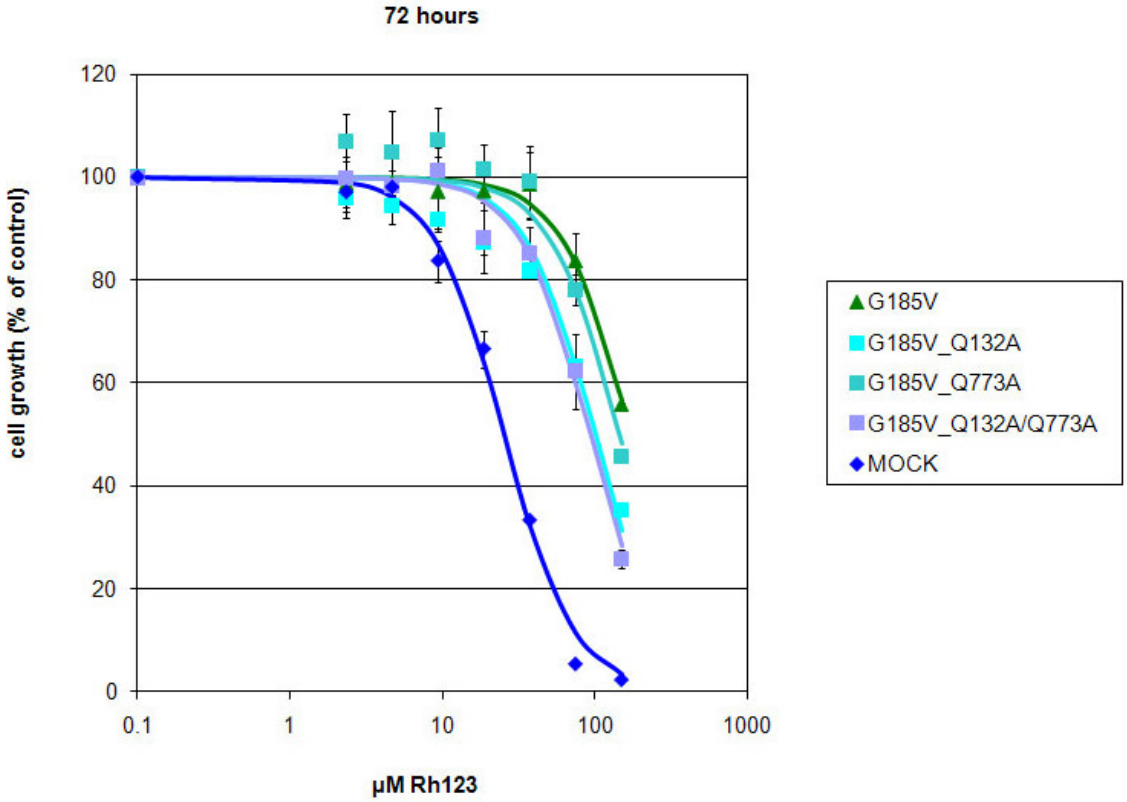

Figure 4.21: Cell growth expressed as percentage of control for G185V P-gp, G185V A mutants and mock transfected NIH3T3 cells after 72 hours rhodamine 123 incubation at 37°C. Each experiment was performed in duplicate.

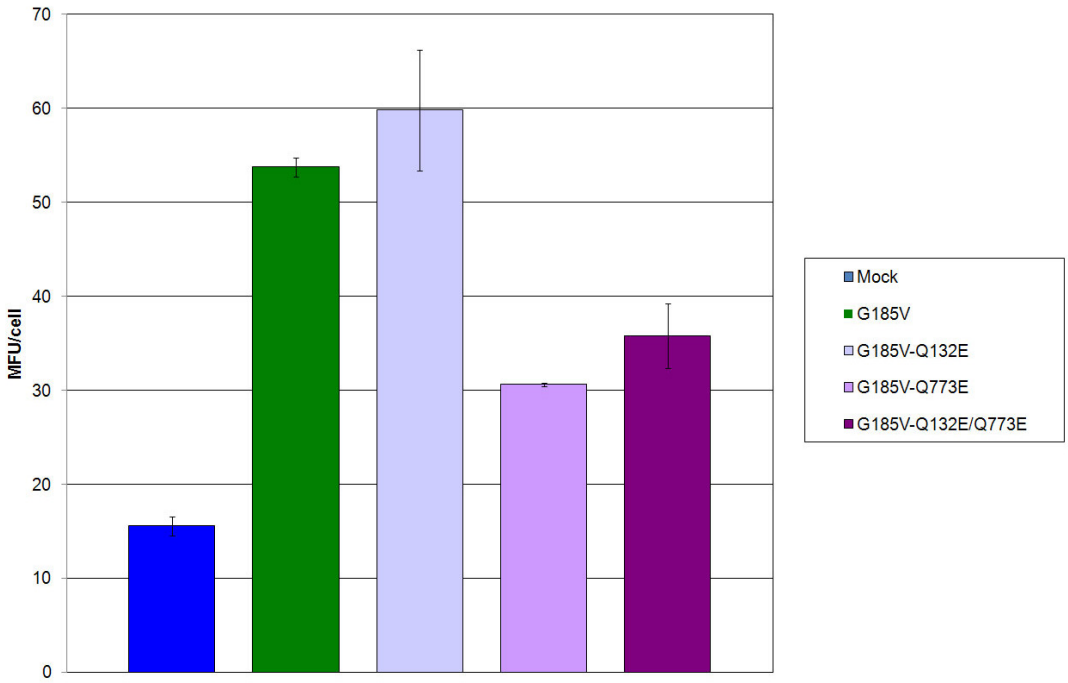

Figure 4.22: MRK16 staining of G185V P-gp, G185V E mutants and mock transfected cells. All mutants were expressed. Each experiment was performed in duplicate.

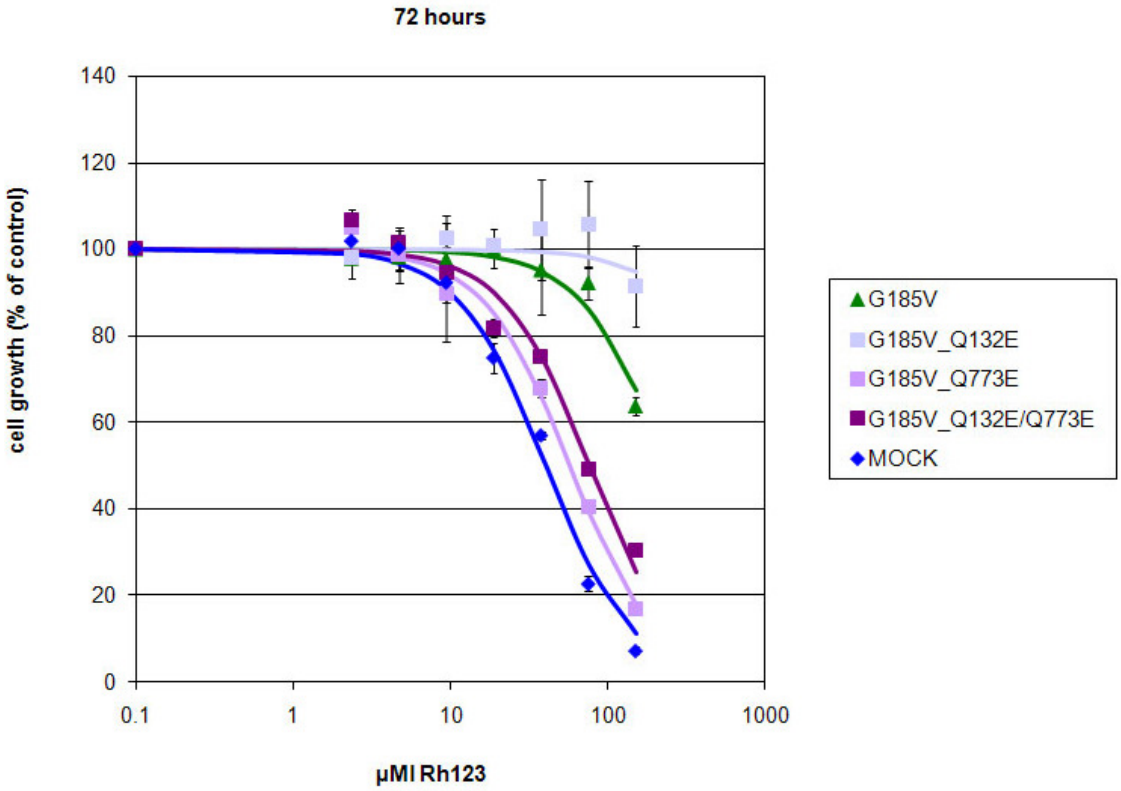

Figure 4.23: Cell growth expressed as a percentage of control for G185V P-gp, G185V E mutants and mock transfected NIH3T3 cells after 72 hours rhodamine 123 incubation at 37°C. Each experiment was performed in duplicate.

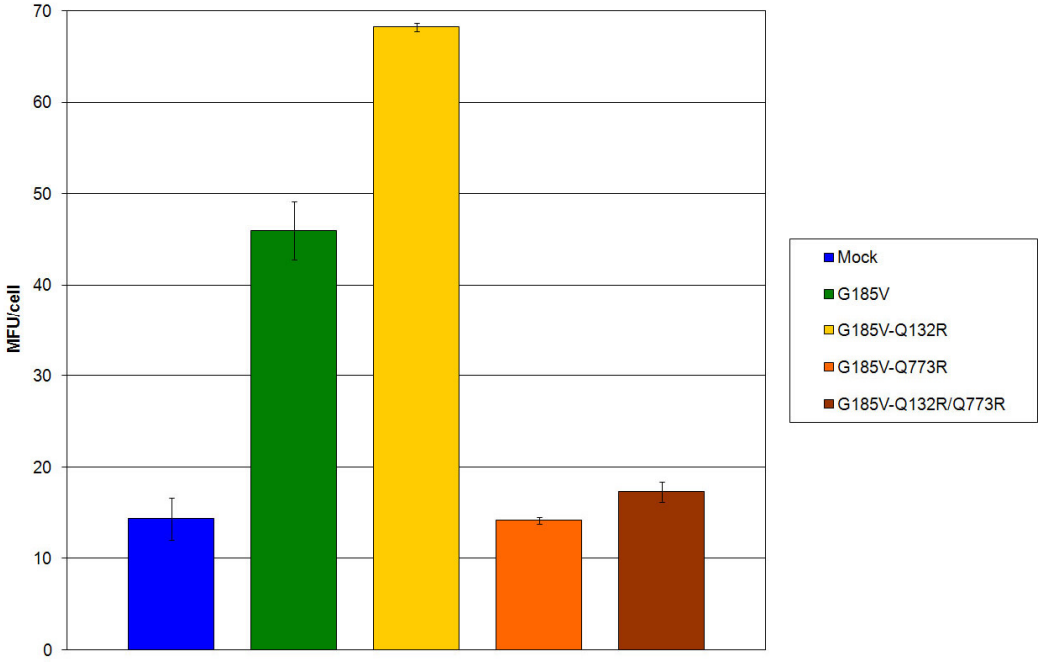

Figure 4.24: MRK16 staining of G185V P-gp, G185V R mutants and mock transfected cells. Q773R and Q132R/Q773R mutants were not expressed. Each experiment was performed in duplicate.

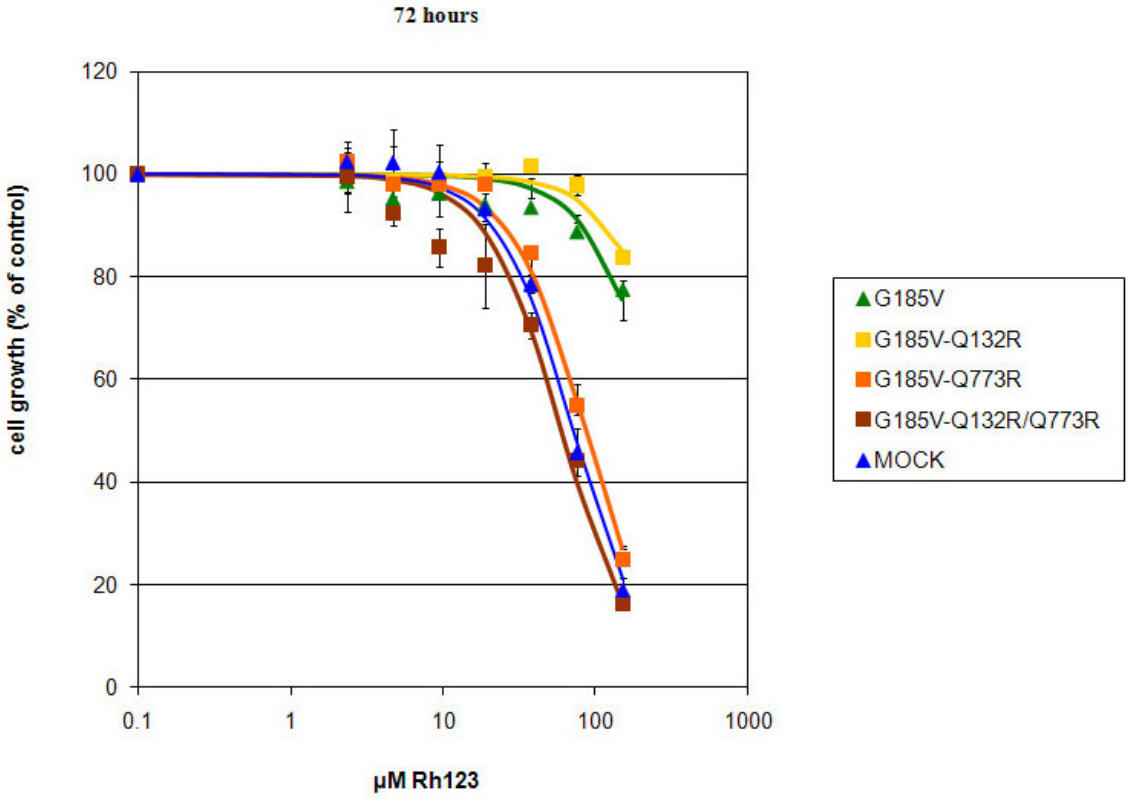

Figure 4.25: Cell growth expressed as percentage of control for G185V P-gp, G185V E mutants and mock transfected NIH3T3 cells after 72 hours rhodamine 123 incubation at 37°C. Each experiment was performed in duplicate.

The IC_{50} values after a 72 hour incubation with G185V P-gp, Q132A, Q773A and Q132A/Q773A in the G185V background, and mock transfected cells were 173 µM, 99

μM, 145 μM, 92 μM and 25 μM (shown in Figure 4.21). These results indicated that an alanine substitution at position 132 and 773, individually or in combination had little influence on the substrate properties of rhodamine 123 and therefore little influence on cell survival.

The IC_{50} values after 72 hours incubation with G185V P-gp, Q132E, Q773E and Q132E/Q773E in the G185V background, and mock transfected cells were 238 μM, 958 μM, 57 μM, 76 μM and 40 μM (shown in Figure 4.23). Surprisingly, we found that Q132E is a "gain of function" mutation because of the fourfold higher IC_{50} value (four-fold higher resistance) as compared to the G185V background.

The IC_{50} values after 72 hours incubation with G185V P-gp, Q132R, Q773R and Q132R/Q773R in the G185V background, and mock transfected cells were 283 μM, 401 μM, 86 μM, 60 μM and 71 μM (shown in Figure 4.25). Although both the Q132R and the Q132E mutant showed a similar behaviour, the Q132R showed essentially identical resistance as compared to the G185V background. The Q132R/Q773R double mutant essentially showed the same IC_{50} value as the mock tranfected cells. Similarly, the difference between IC_{50} values of Q773R and mock transfected cells was negligible.

4.8 Rhodamine 123 zero trans efflux experiments

The pump activity of the transfected cell lines were tested by zero trans efflux experiments. To examine whether rhodamine 123 is recognized as substrate by P-gp mutants, we determined the transport of rhodamine 123 in NIH 3T3 cells stably expressing P-gp mutants' compared to G185V P-gp and mock transfected cells.

Because of the fact that the Q773R and Q132R/Q773R in the G185V background did not traffic to the plasma membrane, the first experiments were performed by adding CsA at a concentration of 10 μM at 37°C for 24 hours. All R mutants and both G185V P-gp and mock transfected cells were incubated with CsA serving as control. After 24 hours the cells were washed three times with 90% DBS and 10% DMEM for 20 minutes at 37°C to remove CsA from the cultures. The time dependent efflux of rhodamine 123 was followed over 6 minutes (time points 60, 120, 180, 240, 300 and 360 seconds). First order rate constants (FORCs) were obtained by simultaneous fit of duplicate datapoints by an exponential function and normalized for expression rates (Figure 4.27).

We also examined the expression level for all cell lines by cell surface labelling of P-gp with MRK16 in parallel to the efflux experiment. Additionally, unstimulated cells

served as control. Thus we carried out seven stimulated and five unstimulated independent MRK16 stainings for each cell line (shown in Figure 4.26). CsA incubation promoted expression of all mutant P-gps to levels observed for G185V P-gp. An exactly identical expression was not required, because FORCs are linearly dependent on protein expression rates in a zero trans efflux protocol. Experimental data are presented as the means ± S.D.

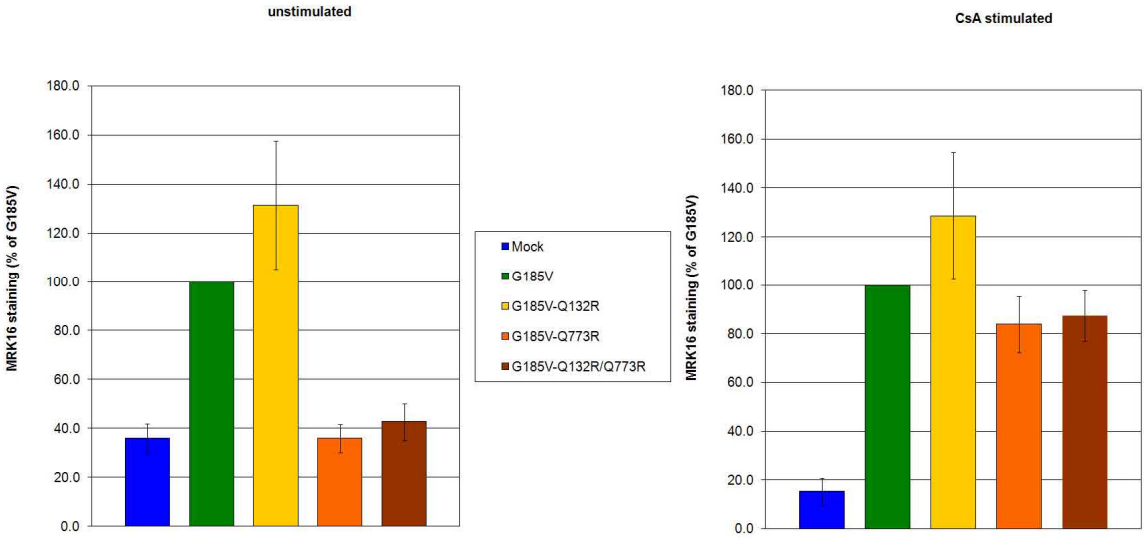

Figure 4.26: MRK16 staining of G185V P-gp, Q132R, Q773R and Q132R/Q773R P-gp mutants in G185V background, and mock transfected cells. The values are expressed as percent of G185V set to 100%. The values are mean ± standard deviations. Left: unstimulated cells (N=5). Right: Cells were incubated with 10 µM CsA for 24 hours (N=7).

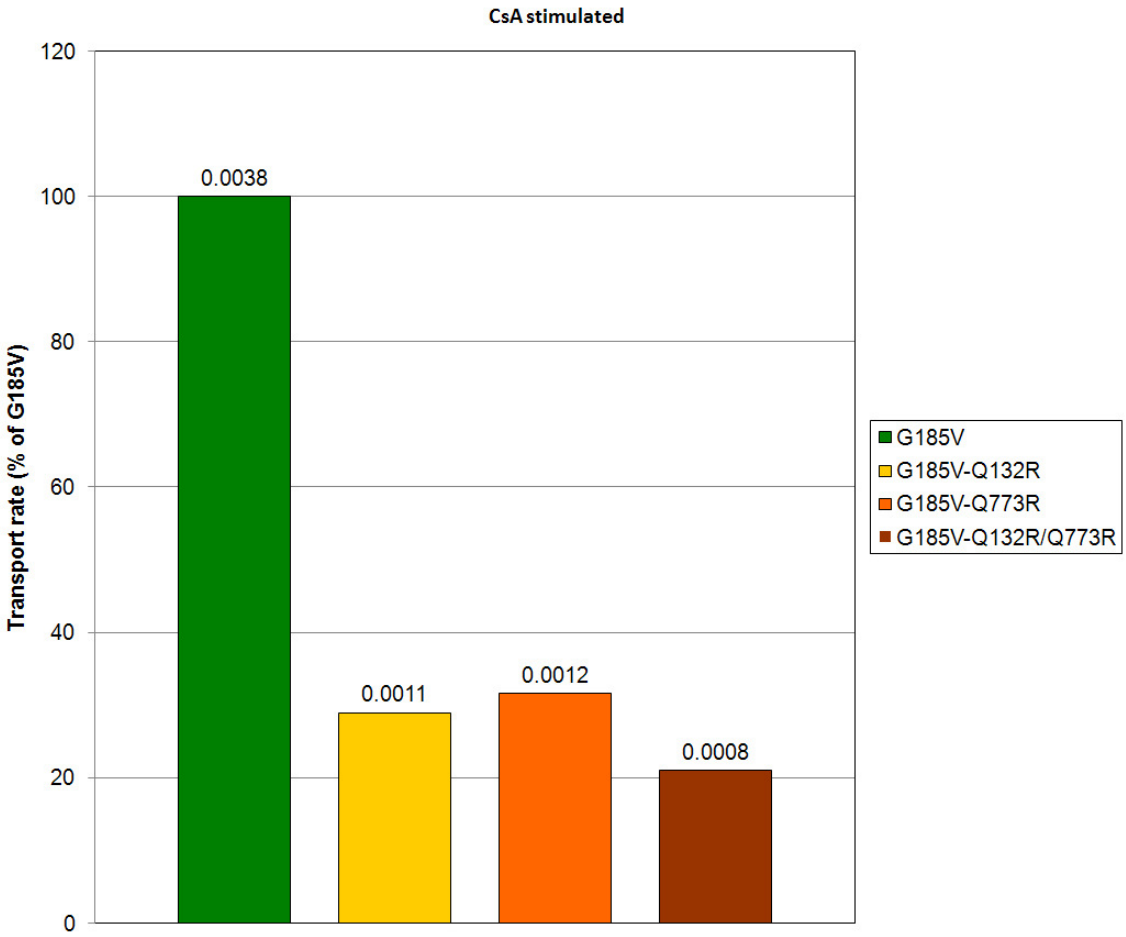

Figure 4.27: Rhodamine 123 zero trans efflux without modulator. The diagramme shows the transport rate of rhodamine 123 of G185V P-gp, Q132R, Q773R and Q132R/Q773R P-gp mutants in G185V background. The slope obtaining through linear regression of FORC versus MFU values of all cell lines are calculated and indicated above the bar. Cells were preincubated with 10 µM CsA for 24 hours (N=7).

To compare different flux rates in mutants to each other the transport rates have to be normalized for expression rate. The Q132R mutant showed 29% efflux rates of G185V control, Q773R and the double mutant showed 32% and 21%, respectively. The rhodamine 123 transport rate for G185V P-gp showed high interexperimental variation, which we interpreted as possibly due to incomplete remove of CsA. To overcome the effect of potentially incomplete CsA removal, surface expression was increased by shifting to a growth temperature of 28°C. The expression level increased in all of the R mutants (Figure 4.55).

Different compounds, GPV01, GPV02, GPV12, GPV31, GPV46, and GPV57, were tested for their modulating activity in the rhodamine 123 efflux assays for wt, G185V P-gp and mock transfected cells (shown in Table 4.3). A time dependent efflux was used with either no modulator, or modulator at eight various concentrations depending on solubility and the expected potency for the modifier. The modulator concentrations for

GPV01 that were used for mutant characterization ranged from 164 nM to 100 µM (1:2.5 serial dilutions). For each concentration of the inhibitor, the time dependent efflux of rhodamine 123 was followed over 6 minutes (time points 90, 180, 270 and 360 seconds). From these data points the initial efflux rate was calculated by determining the slope of the tangent to the extrapolated 0 time point which was normalised to obtain the first order rate constant (FORC). The first order rate constants (V_{max}/K_m) were then plotted as a function of inhibitor concentration in a linear and a half-logarithmic plot (shown in Figure 4.28 - Figure 4.48). Hyperbolic curves were fitted to the data points using the solver add-in of the MS-office Excel computer program. G185V P-gp and wt P-gp expressing cells were loaded with the fluorescent dye rhodamine 123 and the time-dependent decrease of cell-associated fluorescence in the presence of different concentrations of inhibitors was measured. Mock transfected cells served as negative control. Plotting the first order rate constants versus inhibitor concentration led to dose/response curves, which allowed calculation of the IC_{50} values. These IC_{50} values refer to those concentrations, which are required to inhibit efflux first order rate constants of rhodamine 123 by 50%. IC_{50} values were determined by fitting a Hill equation onto data points by the method of nonlinear least-squares. A representative experiment for compound GPV01 is shown in Figure 4.29 - Figure 4.31 and for GPV31 in Figure 4.32 - Figure 4.34. Cell surface labelling was carried out for all cell lines in parallel with the efflux experiment (Figure 4.28).

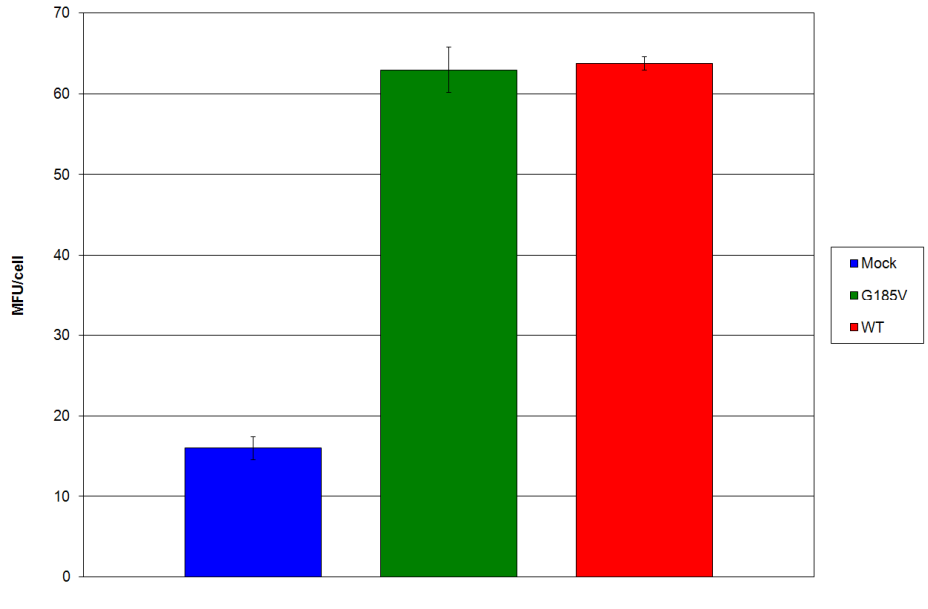

Figure 4.28: MRK16 staining of wt P-gp, G185V P-gp and mock transfectd clells. Each experiment was performed in duplicate.

The expression level for wt and G185V P-gp was similar.

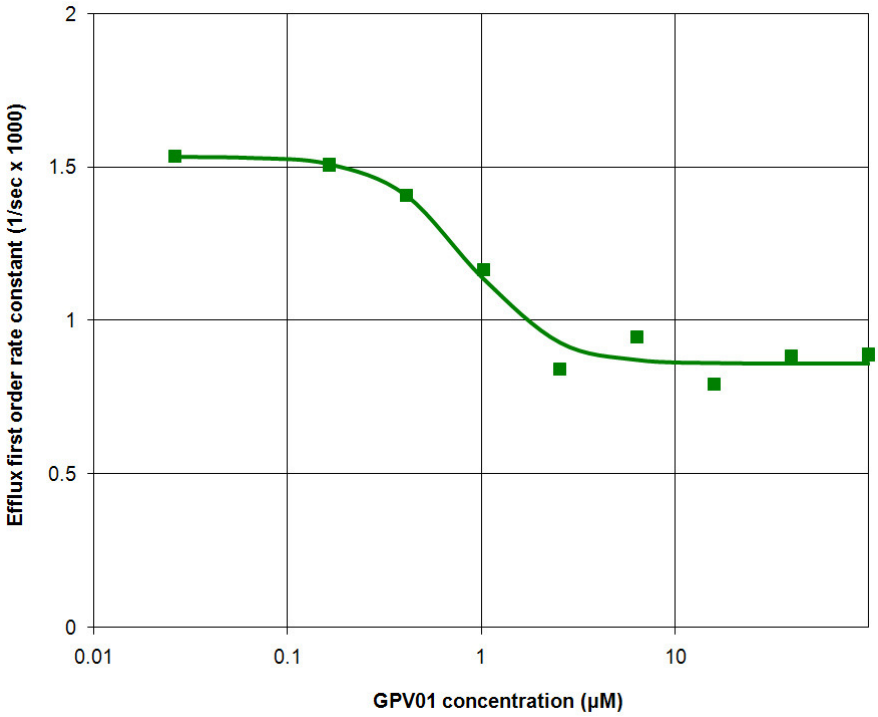

Figure 4.29: Dose-response curve for compound GPV01, showing the effect on the rhodamine 123 efflux rate in G185V P-gp expressing NIH3T3 cells. From measurements in the absence and presence of 8 different concentrations of the propafenone analogue GPV01, IC_{50} values were calculated using a hyperbolic curve fit.

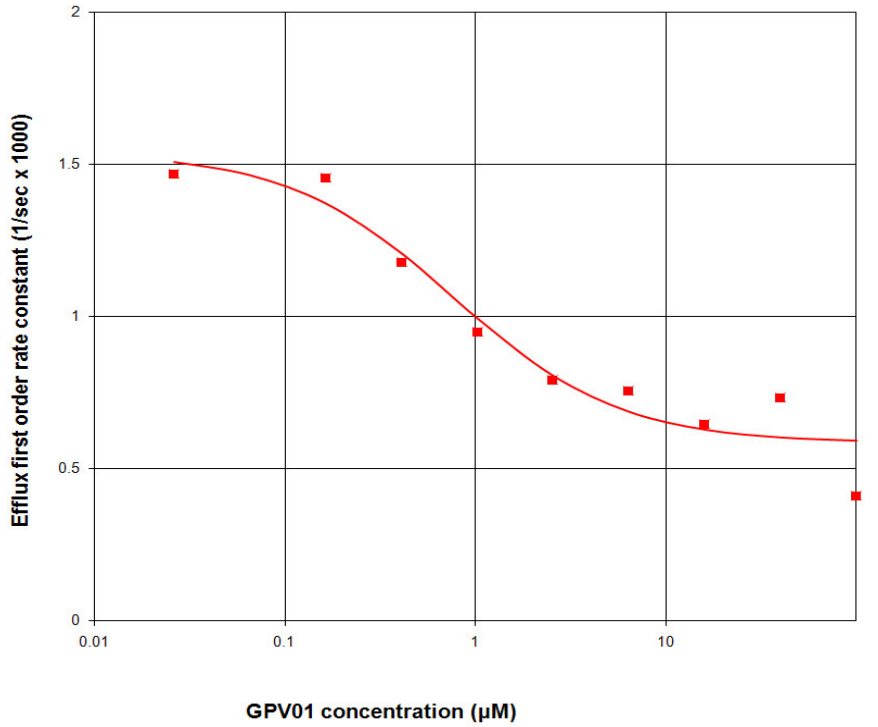

Figure 4.30: Dose-response curve for compound GPV01, showing the effect on the rhodamine 123 efflux rate in wt P-gp expressing NIH3T3 cells. From measurements in the absence and presence of 8 different concentrations of the propafenone analogue GPV01, IC_{50} values were calculated using a hyperbolic curve fit.

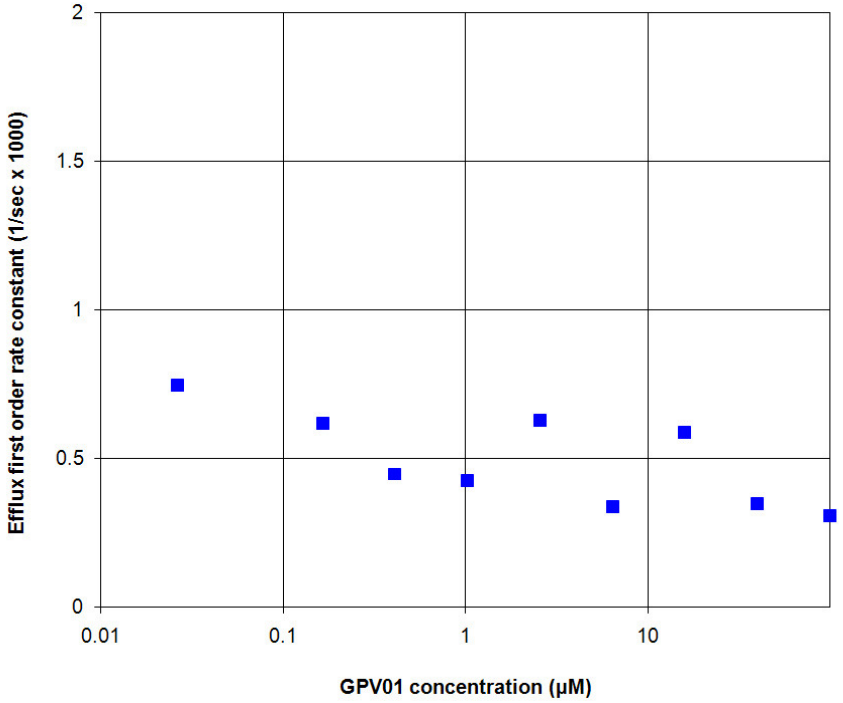

Figure 4.31: Dose-response curve for compound GPV01, showing the effect on the rhodamine 123 efflux rate in mock transfected NIH3T3 cells in the absence and presence of 8 different concentrations of the propafenone analogue GPV01.

For all efflux experiments the IC_{50} values of GPV01 were 0.780 µM (95% CI: 0.49 µM – 1.07 µM, N=10) for G185V and 0.73 µM (95% CI: 0.62 µM – 0.84 µM, N=3) for wt cells. It was not possible to calculate an IC_{50} value for mock transfected cells.

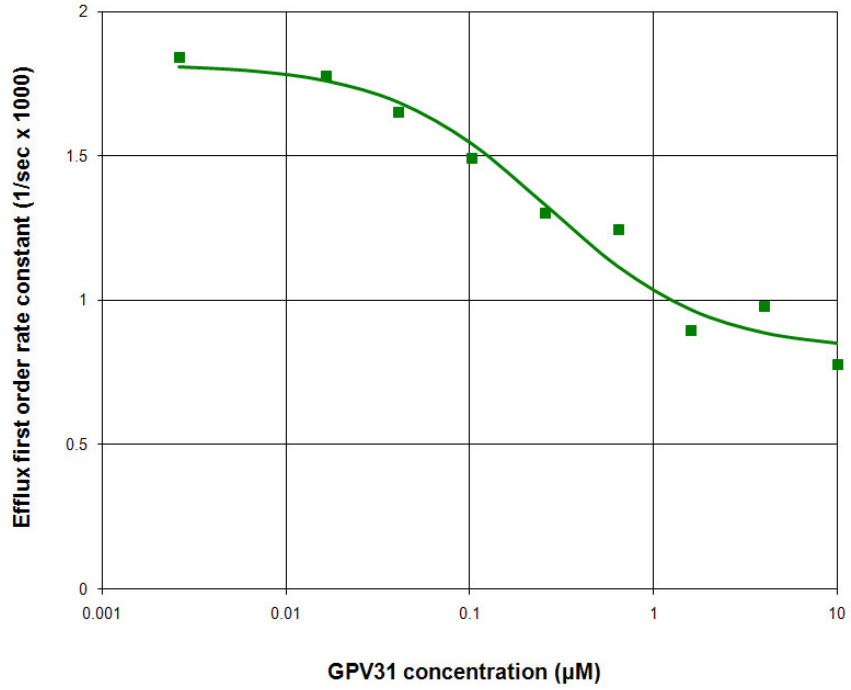

Figure 4.32: Dose-response curve for compound GPV31, showing the effect on the rhodamine 123 efflux rate in G185V P-gp expressing NIH3T3 cells. From measurements in the absence and presence of 8 different concentrations of the propafenone analogue GPV31, IC_{50} values were calculated using a hyperbolic curve fit.

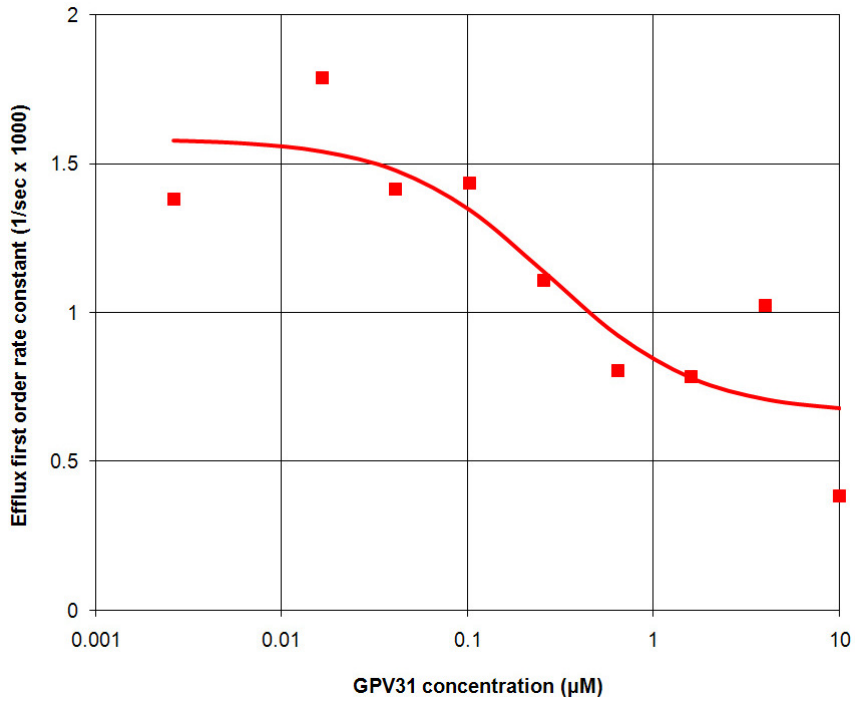

Figure 4.33: Dose-response curve for compound GPV31, showing the effect on the rhodamine 123 efflux rate in wt P-gp expressing NIH3T3 cells. From measurements in the absence and presence of 8 different concentrations of the propafenone analogue GPV31, IC_{50} values were calculated using a hyperbolic curve fit.

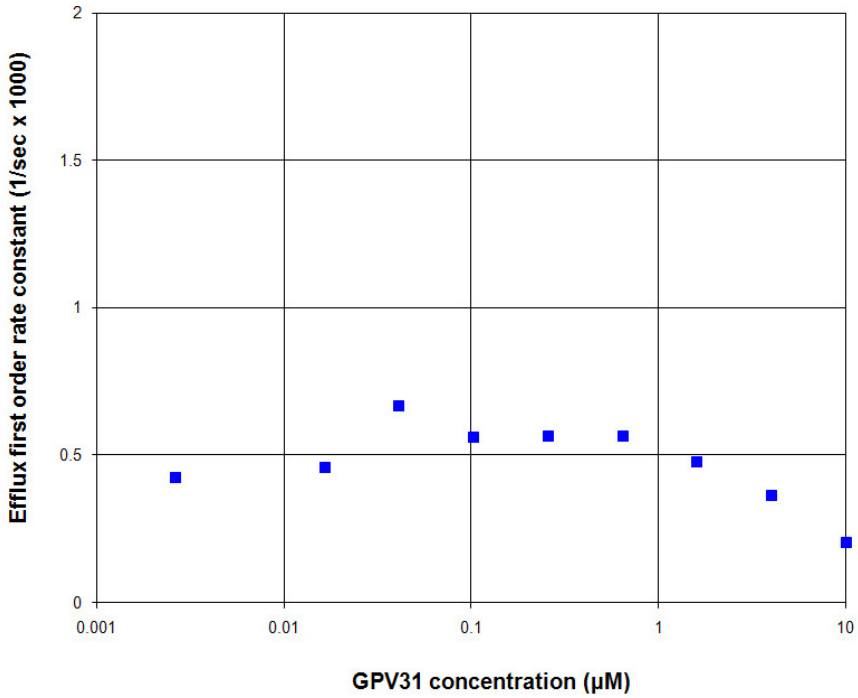

Figure 4.34: Dose-response curve for the compound GPV31, showing the effect on rhodamine 123 efflux rate in mock transfected NIH3T3 cells in the absence and presence of 8 different concentrations of the propafenone analogue GPV31.

For all rhodamine 123 efflux inhibition experiments with GPV31 the IC_{50} values were 0.18 µM (95% CI: 0.10 µM – 0.27 µM, N=3) for G185V P-gp and 0.27 µM (N=1) for wt P-gp. As before, no effect of GPV31 was observed in mock transfected cells, because of a lack of expression of P-gp. The rate constant observed in these cells corresponds to rhodamine 123 diffusion rates.

The IC_{50} values for all 6 propafenone analogues are reported in Table 4.3. It was not possible to calculate IC_{50} values for mock transfected cells for any of the propafenone analogues, because these cells do not express significant levels of P-gp. The most active compounds are GPV01, GPV02, and GPV31. For these three compounds comparably low inhibitor concentrations are needed to modulate activity. IC_{50} values of these compounds are lower than those observed for GPV12, GPV46, and GPV57. The modulators GPV01, GPV02, GPV12, GPV31, GPV46 and GPV57 were tested once before the mutants were characterized.

Cell line	Modulator	IC50 (µM)
G185V	GPV01	0.86
WT	GPV01	0.77
G185V	GPV02	0.78
WT	GPV02	0.63
G185V	GPV12	5.36
WT	GPV12	31.41
G185V	GPV31	0.27
WT	GPV31	0.27
G185V	GPV46	85.57
WT	GPV46	153.98
G185V	GPV57	5.29
WT	GPV57	21.62

Table 4.3: Different propafenone analogues and their respective IC_{50} values for inhibition of G185V P-gp and wt P-gp obtained in rhodamine 123 efflux experiments. It was not possible to calculate IC_{50} values for mock transfected cells.

Because of generally low expression rates of stable transfectants, use of the G185V background was considered to increase the likelihood of being able to functionally characterize mutant P-gp with reduced pump activity. Indeed, the G185V P-gp had higher

rhodamine 123 efflux rates as compared to wt P-gp. This observation is consistent with the cytotoxicity experiments where the G185V P-gp showed a higher resistance to rhodamine 123 compared to wt P-gp. The FORCs for these 6 rhodamine 123 efflux experiments of G185V P-gp, wt P-gp and mock transfected cells are shown in Figure 4.35.

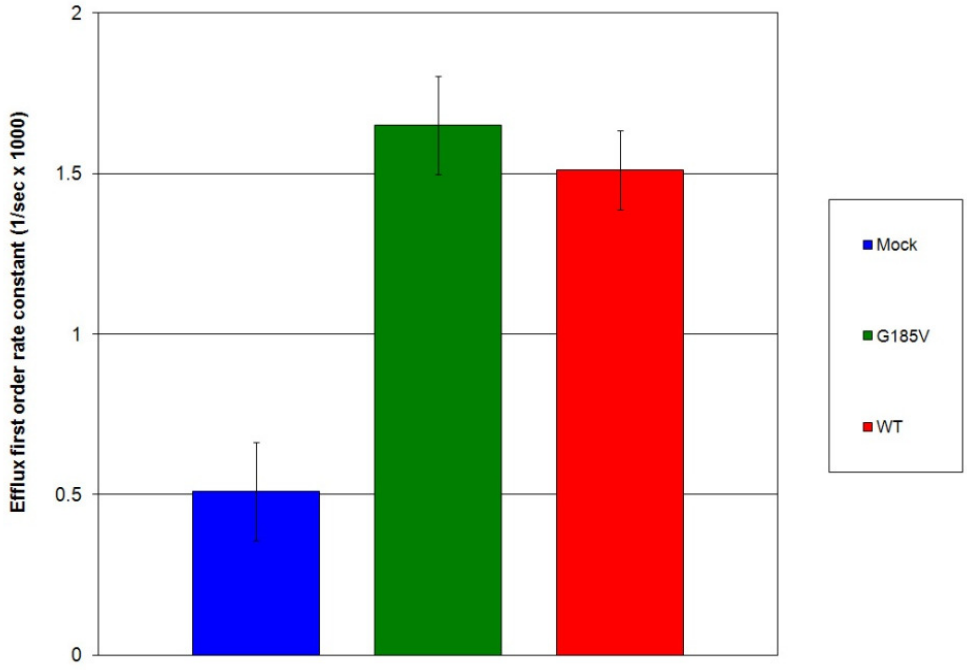

Figure 4.35: Transport rates (FORCs) of G185V P-gp, wt P-gp and mock transfected cells for rhodamine 123.

The mean of all rhodamine 123 zero trans efflux experiments resulted in a FORC of 1.55 1/sec x 1000 (95% CI: 1.44 – 1.65, N=17) for G185V P-gp, 1.46 1/sec x 1000 (95% CI: 1.33 – 1.59, N=8) for wt P-gp and 0.59 1/sec x 1000 (95% CI: 0.51 – 0.67, N=14) for mock transfected cells. These FORCs of G185V P-gp and wt P-gp have been normalized for expression rate to compare flux rates to each other (shown in Figure 4.36). The slope of this relationship provided the pump activity. The slopes of the linear regressions are shown in Table 4.4. The pump activity for wt and G185V P-gp was similar. The mock transfected cells were close to the origin indicating that the rate constant observed in these cells corresponds to rhodamine 123 diffusion rates.

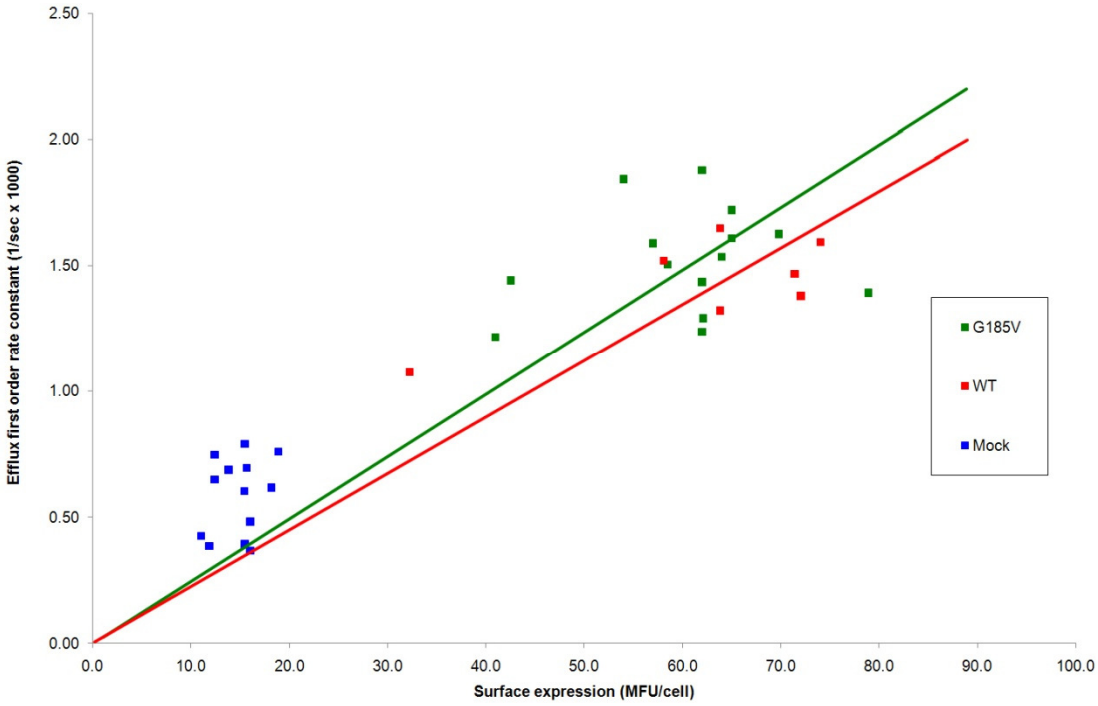

Figure 4.36: Correlation (origin forced to 0) of surface expression (measured by MRK16 staining) and FORC for G185V P-gp and wt P-gp.

Cell line	slope	N	r	p	% of G185V
G185V	0.0247	14	0.997	0.006	100
WT	0.0224	7	0.620	0.240	91

Table 4.4: Pump activity of G185V P-gp and wt P-gp. The slopes were obtained through linear regression of FORC versus surface expression (MFU value). N: number of data points that were used, r: correlation coefficient, and p: significance

The next step was to characterize the P-gp mutants. All three mutant combinations for example Q132A, Q773A and Q132A/Q773A in the G185V background were compared with G185V P-gp and mock transfected cells in rhodamine 123 efflux experiments on the same day. A representative experiment for each cell line for compound GPV01 is shown in Figure 4.38 - Figure 4.42; Figure 4.44 - Figure 4.48; Figure 4.50 - Figure 4.54; and Figure 4.56 - Figure 4.59. In general the rhodamine 123 zero trans efflux experiments were performed in at least two independent experiments and cell surface labelling of P-gp was carried out for all cell lines in parallel in repeat determinations for each experiment (Figure 4.37, Figure 4.43, Figure 4.49, and Figure 4.55).

We tested compound GPV01 as inhibitor for all P-gp mutants.

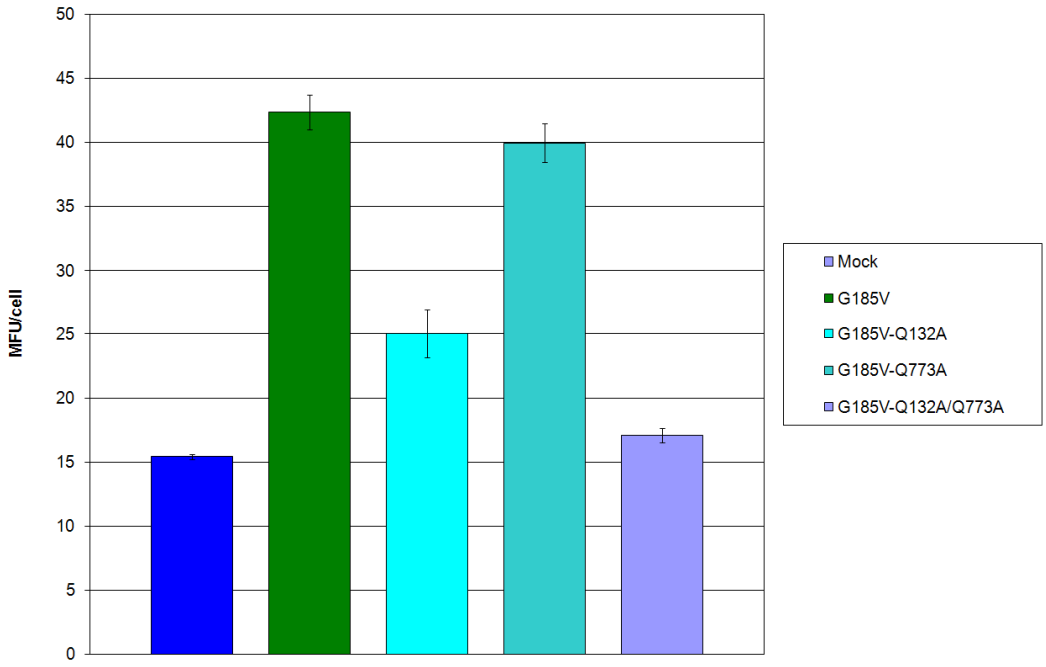

Figure 4.37: MRK16 staining of G185V P-gp, Q132A, Q773A and Q132A/Q773A P-gp mutants in G185V background, and mock transfected cells. Each experiment was performed in duplicate.

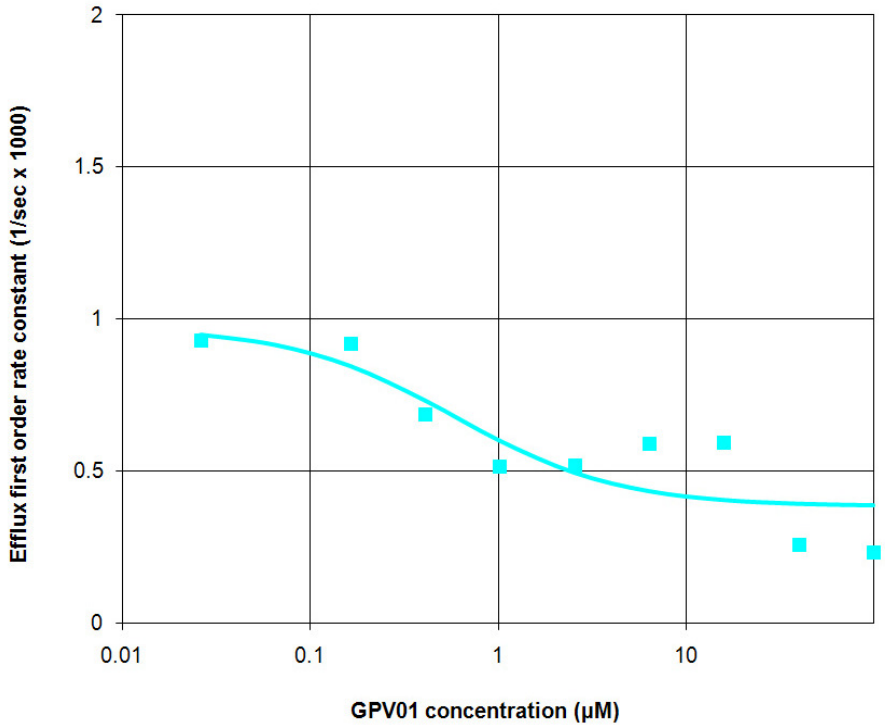

Figure 4.38: Dose-response curve for compound GPV01, showing the effect on the rhodamine 123 efflux rate in G185V-Q132A P-gp expressing NIH3T3 cells. From measurements in the absence and presence of 8 different concentrations of the propafenone analogue GPV01, IC_{50} values were calculated using a hyperbolic curve fit.

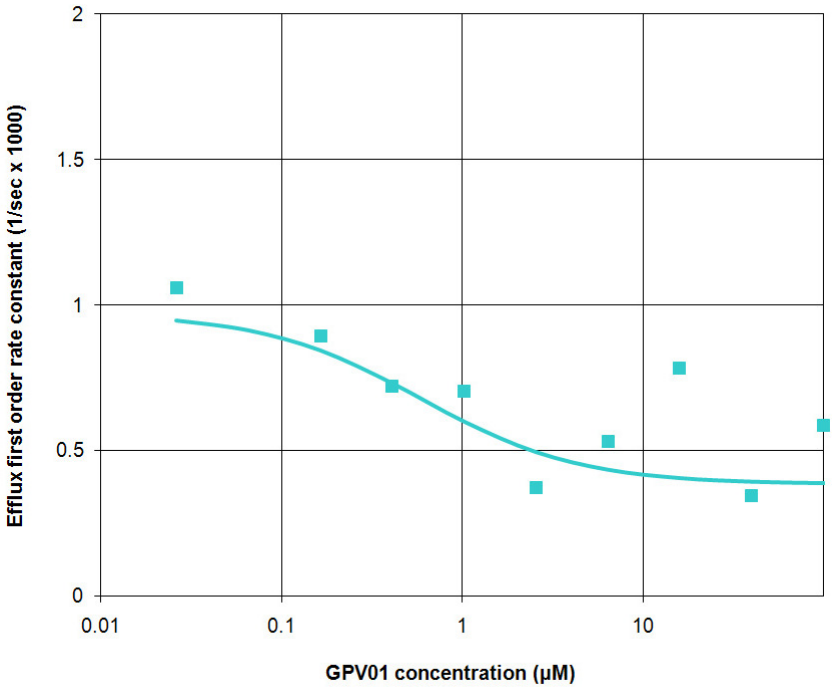

Figure 4.39. Dose-response curve for compound GPV01, showing the effect on the rhodamine 123 efflux rate in G185V-Q773A P-gp expressing NIH3T3 cells. From measurements in the absence and presence of 8 different concentrations of the propafenone analogue GPV01, IC_{50} values were calculated using a hyperbolic curve fit.

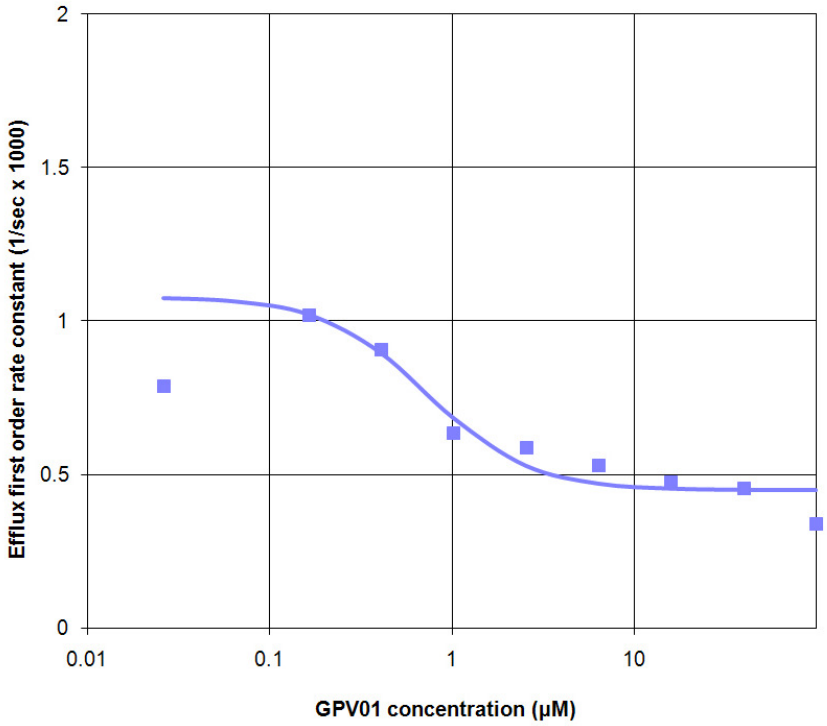

Figure 4.40: Dose-response curve for compound GPV01, showing the effect on the rhodamine 123 efflux rate in G185V-Q132A/Q773A P-gp expressing NIH3T3 cells. From measurements in the absence and presence of 8 different concentrations of the propafenone analogue GPV01, IC_{50} values were calculated using a hyperbolic curve fit.

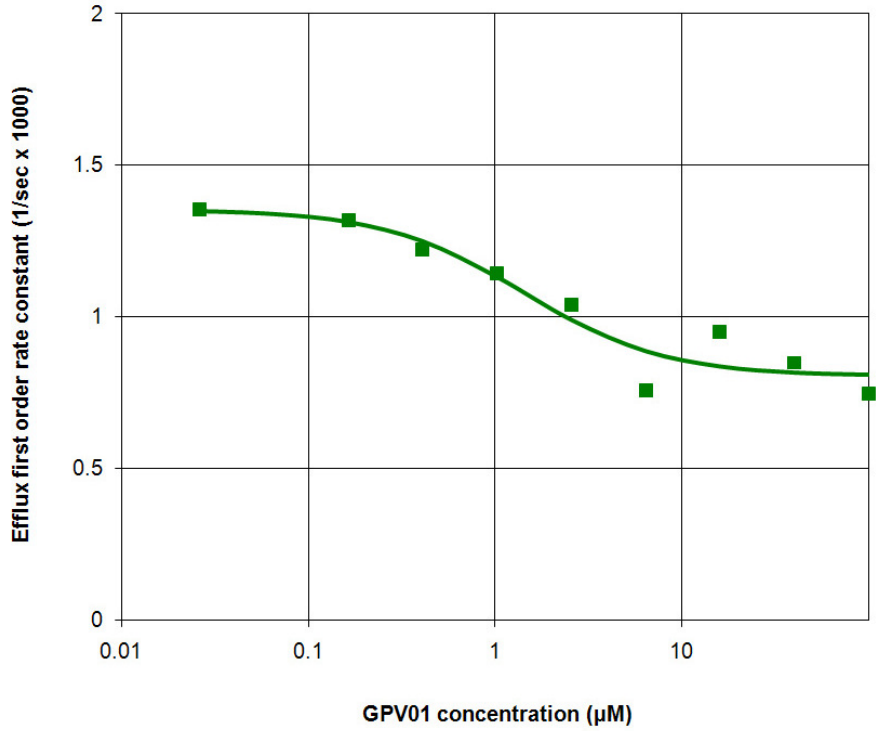

Figure 4.41: Dose-response curve for compound GPV01, showing the effect on the rhodamine 123 efflux rate in G185V P-gp expressing NIH3T3 cells. From measurements in the absence and presence of 8 different concentrations of the propafenone analogue GPV01, IC_{50} values were calculated using a hyperbolic curve fit.

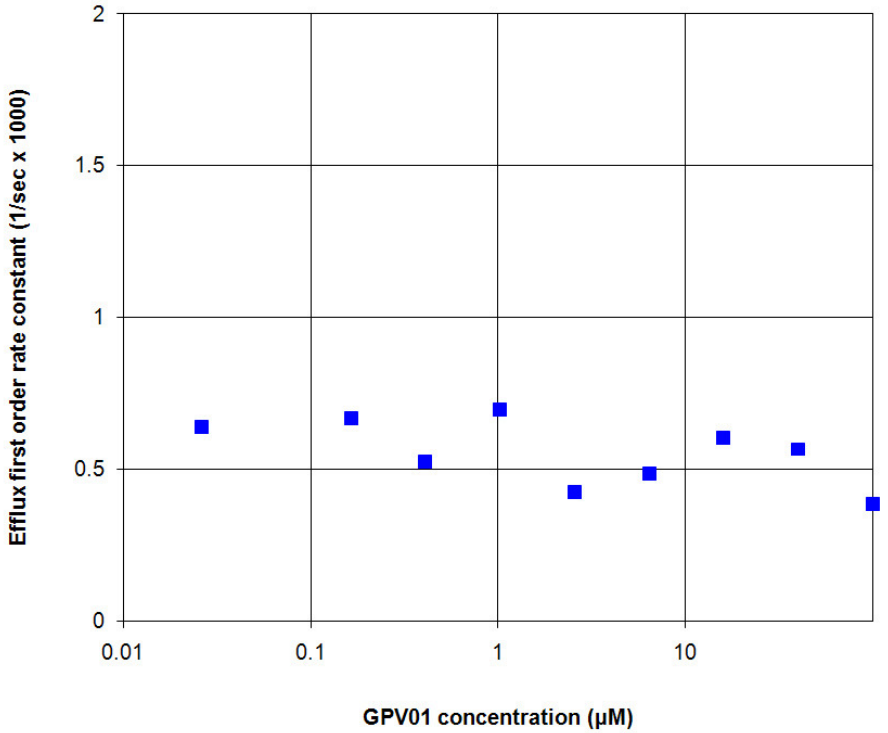

Figure 4.42: Dose-response curve for compound GPV01, showing the effect on the rhodamine 123 efflux rate in mock transfected NIH3T3 cells in the absence and presence of 8 different concentrations of the propafenone analogue GPV01.

IC_{50} values for rhodamine 123 efflux inhibition with GPV01 were 0.66 µM (95% CI: 0.52 µM – 0.81 µM, N=2) for G185V-Q132A, 0.57 µM (95% CI: 0.24 µM – 0.90 µM, N=2) for G185V-Q773A, and 1.64 µM (95% CI: -0.13 µM – 3.40 µM, N=2) for the double A mutant.

Because of the fact that the G185V-Q132A/Q773A P-gp mutant had a very low expression level the experiments were performed again. To enhance expression of P-gp, the G185V, all alanine mutants in the G185V background as well as the mock transfected cells were shifted to a growth temperature of 28°C prior to assessing substrate flux. The expression level increased in all mutants (shown in Figure 4.43).

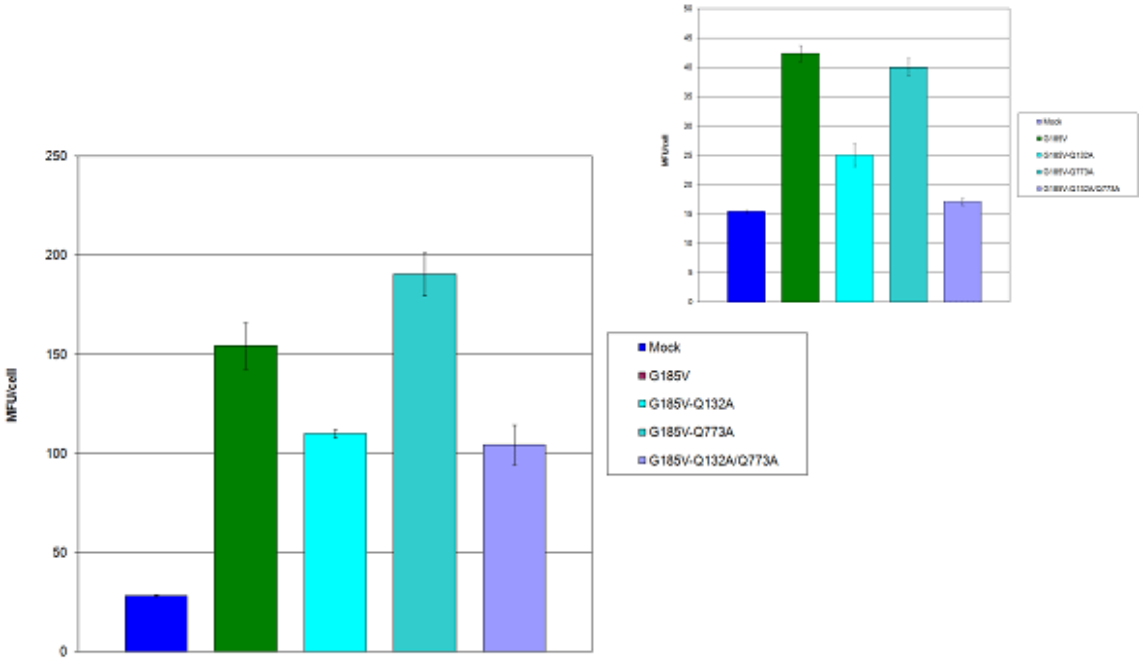

Figure 4.43: MRK16 staining of G185V P-gp, Q132A, Q773A and Q132A/Q773A P-gp mutants in G185V background, and mock transfected cells. Comparison of incubation at 28°C (left) and 37°C (top-right, see Figure 4.37). The cells were shifted to a growth temperature of 28°C / 37°C prior to assessing substrate flux. Each experiment was performed in duplicate.

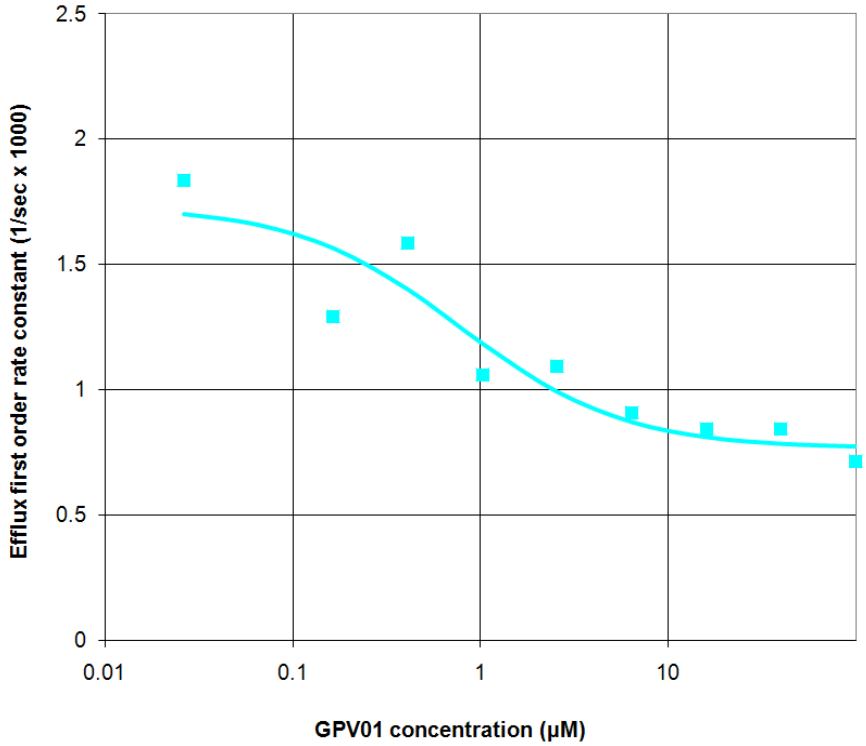

Figure 4.44: Dose-response curve for compound GPV01, showing the effect on the rhodamine 123 efflux rate in G185V-Q132A P-gp expressing NIH3T3 cells. From measurements in the absence and presence of 8 different concentrations of the propafenone analogue GPV01, IC_{50} values were calculated using a hyperbolic curve fit. The cells were shifted to a growth temperature of 28°C prior to assessing substrate flux.

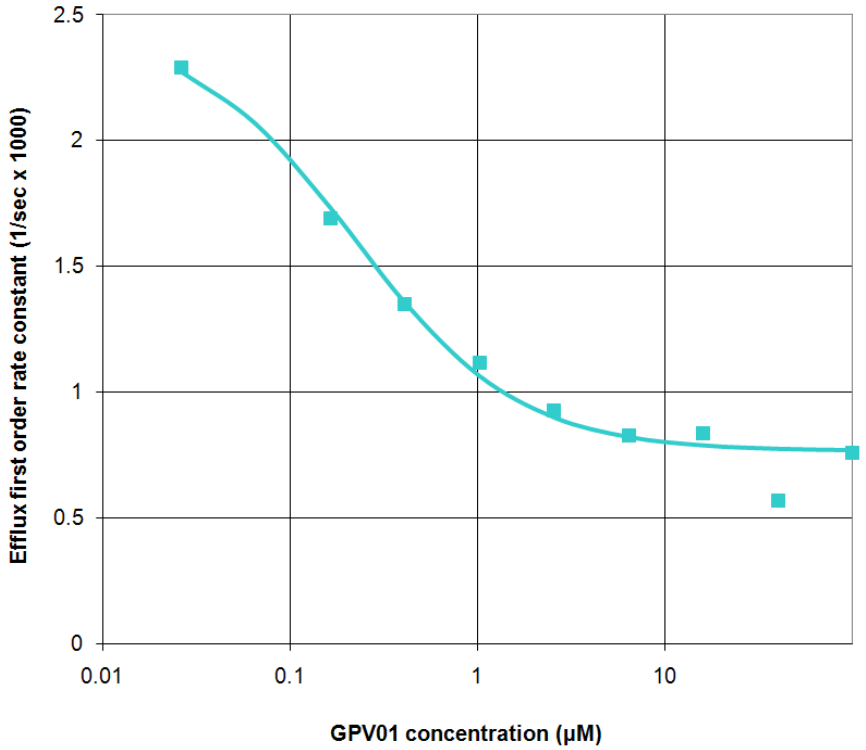

Figure 4.45: Dose-response curve for compound GPV01, showing the effect on the rhodamine 123 efflux rate in G185V-Q773A P-gp expressing NIH3T3 cells. From measurements in the absence and presence of 8 different concentrations of the propafenone analogue GPV01, IC_{50} values were calculated using a hyperbolic curve fit. The cells were shifted to a growth temperature of 28°C prior to assessing substrate flux.

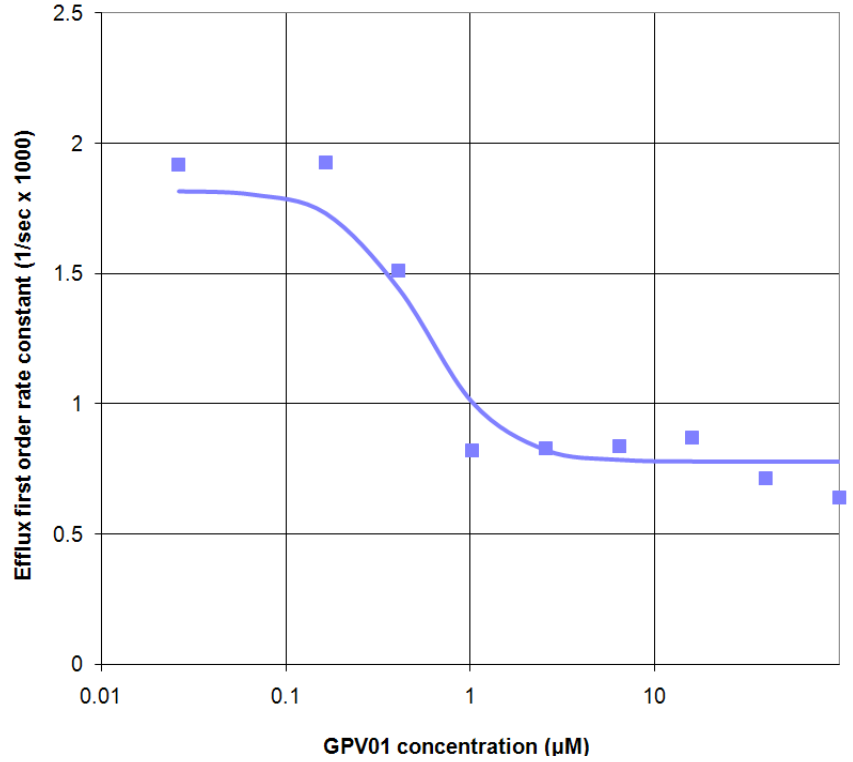

Figure 4.46: Dose-response curve for compound GPV01, showing the effect on the rhodamine 123 efflux rate in G185V-Q132A/Q773A P-gp expressing NIH3T3 cells. From measurements in the absence and presence of 8 different concentrations of the propafenone analogue GPV01, IC_{50} values were calculated using a hyperbolic curve fit. The cells were shifted to a growth temperature of 28°C prior to assessing substrate flux.

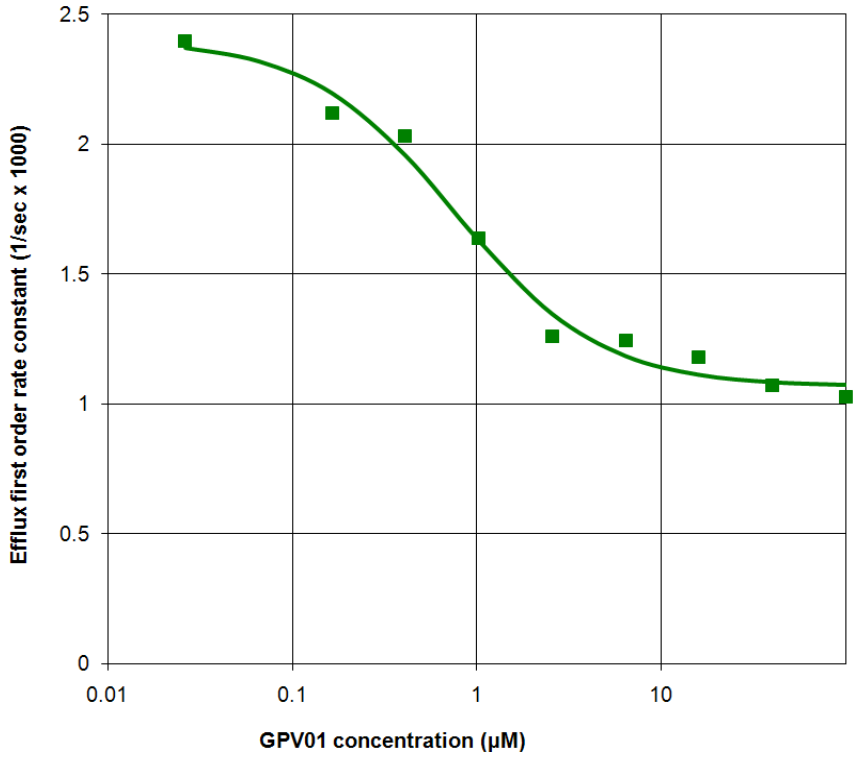

Figure 4.47: Dose-response curve for compound GPV01, showing the effect on the rhodamine 123 efflux rate in G185V P-gp expressing NIH3T3 cells. From measurements in the absence and presence of 8 different concentrations of the propafenone analogue GPV01, IC_{50} values were calculated using a hyperbolic curve fit. The cells were shifted to a growth temperature of 28°C prior to assessing substrate flux.

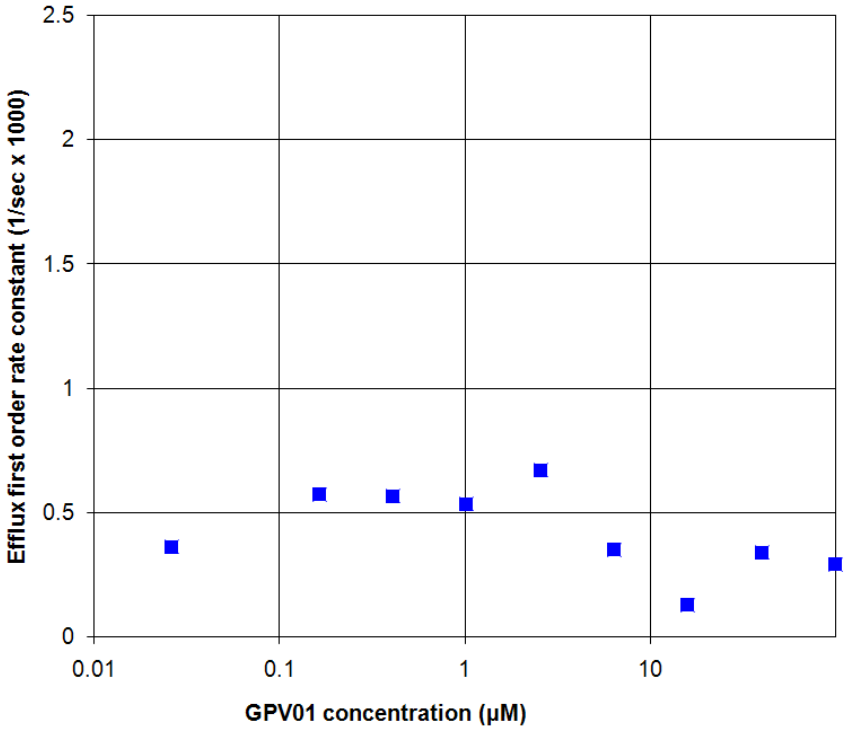

Figure 4.48: Dose-response curve for compound GPV01, showing the effect on the rhodamine 123 efflux rate in mock transfected NIH3T3 cells in the absence and presence of 8 different concentrations of the propafenone analogue GPV01. The cells were shifted to a growth temperature of 28°C prior to assessing substrate flux.

After shifting the cells to a growth temperature of 28°C prior to assessing substrate flux, the IC_{50} values for rhodamine 123 efflux inhibition with GPV01 were 0.58 µM (95% CI: 0.20 µM – 0.95 µM, N=3 for G185V-Q132A, 0.24 µM (95% CI: 0.18 µM – 0.31 µM, N=3) for G185V-Q773A, and 1.06 µM (95% CI: -0.19 µM – 2.31 µM, N=3) for the double A mutant. For G185V P-gp an IC_{50} value of 0.76 µM (95% CI: 0.62 µM – 0.94 µM, N=6) was obtained. At both temperatures, 28°C and 37°C, the G185V-Q773A and G185V-Q132A mutants showed a better modulating activity for compound GPV01 compared to G185V P-gp and wt P-gp, however confidence intervals indicate that this is not a significant difference.

The next three mutant combinations Q132E, Q773E and Q132E/Q773E in the G185V background were tested and compared with G185V P-gp and mock transfected cells in rhodamine 123 efflux experiments on the same day.

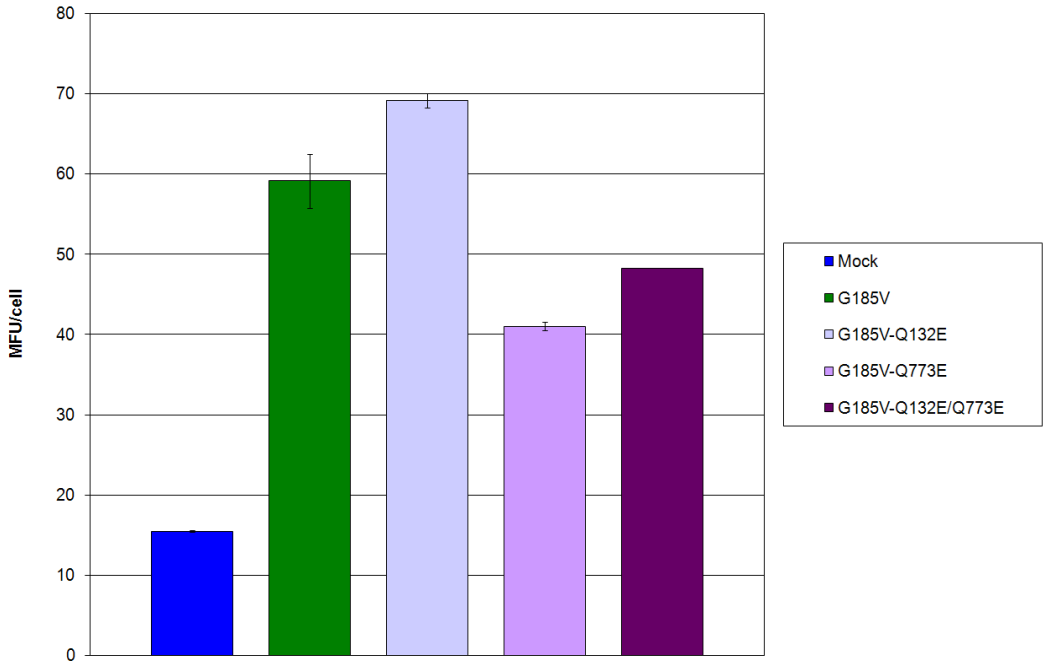

Figure 4.49: MRK16 staining of G185V P-gp, Q132E, Q773E and Q132E/Q773E P-gp mutants in G185V background, and mock transfected cells. The cells grew at 37°C prior to assessing substrate flux. Each experiment was performed in duplicate.

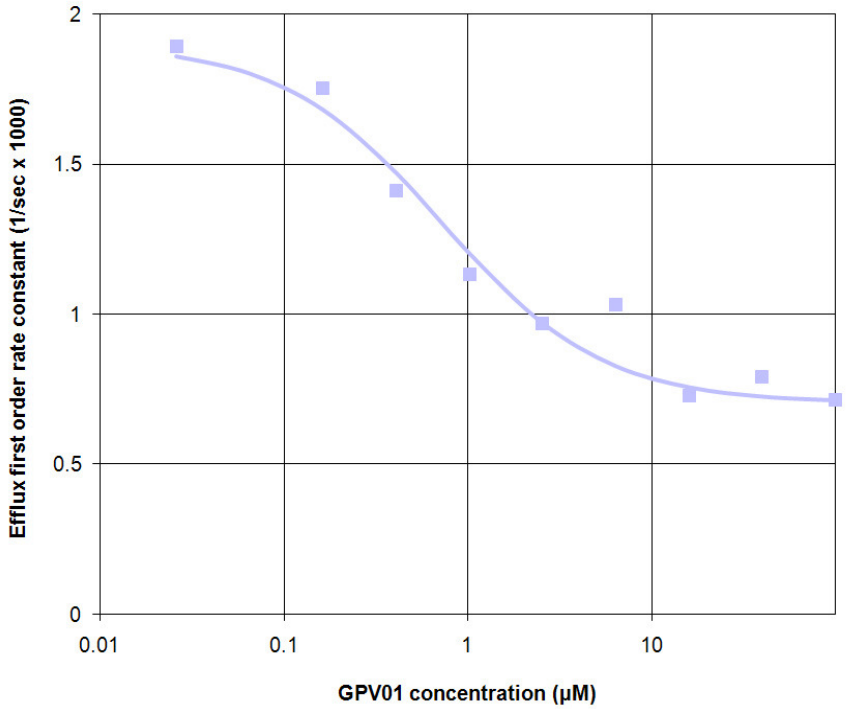

Figure 4.50: Dose-response curve for compound GPV01, showing the effect on the rhodamine 123 efflux rate in G185V-Q132E P-gp expressing NIH3T3 cells. From measurements in the absence and presence of 8 different concentrations of the propafenone analogue GPV01, IC_{50} values were calculated using a hyperbolic curve fit.

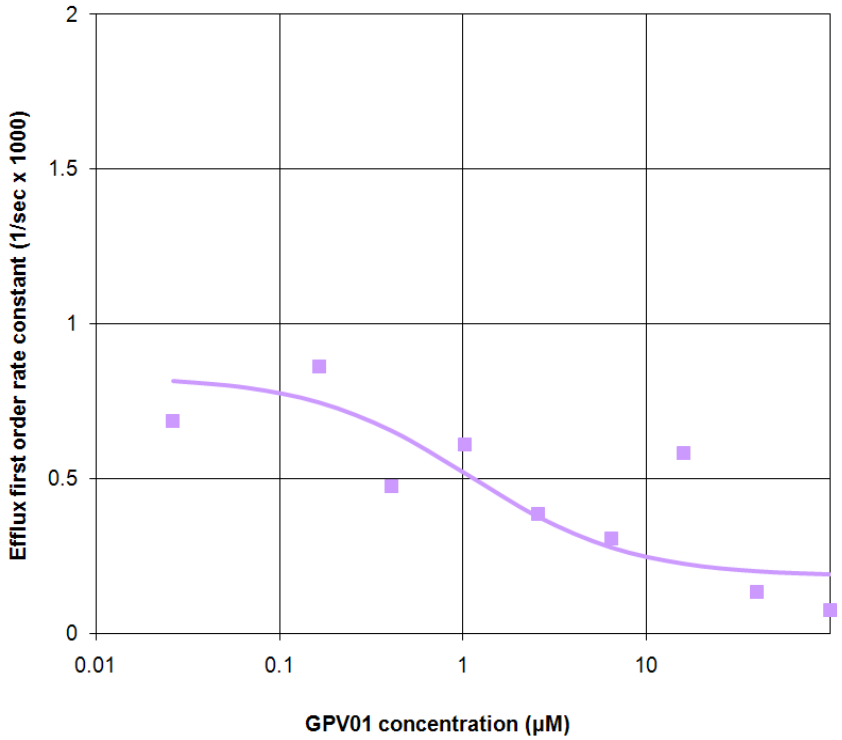

Figure 4.51: Dose-response curve for compound GPV01, showing the effect on the rhodamine 123 efflux rate in G185V-Q773E P-gp expressing NIH3T3 cells. From measurements in the absence and presence of 8 different concentrations of the propafenone analogue GPV01, IC_{50} values were calculated using a hyperbolic curve fit.

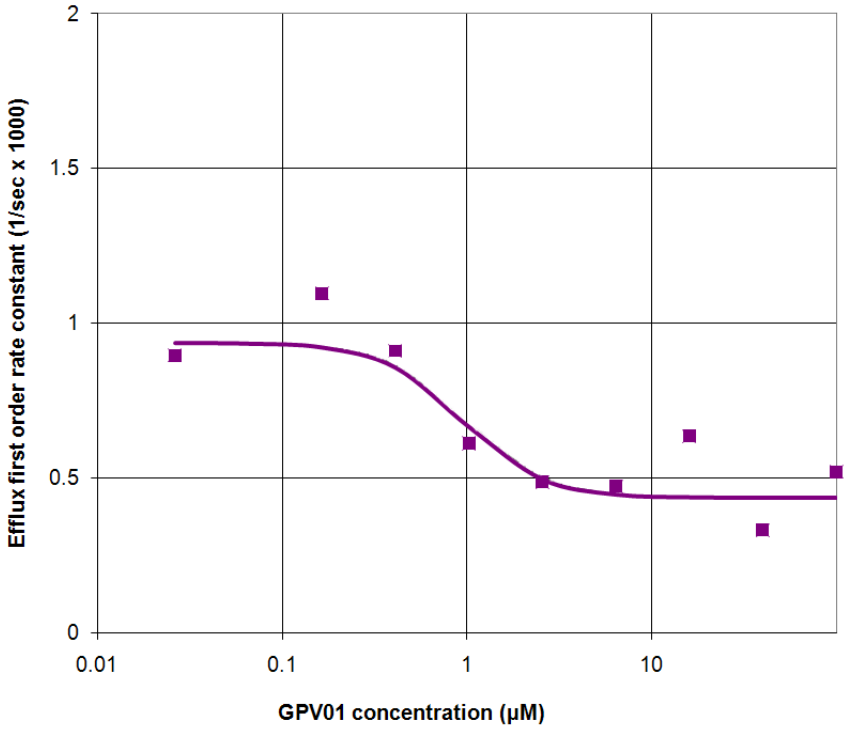

Figure 4.52: Dose-response curve for compound GPV01, showing the effect on the rhodamine 123 efflux rate in G185V-Q132E/Q773E P-gp expressing NIH3T3 cells. From measurements in the absence and presence of 8 different concentrations of the propafenone analogue GPV01, IC_{50} values were calculated using a hyperbolic curve fit.

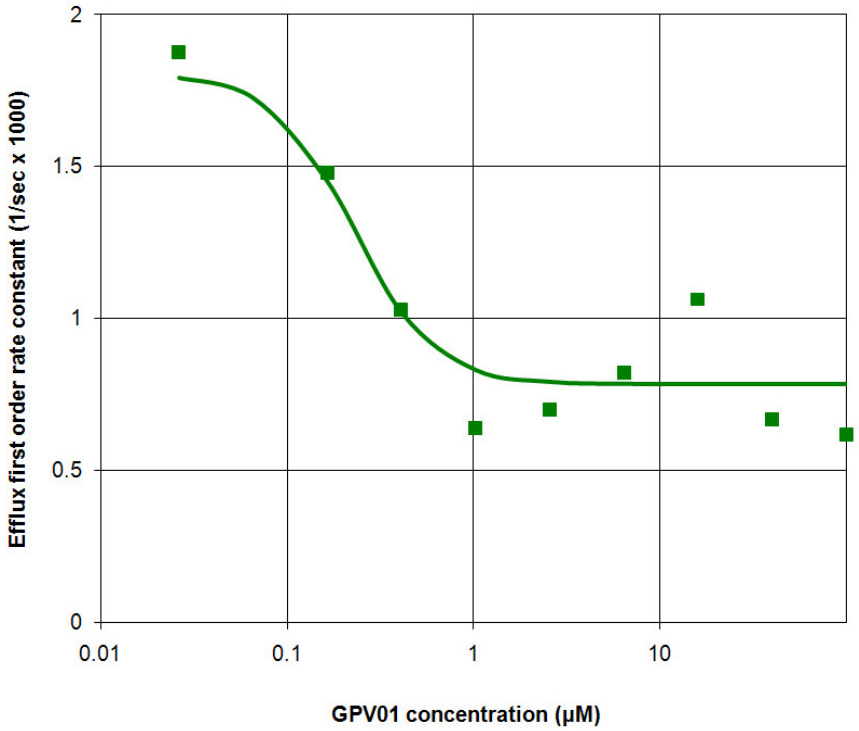

Figure 4.53: Dose-response curve for compound GPV01, showing the effect on the rhodamine 123 efflux rate in G185V P-gp expressing NIH3T3 cells. From measurements in the absence and presence of 8 different concentrations of the propafenone analogue GPV01, IC_{50} values were calculated using a hyperbolic curve fit.

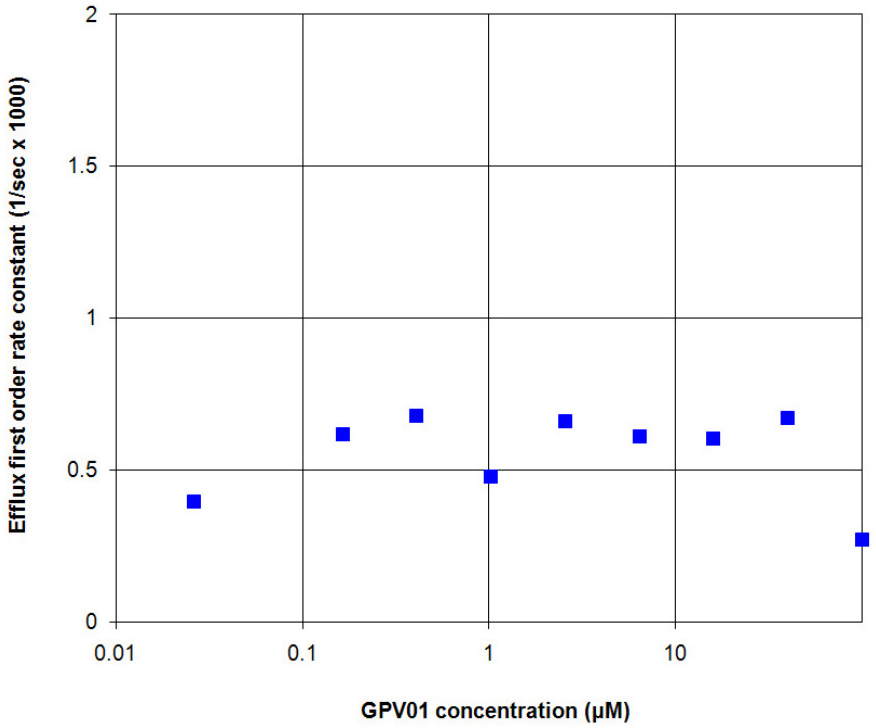

Figure 4.54: Dose-response curve for compound GPV01, showing the effect on the rhodamine 123 efflux rate in mock transfected NIH3T3 cells in the absence and presence of 8 different concentrations of the propafenone analogue GPV01.

The IC_{50} values for Q132E and Q773E in the G185V background were 0.74 µM (95% CI: 0.40 µM – 1.08 µM, N=3) and 0.98 µM (95% CI: 0.78 µM – 1.19 µM, N=2). For the double E mutant the IC_{50} value was 0.98 µM (95% CI: 0.91 µM – 1.04 µM, N=2). All E mutants showed similar IC_{50} values compared to G185V and wt P-gp.

The R mutants' combination Q132R, Q773R and Q132R/Q773R in the G185V background were also tested and compared with G185V P-gp and mock transfected cells in the same rhodamine 123 efflux experiments.
Because of the fact that the R mutants did not show trafficking to the plasma membrane the cells were shifted to a growth temperature of 28°C. Cells cultured at a growth temperature of 37°C were analyzed in parallel. The expression level increased in all of the R mutants at 28°C (Figure 4.55).

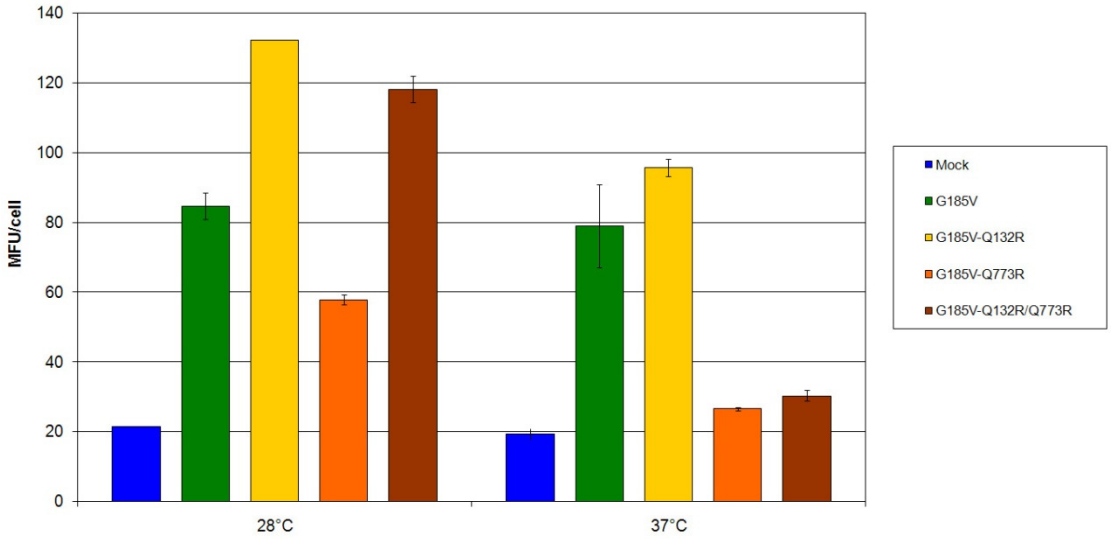

Figure 4.55: MRK16 staining of G185V P-gp, Q132R, Q773R and Q132R/Q773R P-gp mutants in G185V background, and mock transfected cells. The cells were shifted to a growth temperature of 28°C prior to assessing substrate flux. In parallel, a growth temperature of 37°C was selected for comparison. Experiments in each cell line were performed in duplicate.

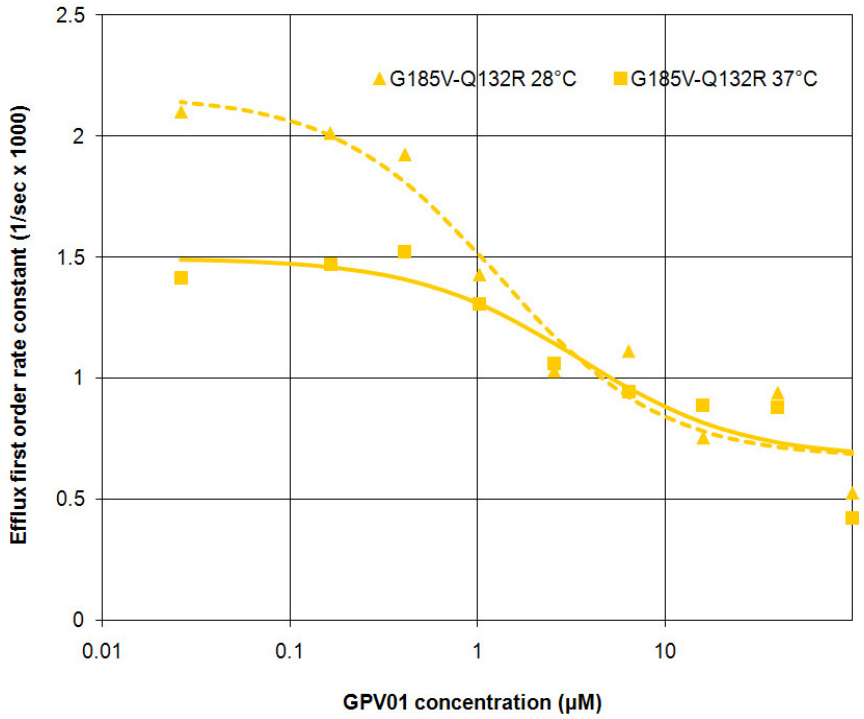

Figure 4.56: Dose-response curve for compound GPV01, showing the effect on the rhodamine 123 efflux rate in G185V-Q132R P-gp expressing NIH3T3 cells at 28°C and 37°C. From measurements in the absence and presence of 8 different concentrations of the propafenone analogue GPV01, IC_{50} values were calculated using a hyperbolic curve fit.

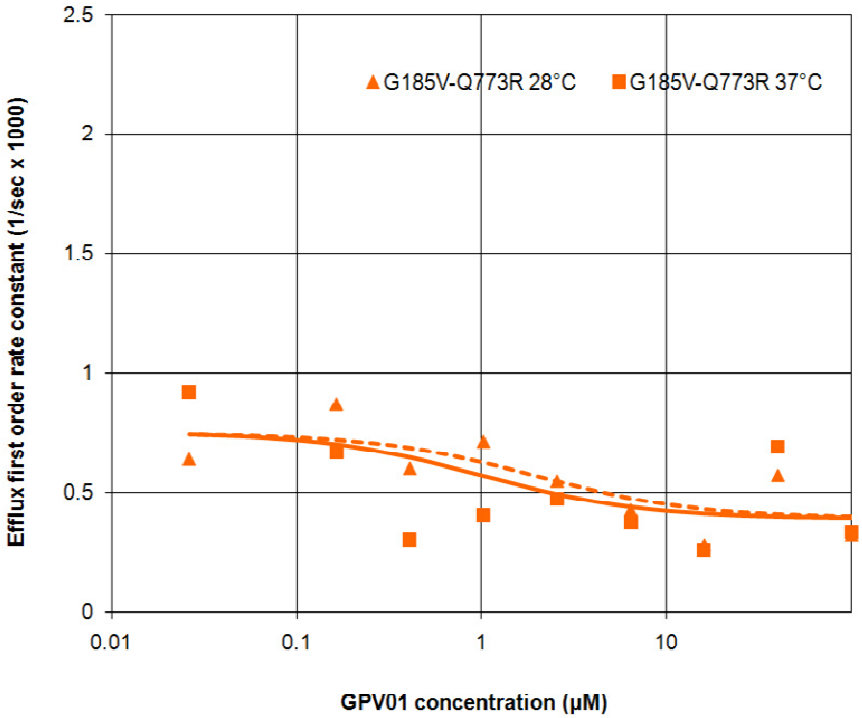

Figure 4.57: Dose-response curve for compound GPV01, showing the effect on the rhodamine 123 efflux rate in G185V-Q773R P-gp expressing NIH3T3 cells at 28°C and 37°C. From measurements in the absence and presence of 8 different concentrations of the propafenone analogue GPV01, IC_{50} values were calculated using a hyperbolic curve fit.

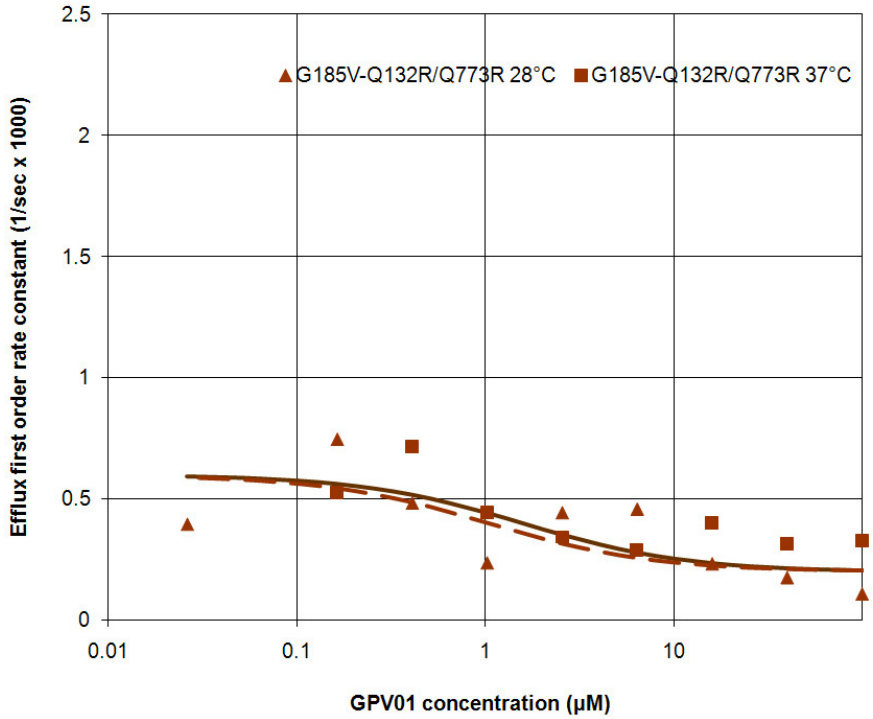

Figure 4.58: Dose-response curve for compound GPV01, showing the effect on the rhodamine 123 efflux rate in G185V-Q132R/Q773R P-gp expressing NIH3T3 cells at 28°C and 37°C. From measurements in the absence and presence of 8 different concentrations of the propafenone analogue GPV01, IC_{50} values were calculated using a hyperbolic curve fit.

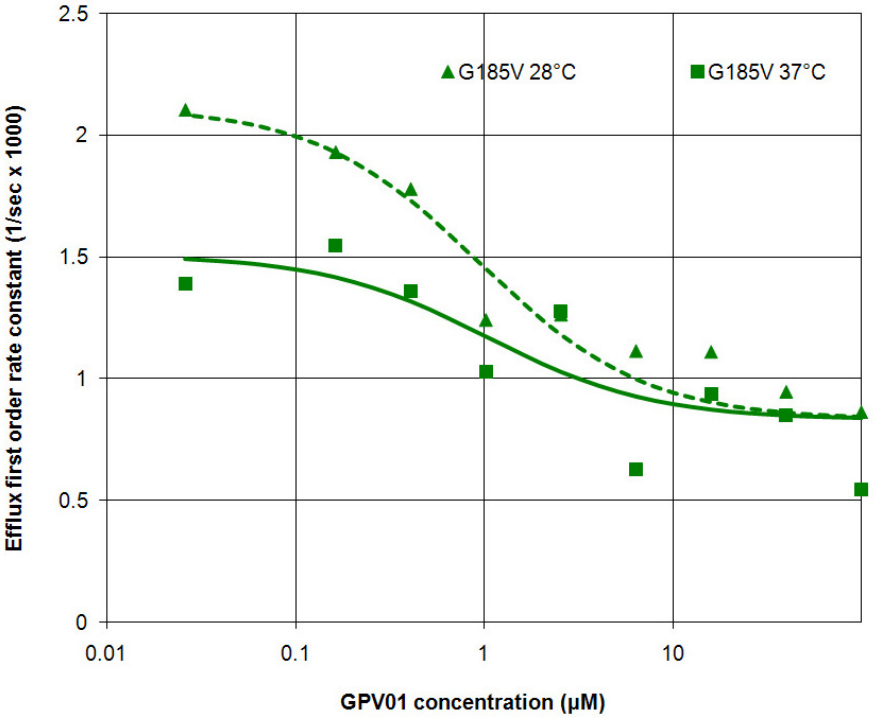

Figure 4.59: Dose-response curve for compound GPV01, showing the effect on the rhodamine 123 efflux rate in G185V P-gp expressing NIH3T3 cells at 28°C and 37°C. From measurements in the absence and presence of 8 different concentrations of the propafenone analogue GPV01, IC_{50} values were calculated using a hyperbolic curve fit.

At 37°C the IC_{50} values for Q132R and Q773R in the G185V background were 2.89 µM (95% CI: 1.77 µM – 4.01 µM, N=2) and 1.10 µM. For the double mutant Q132R/Q773R the IC_{50} value was 1.59 µM.

The IC_{50} values at 28°C for Q132R and Q773R in the G185V background were 1.30 µM (95% CI: 1.30 µM – 1.30 µM, N=2) and 1.16 µM (95% CI: -0.42 µM – 2.74 µM, N=2). For the double R mutant the IC_{50} value was 2.20 µM.

It was not possible to calculate IC_{50} values for all rhodamine 123 efflux experiments for the Q773R at 37°C and for the double R mutant at either temperature, 28°C or 37°C, in the G185V background, since some mutants showed a similar behaviour as the mock transfected cells – i.e. did not show a concentration dependent difference in flux rates.

For compound GPV01 as an inhibitor, the IC_{50} values for G185V were 0.78 µM (95% CI: 0.49 µM – 1.07 µM, N=10) at 37°C and 0.78 µM (95% CI: 0.62 µM – 0.94 µM, N=6) at 28°C. Mock transfected cells did not show a concentration dependent difference in flux rates indicating that membrane diffusion is not changed by the inhibitor.

All rhodamine 123 zero trans experiments are summarized in Table 4.5.

Temperature	Cell line	average IC50 (µM)	95% CI lower limit	95% CI upper limit	N for IC50	average FORC (1/sec x 1000)	95% CI lower limit	95% CI upper limit	N for FORC
37°C	G185V	0.78	0.49	1.07	10	1.55	1.44	1.65	17
37°C	WT	0.73	0.62	0.84	3	1.46	1.33	1.59	8
37°C	G185V-Q132A	0.66	0.52	0.81	2	0.82	0.61	1.03	2
37°C	G185V-Q773A	0.57	0.24	0.90	2	0.92	0.65	1.19	2
37°C	G185V-Q132A/Q773A	1.64	-0.13	3.40	2	0.69	0.50	0.88	2
37°C	G185V-Q132E	0.74	0.40	1.08	3	1.72	1.53	1.92	4
37°C	G185V-Q773E	0.98	0.78	1.19	2	0.74	0.62	0.86	4
37°C	G185V-Q132E/Q773E	0.98	0.91	1.04	2	0.91	0.86	0.97	4
37°C	G185V-Q132R	2.89	1.77	4.01	2	1.35	1.22	1.48	2
37°C	G185V-Q773R	1.10			1	0.75	0.58	0.92	3
37°C	G185V-Q132R/Q773R	1.59			1	0.63	0.59	0.67	2
37°C	Q773A	0.67	-0.30	1.64	2	1.40	1.00	1.81	2
37°C	Q773E	1.80	0.11	3.49	2	1.07	0.96	1.18	2
37°C	Q773R	3.02	-0.60	6.64	2	0.71	0.70	0.72	2
37°C	Mock				13	0.59	0.51	0.67	14
28°C	G185V	0.78	0.62	0.94	6	1.79	1.66	2.31	6
28°C	WT	0.60			1	1.58			1
28°C	G185V-Q132A	0.58	0.20	0.95	3	1.32	1.81	2.35	3
28°C	G185V-Q773A	0.24	0.18	0.31	3	1.14	1.31	2.28	3
28°C	G185V-Q132A/Q773A	1.06	-0.19	2.31	3	1.32	1.38	2.30	3
28°C	G185V-Q132R	1.30	1.30	1.30	2	2.01	1.84	2.19	2
28°C	G185V-Q773R	1.16	-0.42	2.74	2	0.72	0.56	0.88	2
28°C	G185V-Q132R/Q773R	2.20			1	0.47	0.34	0.59	2
28°C	Q773A	0.52			1	1.79			1
28°C	Q773E	1.03			1	2.82			1
28°C	Q773R	0.77			1	1.35			1
28°C	Mock				4	1.20	0.42	0.83	4

Table 4.5: IC_{50} and FORC values of the propafenone analogue GPV01 for G185V P-gp, wt P-gp, and P-gp mutants in the G185V and wt background. IC_{50} values for inhibition of P-gp and P-gp mutants were obtained in rhodamine 123 efflux experiments. It was not possible to calculate IC_{50} values for mock transfected cells. In addition to the IC_{50} values, FORCs were calculated for P-gp, P-gp mutants and mock transfected cells. Values in parentheses brackets correspond to the 95% confidence interval (CI).

Rhodamine 123 zero trans efflux analysis revealed that all mutants except G185V-Q773R and G185V-Q132R/Q773R showed similar activity as compared to G185V cells. Each mutant in the G185V background was tested in at least two independent experiments. IC_{50} values for G185V P-gp and P-gp mutants in the G185V background inhibition using GPV01 were compared. Wt P-gp and some P-gp mutants in the wt background were also tested. Table 4.5 summarizes the IC_{50} values for inhibition of P-gp mediated rhodamine 123 efflux. Values in parentheses correspond to the 95% confidence interval (CI). The transporters behaved differently with respect to inhibition by GPV01 resulting in different IC_{50} values for each mutant. GPV01 showed the strongest modulating activity for G185V-Q773A, followed by G185V-Q132A both at 37°C and 28°C (see Table 4.5). The IC_{50} value for G185V-Q132A was 0.66 µM (95% CI: 0.52 µM – 0.81 µM, N=2) at 37°C and 0.58 µM (95% CI: 0.20 µM – 0.95 µM, N=3) at 28°C. The arginine mutants required expression at 28°C for maturation of P-gp.

Table 4.5 shows the non-normalized FORCs. The mock transfected cells showed a FORC of 0.59 1/sec x 1000 (95% CI: 0.51 – 0.67, N=14) at 37°C and 0.62 1/sec x 1000 (95% CI: 0.42 – 0.83, N=4) at 28°C. These results showed that the temperature shift had no influence on flux (diffusion) rates in NIH 3T3 cells and that expression of endogenous mouse P-gp was thus not detectable. To compare different flux rates in mutants to each other, transport rates have to be normalized for expression rates (shown in Figure 4.60, Figure 4.61 and Figure 4.62). As noted before, the slope of this relationship is a reflection of the pump activity. The slopes of the linear regressions are summarized in Table 4.6.

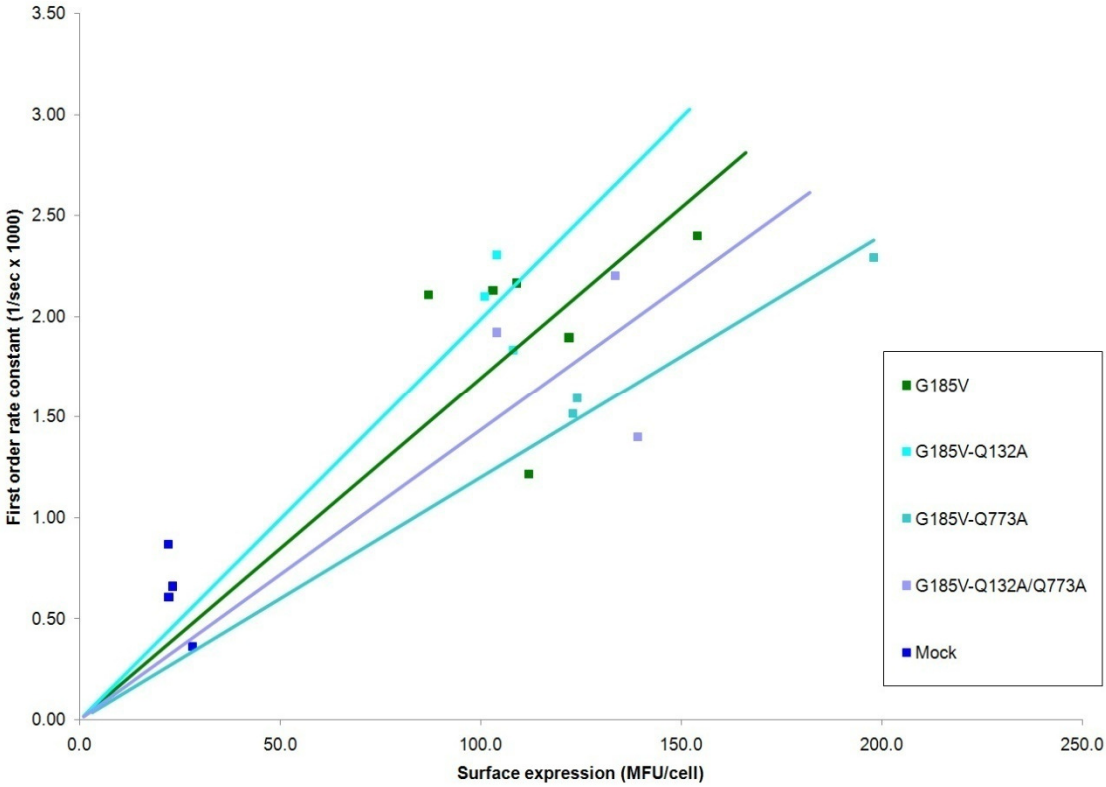

Figure 4.60: Correlation (origin forced to 0) of surface expression (measured by MRK16 staining) and FORC for G185V P-gp, Q132A, Q773A and Q132A/Q773A P-gp mutants in G185V background. The cells were shifted to a growth temperature of 28°C prior to performing the experiments.

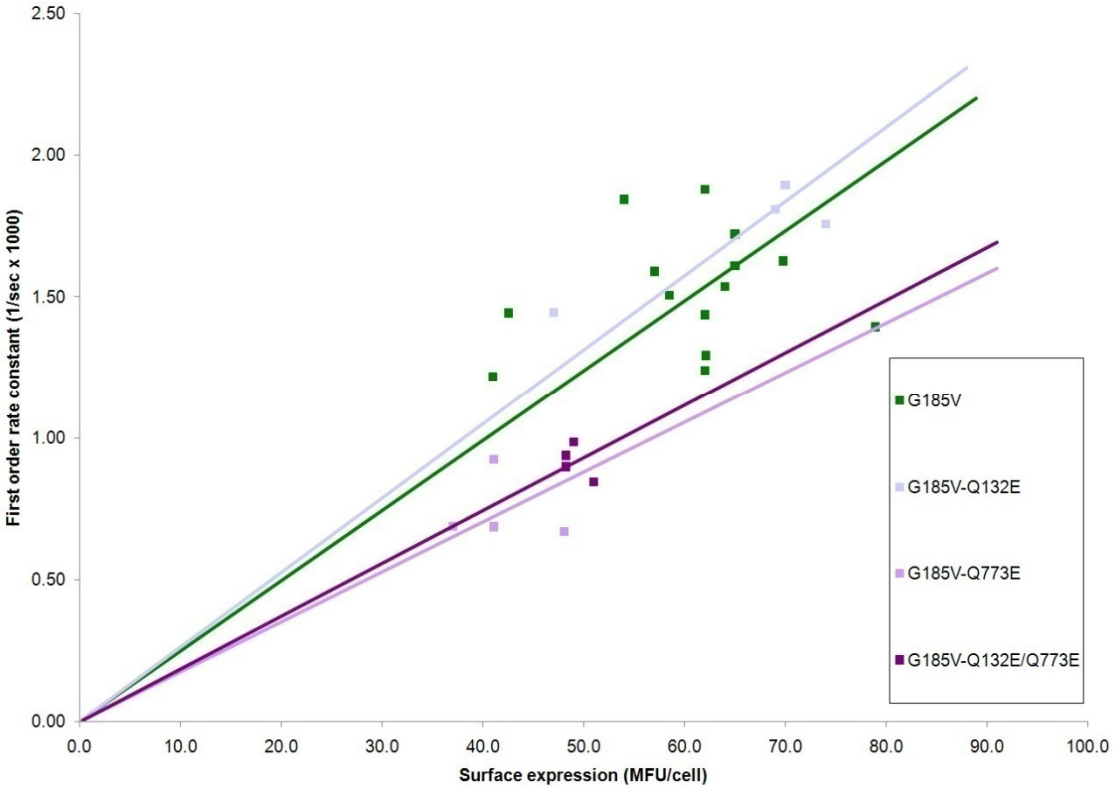

Figure 4.61: Correlation (origin forced to 0) of surface expression (measured by MRK16 staining) and FORC for G185V P-gp, Q132E, Q773E and Q132E/Q773E P-gp mutants in G185V background.

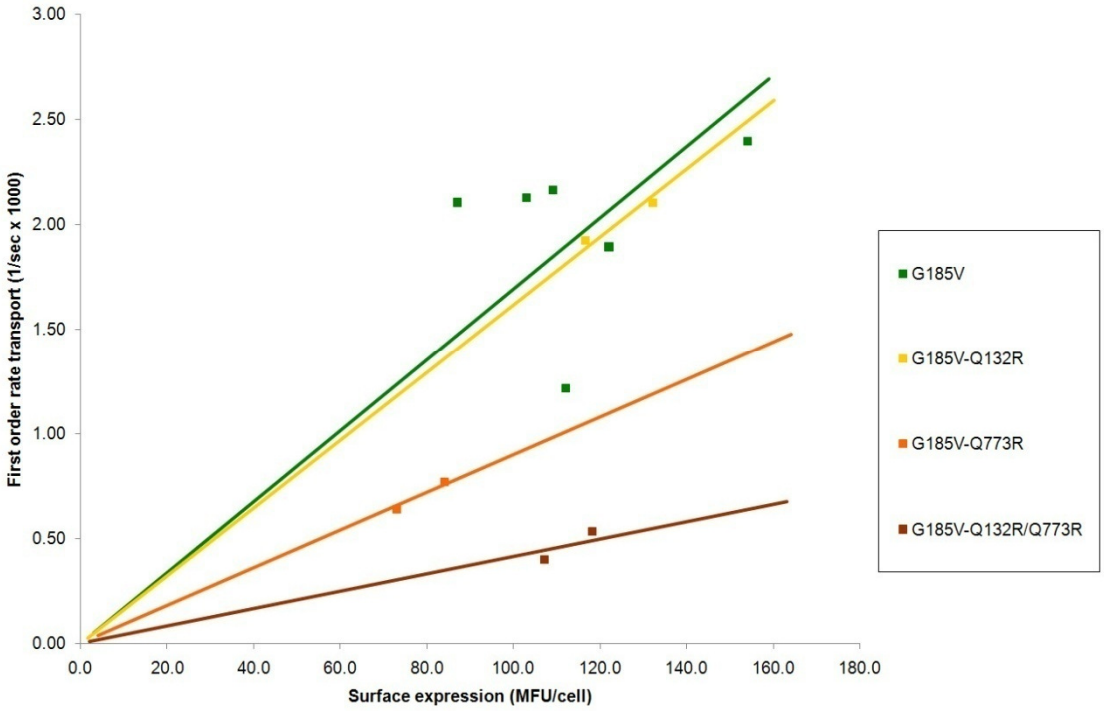

Figure 4.62: Correlation (origin forced to 0) of surface expression (measured by MRK16 staining) and FORC for G185V P-gp, Q132R, Q773R and Q132R/Q773R P-gp mutants in G185V background. The cells were shifted to a growth temperature of 28°C prior to performing the experiments.

Temperature	Cell line	slope	N	r	p	% of G185V
37°C	G185V	0.0247	14	0.997	0.006	100
37°C	G185V-Q132E	0.0262	4	0.999	0.079	106
37°C	G185V-Q773E	0.0176	4	0.999	0.444	71
37°C	G185V-Q132E/Q773E	0.0186	4	1.000	0.444	75
28°C	G185V	0.0169	6	1.000	0.288	100
28°C	G185V-Q132A	0.0199	3	1.000	0.706	118
28°C	G185V-Q773A	0.0120	3	1.000	0.860	71
28°C	G185V-Q132A/Q773A	0.0144	3	1.000	0.799	85
28°C	G185V-Q132R	0.0162	2	1.000		96
28°C	G185V-Q773R	0.0090	2	1.000		53
28°C	G185V-Q132R/Q773R	0.0042	2	1.000		25

Table 4.6: Pump activity of G185V P-gp and mutant P-gps. The slopes were obtained through linear regression of FORC versus surface expression (MFU value). N: number of data points that were used, r: correlation coefficient, and p: significance.

The most active mutants in the G185V background were Q132A, Q132E and Q132R. The Q132A mutant showed 118% pump activity of G185V control, Q773A and the double A mutant showed 71% and 85%, respectively. The pump activity for the Q132E, Q773E and double E mutants were 106%, 71% and 75% of G185V control. The results for Q132R, Q773R and Q132R/Q773R mutants were 96%, 53% and 25%. The most A and R mutants at 37°C were not analyzed due to their poor efflux pump activity which was close to that of the mock transfected cells and as such not interpretable by linear regression.

5 Discussion

The escape of cancer cells from chemotherapy through activation of MDR mechanisms is a major reason for treatment failure in systemic (metastasized) cancers. Since the discovery of P-gp, many groups have focussed on understanding how a single protein is capable of transporting so many unrelated compounds. Due to the broad substrate recognition, it has been a challenge to predict effects of disrupting P-gp-mediated transport (Yang, Wu et al. 2008).

During the course of this project, four structures for complete ABC transporters were published: the metal-chelate-type transporter HI1470/1 from *Haemophilus influenzae* (Pinkett, Lee et al. 2007), the molybdate transporter ModBC from *Archaeoglobus fulgidus* in complex with its binding protein (ModA) (Hollenstein, Frei et al. 2007), and two structures of Sav1866 (one bound to the nucleotide analogue AMP-PNP, and another with ADP) (Dawson and Locher 2006; Dawson and Locher 2007). The recent publication of the high resolution crystal structure of Sav1866 was a significant advance in the understanding of the molecular mechanism of ABC transporter function (Zolnerciks, Wooding et al. 2007). Following publication of the Sav1866 structure several previously lower resolution MsbA structures were retracted.

Upon issuing of this thesis, the x-ray structure of mouse P-gp (ABCB1), which has 87% sequence identity to human P-gp, was described by Aller et al. in Chang's group (Aller, Yu et al. 2009). Chang's group determined apo and drug-bound P-gp structures. The apo P-gp at 3.8 Å represents a nucleotide-free inward-facing conformation forming two bundles of six transmembrane helices (TMs 1, 2, 3, 6, 10, 11 and TMs 4, 5, 7, 8, 9, 12). This results in a large internal cavity of ~6000 Å open to both the cytoplasm and the inner leaflet, cubed with a 30 Å separation of the two nucleotide-binding domains. In addition, Chang's group described two P-gp structures with cyclic peptide inhibitors, cyclic-*tris*-(R)-valineselenazole (QZ59-RRR) and cyclic-*tris*-(S)-valineselenazole (QZ59-SSS). These drug-bound P-gp structures reveal distinct drug-binding sites in the internal cavity.

The Sav1866 structures represented good templates for the clinically relevant P-gp. This ABC-half transporter is a member of the MDR-class, and is homologous to both the N- and C-terminal halves of human P-gp.

The ATP-switch model is the product of biochemical data interpreted in the light of advances in structure determination for several ABC transporters. Recently, Linton and

Higgins (Linton and Higgins 2007) postulated that the different conformations of P-gp might have different affinities for drug substrates. It is possible that conversion of different sites, from high- to low-affinity states, may take place during different stages of the reaction cycle (Loo, Bartlett et al. 2007).

The aim of this project at initiation was to investigate the role of conserved amino acids in the molecular mechanism of the human multidrug transporter, P-glycoprotein. Identification of the drug-binding sites in P-gp would help to understand the mechanism of drug interaction and transport. Studies on the TMDs suggested that the drug-binding sites lie within the TMDs because the TMDs alone retain the ability to interact with a variety of drug substrates in the absence of both ATP-binding domains (Loo and Clarke 1999). P-gp has been reported to contain multiple operationally defined drug-binding sites. It contains two distinct binding sites for rhodamine 123 (R-site) and Hoechst 33342 (H-site) and a third site which binds prazosin and progesterone (Shapiro and Ling 1997; Shapiro, Fox et al. 1999). The presence of at least four distinct drug interaction sites on P-gp was detected using radioligand binding studies (Martin, Berridge et al. 2000). Mapping the residues that line the drug-binding sites has been a challenging task. P-gp can bind dozens of structurally unrelated compounds, multiple drug substrates can bind at the same time (Loo, Bartlett et al. 2003; Lugo and Sharom 2005), and binding of drug substrate may occur by an induced-fit mechanism (Loo, Bartlett et al. 2003). However, the mechanism of drug binding is complex. The group of David Clarke used cysteine mutagenesis and reaction with thiol-reactive drug substrates such as MTS-verapamil (Loo and Clarke 2001; Loo, Bartlett et al. 2006; Loo, Bartlett et al. 2006) and MTS-rhodamine (Loo and Clarke 2002; Loo, Bartlett et al. 2007) to map the locations of the drug-binding sites. The generation of a cysteine-less P-gp mutant in which all cysteine residues were replaced with alanine was first described by Loo and Clarke (Loo and Clarke 1995). The removal of endogenous cysteine residues from P-gp has a minimal impact upon the function of the protein, thus the use of cysteine-less P-gp in cysteine mutagenesis and cross-linking studies is justified. For example, Blott *et al.* showed, that this cysteine-less P-gp transported the fluorescent dye rhodamine 123 with similar efficiency to wild-type protein (Blott, Higgins et al. 1999).
The observation that TMD-NBD interactions are important for folding and activity has been reported for CFTR (Serohijos, Hegedus et al. 2008).

Our group showed the participation of multiple TM segments in mediating P-gp-drug interactions by photolabelling of P-gp with drug analogues, followed by analysis by MALDI-TOF mass spectrometry (Ecker, Csaszar et al. 2002; Pleban, Kopp et al. 2005). The initial homology model of P-gp generated by our group was generated based on the MsbA template structure, which was the only available structure at this time (Chang and Roth 2001; Chang 2003; Seigneuret and Garnier-Suillerot 2003; Stenham, Campbell et al. 2003; Pleban, Kopp et al. 2005; Reyes and Chang 2005). In the resulting homology model both amino acids Q132 (TM2) in the N-terminal half and Q773 (TM8) in the C-terminal half were in close proximity to the binding sites that were detected using the photoaffinity labelling. These glutamine residues align with each other in alignments of the N- and C-terminal half of P-gp and were considered to be located between the most strongly photolabelled residues F951 and M197 at the TM3/TM11 interface, and A311 and T769 at the TM5/TM8 interface. Q132 and Q773 were also predicted to form H-bonds with propafenone type ligands in data driven docking experiments (Shown in Figure 2.8 and Figure 2.9). Studies in our lab were performed to clarify the P-gp-mediated transport mechanisms by replacement of Q132 and Q773 by nonpolar alanine residues, positively charged arginine or negatively charged glutamic acid residue, individually, or in combination. Results indicating that a charge is tolerated in this position of the protein were obtained. A replacement was expected to lead to altered substrate binding characteristics and transport. This was confirmed for rhodamine 123 efflux. P-gp drug transport activity requires interactions between the two halves of the molecule, although they do not have to be covalently linked. A functional transporter could only be generated when the two half-molecules were co-expressed in the same cells (Loo and Clarke 1996; Loo and Clarke 1998). We expected that the substitution of Q132 and Q773 with alanine, individually or in combination, does not cause a change that is large enough to abolish binding of a drug completely, but if these residues would be close to the substrate recognition site, a substitution with arginine was expected to disrupt P-gp interactions with some drug substrates because of its relatively large and positively charged side chain. Initial studies on P-gp using arginine mutagenesis showed that introduction of arginines at some positons in TM1 disrupts binding of some drugs (Taguchi, Kino et al. 1997). For a negatively charged substitution glutamic acid was chosen.

To examine our hypothesis, nine P-gp mutants were generated in the pEF5 vector in order to examine their impact on P-gp cell surface expression and on P-gp function.

Using stable FlpIn HEK 293 or NIH 3T3 cell lines, expressing either *MDR,* wild-type or *MDR1* mutants, we have characterised the functional differences between cells expressing wild-type and mutant P-gp. Expression and function were measured by FACS analysis using MRK16 staining, cytotoxicity assays and rhodamine 123 efflux in the presence of propafenone analogues. The mutants were generated in the wt and in the G185V background. The latter represents a gain of function mutation for the transport of rhodamine 123 and was thus expected to improve the signal to noise ratio for mutants with low expression levels of P-gp. The amino acid sequence of proteins is generally believed to determine protein expression, folding and function. Thus, mutations which alter the primary structure of a protein can affect these properties. Mutations that cause an amino acid change in a corresponding protein are often responsible for genetic changes known to cause disease. A common observation is, that mutant proteins synthesized in the endoplasmatic reticulum are defective in folding and trafficking, leading to reduced levels or absence of functional protein at a required location, because most is degraded soon after synthesis in the endoplasmic reticulum. Maturation of processing mutants can be induced by chemical or pharmacological chaperones or by expression at low temperature.

Because of the fact that our mutations are located at the TMD domain interface, not all mutants showed uncompromised trafficking to the plasma membrane. This was remedied by either adding cyclosporin A at a concentration of 10 µM for 24 hours or by shifting cells to a growth temperature of 28°C. Expression in the presence of drug substrate CsA induced maturation of the P-gp mutants. Inducing maturation of P-gp mutants by growth at lower temperatures also correctly targeted the protein to the membrane. We found that CsA does not modify the expression of any of the *MDR1* genes containing the mutation by SYBR green real-time reverse transcription PCR. Nevertheless, shifting the cells to a growth temperature of 28°C to induce maturation of processing mutants was given preference, because it proved difficult to completely remove CsA from the cultures prior to assessing substrate efflux.

The expression level of P-gp in different mutants was shown in comparison to wt P-gp, G185V P-gp and mock transfected cells. P-gp expression was similar for wt and G185V P-gp. The Q132E mutant in the G185V background showed a slightly higher expression level in comparison to G185V P-gp. The same effect was observed for the Q132R, the double R and Q773A mutants in the G185V background after a shift to a growth temperature of 28°C. A temperature shift promoted expression of all mutant P-gps. The

expression level was similar for the Q132A and Q132A/Q773A mutants in the G185V background after a shift to a growth temperature of 28°C. At 37°C the double A mutant had a somewhat higher expression level than the mock transfected cells. Reducing the growth temperature of the cells expressing double A, Q773R or double R mutation below 30°C resulted in a portion of the mutant protein trafficking to the plasma membrane. The Q132A and double A mutants showed a somewhat decreased expression compared to the G185V P-gp. The same pattern was observed for the Q773R, Q773E and double E mutants in the G185V background. An exactly identical expression was not required, because first order rate constants of efflux were determined in a zero trans efflux protocol. These rate constants can directly be related to protein expression rates.

In order to obtain evidence that the resulting protein products are indeed functionally expressed, rhodamine 123 zero trans efflux studies were used for mutant characterisation, because they yield first order rate constants which are directly related to transporter expression rates. Cells were preloaded with rhodamine 123 for 30 min; after this time a steady state of fluorophore accumulation was reached. Transport activities of mutated P-gps were measured by determining the accumulation of rhodamine 123 in the absence and presence of different concentrations of the P-gp inhibitor GPV01. When cells were incubated at 37°C, there was a decrease in the fluorescence of cells due to P-gp-mediated rhodamine 123 efflux, indicating that P-gp actively extruded rhodamine 123 from the cells.

In contrast, in the presence of GPV01, rhodamine 123 fluorescence increased depending on the GPV01 concentration, indicative of inhibition of P-gp transport. IC_{50} values of GPV01 were calculated from dose-response curves of FORC (V_{max}/K_m) versus GPV01 concentration. Different IC_{50} values were observed for each kind of P-gp mutant indicating different modulating activity and interaction properties with those membrane pumps.

All alanine single mutants were active. The Q773A and Q132A/Q773A showed only somewhat decreased pump activity as compared to wt and G185V P-gp. In contrast to the G185V background, the Q132A mutant showed an increased pump activity. This indicated that the glutamine residues are not directly involved in interaction with rhodamine 123. The Q132E, showing a slightly increased pump activity, and Q132R mutants also were fully functional. Compared to the G185V background, the Q773E mutant showed a decreased pump activity, while the Q773R mutant showed a deficient pump activity compared to G185V P-gp. The Q132A/Q773A and Q132E/Q773E mu-

tants also were functional, while the Q132R/Q773R mutant was dysfunctional, the latter apparently being impaired functionally by the Q773R mutation alone.
The reduction in affinity of mutants Q773R and Q132R/Q773R in the G185V background for rhodamine at both 28°C and 37°C growth temperatures is consistent with the observation that they had reduced ability to confer resistance to rhodamine123 in cytotoxicity studies. The mock transfected cells showed a higher IC_{50} value than the Q132R/Q773R double mutant, suggesting that the negative effect of the Q773R mutation could not be compensated by a Q132R mutation. The higher IC_{50} value of the Q132E/Q773E double mutant compared to the Q773E mutant in cytotoxicity assays may thus also be explained by a compensatory influence of the Q132E mutation.

An explanation for the observation that the mutants Q773R had much lower and Q132R/Q773R had no transport activity may be explained by the fact that an arginine residue in position 773 appears to reduce P-gp interaction with rhodamine 123 because of its positively charged side chain.

Like many P-gp substrates, rhodamine 123 is a protonatable compound, which, after entering the central water filled cavity, is likely to be present in a charged form. This indicates that charge repulsion might be responsible for the inability of the mutant to transport rhodamine 123. In addition, these results indicate that residue 773 but not residue 132 may be close to the rhodamine binding site.
Our data show that the nature of the amino acid side chain at position 132 and 773 strongly influences the function of P-gp. Nevertheless, the majority of the mutants were capable of transporting rhodamine 123. Small side chains at these positions result in proteins with only modest changes in substrate specificity. One mutant, G185V-Q773R, did not transport rhodamine 123 well. Transmembrane segments can change their shape to accommodate structurally different compounds. Thus, slight rotational and/or lateral movement in any transmembrane segment could result in numerous permutations of residues contributing to the drug-binding site. A substrate with one structure would cause specific shifts in the different transmembrane segments responsible for its binding (induced-fit) (Rosenberg, Velarde et al. 2001).
Several residues line the TMD/TMD contact interfaces in helices 2, 5, 8 and 11, indicating that mobility at these interfaces is required for function (Loo, Bartlett et al. 2004).

In summary our data indicate that residue 773 in P-gp plays an important role in the activity of the transporter, but may not be directly involved in the interaction between P-gp and its substrates. During the transport cycle, P-gp displays different affinities for its substrates and alternates between high-affinity and low-affinity binding sites (Sauna and Ambudkar 2000; Higgins and Linton 2004). It is possible that the transport-deficient P-gp Q773R mutant is unable to undergo conformational changes required for substrate transport. Substrate might be bound, but not released and therefore not be transported effectively. ABC transporters change conformations and affinities for substrates throughout the transport cycle. It is difficult to draw conclusions about the role this specific arginine residue may play in determining conformational changes, substrate interactions and transport function of P-gp. These results are consistent with alanine-scanning mutagenesis of P-gp which was not successful in mapping the drug-binding sites in P-gp (Loo and Clarke 1993) because most mutations either had no effect or caused only modest changes in substrate specificity. Initial studies on P-gp using arginine mutagenesis showed that introduction of arginines at some positions appeared to disrupt P-gp interactions with some drug substrates (Taguchi, Kino et al. 1997). Based on these considerations, we propose that the amino acid replacements at these two sites affect the ability of a drug to enter the binding pocket or to make appropriate binding contacts that trigger hydrolysis of ATP and the subsequent efflux of the drug.

The transfer of rhodamine 123 through the cell membrane from the inside to the outside involves both, passive diffusion and active transport by either P-gp or other transporters. To control for passive diffusion as well as the action of other transporters, FlpIn 3T3 cells were transfected with the empty pEF5 vector. These mock transfected cells served as control.

In particular, we hoped to determine whether the charged side chains participated in substrate recognition and binding. Mutations to A132, E132, R773 and R132/R773, substantially altered the ability of the protein to confer resistance to rhodamine 123. The R132 mutation had a surprisingly high level of activity.

Further studies are necessary to clarify the role of these two glutamine residues. The present analyses have not yet reveiled changes in substrate specificity of P-gp because only a limited number of substrates and inhibitors was used. Therefore, investigating additional substrates and inhibitors will be necessary to demonstrate the relevance of these two amino acids. We also attempted to study mitoxantrone as a solute in steady state experiments. Here the endogenous P-gp was a handicap because no difference be-

tween G185V P-gp and mock transfected cells was observed (data not shown). An explanation for this observation may be that the expression level of the G185V P-gp is too low and/or mitoxantrone is not as good a P-gp substrate as rhodamine 123.

Another objective of this work was to evaluate the influence of various specific P-gp substrates/ ligands as pharmacological chaperones in order to study the ability of the protein to bind these solutes by monitoring surface expression of trafficking deficient mutants. Several mutations lead to reduced levels or absence of functional protein at the plasma membrane.

In these experiment, we tested whether mutations introduced in TM segments 2 and 8 inhibit maturation of the protein. Surface expression of P-gp and P-gp mutants in HEK 293 and NIH 3T3 cells was monitored by flow cytometry using the selective monoclonal antibody MRK16 and an FITC-labelled secondary antibody. The fluorescence intensity of some P-gp mutants was comparable to the background fluorescence intensity, thus the level of P-gp expression was negligible. Pharmacological chaperones such as cyclosporin A and verapamil are predicted to promote maturation of P-gp processing mutants. In fact, most trafficking deficient P-gp mutants have been shown to be rescued by using CsA as a pharmacological chaperone (Loo, Bartlett et al. 2005). The binding sites for propafenones have previously been characterized by our group using photolabelling (Pleban, Kopp et al. 2005). These sites were suggested to be different from those for verapamil and cyclosporin A. This allowed a screening concept to be applied, which uses the property of specific P-glycoprotein ligands to act as pharmacological chaperones. When the mutants show impaired binding, surface expression of the protein is not altered. The minimal effect the pharmacological chaperones had on P-gp expression in mock transfected cells indicaed that the expression of endogenous mouse P-gp was low.

We used 10 µM CsA, 50 µM verapamil and 50 µM GPV51 as pharmacological chaperones. Interestingly, we noticed that higher GPV51 levels, especially the presence of 300 µM GPV51, did not stimulate maturation of G185V P-gp to an extent that was observed with lower concentrations. The impact of GPV51 on the 773R mutant is higher than on the 132R mutant. This indicates preferential binding to the 2/11 interface. At a concentration of 300 µM GPV51, an increased cell death rate in the mock transfected cell cultures was observed (data not shown), this might be interpreted as a negative influence of GPV51 on protein assembly at this concentration.

DMSO was required as a solvent to prepare solutions of the highly lipophilic compounds CsA and GPV51 stocks. The solvent alone was shown not to have an influence on P-gp expression levels (data not shown). The G185V P-gp, and all mutants in the G185V background were stably expressed in NIH 3T3 fibroblasts. The expression levels of the mutants were increased by a 24 hour pre-treatment with the pharmacological chaperones cyclosporine A, verapamil and GPV51, indicating that these chaperones are still able to bind to the protein. In the case of CsA, these results are consistent with those of Loo and Clarke.

However, GPV51 did not have a considerable impact on P-gp expression in NIH 3T3 cells. G185V P-gp, Q773R and the double mutant Q132R/Q773R in the G185V background were stably expressed in HEK 293 cells, too. The expression level of the 132R/773R double mutant was increased by a 24 hour pre-treatment with CsA, indicating that CsA was still able to bind to the protein. Verapamil increased the expression level, too. As with the NIH 3T3 cell line, the propafenone analogue GPV51 did not have a major impact on the expression level, however relative expression gain was still higher than in the NIH 3T3 cell line.

These observations support our hypothesis that propafenones might have a different binding site than the classical pharmacological chaperones CsA and verapamil, establishing the propafenones as a solitary class of P-gp chaperones.

An understanding of multidrug resistance is of wide clinical importance. MDR1 is associated with drug failure in various cancers. MDR1 is associated with drug resistance in malaria, too. The human malaria parasite *Plasmodium falciparum* possesses a P-gp homologue termed Pgh-1 (Foote, Thompson et al. 1989). Pgh-1 exhibits a domain structure typical of a P-gp-type ABC transporter. Both P-gp and Pgh-1 pump vinblastine (Sanchez, Rotmann et al. 2008). Analogies with P-gp may help explain the transport properties and substrate specificity of Pgh-1, possibly opening a window of opportunity for treatment of patients infected with highly drug resistant malaria parasites.

6 Conclusion

In this study, mutational analyses of two conserved residues within the TMDs of P-gp have shown that the nature of the amino acid residues at position 132 and 773 affects the function of P-gp. These two residues were selected for substitution with alanine, glutamic acid and arginine, individually or in combination. Residue 773 is involved in the active rhodamine 123 efflux transport. The substitution of glutamine at position 773 with arginine markedly decreased the active transport of rhodamine 123. These results indicate that residue 773 but not residue 132 is close to the rhodamine binding site.

7 Outlook

In the present study, we have studied rhodamine 123 transport to evaluate functional changes associated with replacement at amino positions Q132 and Q773 by a nonpolar alanine residue, a positively charged arginine or a negatively charged glutamic acid residue, individually or in combination. Based on ATPase activity measurements of P-gp, we will be able to gain insight into the impact of these replacements. The measurement of drug-stimulated ATPase activity was widely used by different research groups to investigate the function of P-gp. The aim will be to establish whether the different effects described in the previous chapter correlate with ATPase activity. For the analysis of the ATPase activity of the wt and mutant proteins, insect cells are convenient expression systems to produce large quantities of proteins. Therefore, preparation of plasma membrane vesicles from insect cells should be performed. In our lab the preparation of plasma membrane vesicles was performed as described by Schlemmer and Sirotnak (Schlemmer and Sirotnak 1994; Schmid, Ecker et al. 1999). For high yield expression in Sf9 insect cells, the gene was inserted into a baculovirus destination vector, which is compatible with the entry vector. Baculovirus transfer vectors containing G185V, G185V-Q132R, G185V-Q773R, and G185V-Q132R/Q773R are presently ready for transfection of monolayers of Sf9 cells.

References

Aller, S. G., J. Yu, et al. (2009). "Structure of P-glycoprotein reveals a molecular basis for poly-specific drug binding." Science **323**(5922): 1718-22.

Altschul, S. F., W. Gish, et al. (1990). "Basic local alignment search tool." J Mol Biol **215**(3): 403-10.

AmershamBiosciences. (2005). "Manual: GFX PCR DNA and Gel Band Purification Kit." Retrieved 21.06.2009, from http://www.molbiotech.uni-freiburg.de/km/lehre/kurs/GenKurs_2006/Amersham%20GFX%20PCR%20DNA%20and%20Gel%20Band%20Purification%20Kit.pdf.

BectonDickinson. "Simultest™ Control γ2a/γ1 Datasheet." Retrieved 20.06.2009, from http://www.bdbiosciences.com/external_files/is/doc/tds/Datasheets_RUO/live/web_enabled/23-3043-00_g2a_g1_ruo.pdf.

Bernard, P. and M. Couturier (1992). "Cell killing by the F plasmid CcdB protein involves poisoning of DNA-topoisomerase II complexes." J Mol Biol **226**(3): 735-45.

Bernard, P., K. E. Kezdy, et al. (1993). "The F plasmid CcdB protein induces efficient ATP-dependent DNA cleavage by gyrase." J Mol Biol **234**(3): 534-41.

BioRad. (1994). "Manual: Bio-Rad Protein Assay." Retrieved 21.06.2009, from http://www3.bio-rad.com/LifeScience/pdf/Bulletin_9004.pdf.

Birnboim, H. C. and J. Doly (1979). "A rapid alkaline extraction procedure for screening recombinant plasmid DNA." Nucleic Acids Res **7**(6): 1513-23.

Bishop, L., R. Agbayani, Jr., et al. (1989). "Reconstitution of a bacterial periplasmic permease in proteoliposomes and demonstration of ATP hydrolysis concomitant with transport." Proc Natl Acad Sci U S A **86**(18): 6953-7.

Blott, E. J., C. F. Higgins, et al. (1999). "Cysteine-scanning mutagenesis provides no evidence for the extracellular accessibility of the nucleotide-binding domains of the multidrug resistance transporter P-glycoprotein." Embo J **18**(23): 6800-8.

Bodor, M., E. J. Kelly, et al. (2005). "Characterization of the human MDR1 gene." Aaps J **7**(1): E1-5.

Borst, P., R. Evers, et al. (2000). "A family of drug transporters: the multidrug resistance-associated proteins." J Natl Cancer Inst **92**(16): 1295-302.

Broach, J. R., V. R. Guarascio, et al. (1982). "Recombination within the yeast plasmid 2mu circle is site-specific." Cell **29**(1): 227-34.

Broach, J. R. and J. B. Hicks (1980). "Replication and recombination functions associated with the yeast plasmid, 2 mu circle." Cell **21**(2): 501-8.

Brown, C. R., L. Q. Hong-Brown, et al. (1996). "Chemical chaperones correct the mutant phenotype of the delta F508 cystic fibrosis transmembrane conductance regulator protein." Cell Stress Chaperones **1**(2): 117-25.

Buchholz, F., L. Ringrose, et al. (1996). "Different thermostabilities of FLP and Cre recombinases: implications for applied site-specific recombination." Nucleic Acids Res **24**(21): 4256-62.

Bushman, W., J. F. Thompson, et al. (1985). "Control of directionality in lambda site specific recombination." Science **230**(4728): 906-11.

Campain, J. A., M. M. Gottesman, et al. (1994). "A novel mutant topoisomerase II alpha present in VP-16-resistant human melanoma cell lines has a deletion of alanine 429." Biochemistry **33**(37): 11327-32.

Cartier, E. A., L. R. Conti, et al. (2001). "Defective trafficking and function of KATP channels caused by a sulfonylurea receptor 1 mutation associated with persistent hyperinsulinemic hypoglycemia of infancy." Proc Natl Acad Sci U S A **98**(5): 2882-7.

Chang, G. (2003). "Structure of MsbA from Vibrio cholera: a multidrug resistance ABC transporter homolog in a closed conformation." J Mol Biol **330**(2): 419-30.

Chang, G. and C. B. Roth (2001). "Structure of MsbA from E. coli: a homolog of the multidrug resistance ATP binding cassette (ABC) transporters." Science **293**(5536): 1793-800.

Chang, G., C. B. Roth, et al. (2006). "Retraction." Science **314**(5807): 1875.

Chen, C. J., J. E. Chin, et al. (1986). "Internal duplication and homology with bacterial transport proteins in the mdr1 (P-glycoprotein) gene from multidrug-resistant human cells." Cell **47**(3): 381-9.

Chen, E. Y., M. C. Bartlett, et al. (2000). "Cystic fibrosis transmembrane conductance regulator has an altered structure when its maturation is inhibited." Biochemistry **39**(13): 3797-803.

Chen, J., G. Lu, et al. (2003). "A tweezers-like motion of the ATP-binding cassette dimer in an ABC transport cycle." Mol Cell **12**(3): 651-61.

Cheng, S. H., R. J. Gregory, et al. (1990). "Defective intracellular transport and processing of CFTR is the molecular basis of most cystic fibrosis." Cell **63**(4): 827-34.

Chiba, P., S. Burghofer, et al. (1995). "Synthesis, pharmacologic activity, and structure-activity relationships of a series of propafenone-related modulators of multidrug resistance." J Med Chem **38**(14): 2789-93.

Chiba, P., G. Ecker, et al. (1996). "Structural requirements for activity of propafenone-type modulators in P-glycoprotein-mediated multidrug resistance." Mol Pharmacol **49**(6): 1122-30.

Chiba, P., W. Holzer, et al. (1998). "Substituted 4-acylpyrazoles and 4-acylpyrazolones: synthesis and multidrug resistance-modulating activity." J Med Chem **41**(21): 4001-11.

Choi, K. H., C. J. Chen, et al. (1988). "An altered pattern of cross-resistance in multidrug-resistant human cells results from spontaneous mutations in the mdr1 (P-glycoprotein) gene." Cell **53**(4): 519-29.

Cordon-Cardo, C., J. P. O'Brien, et al. (1989). "Multidrug-resistance gene (P-glycoprotein) is expressed by endothelial cells at blood-brain barrier sites." Proc Natl Acad Sci U S A **86**(2): 695-8.

Dano, K. (1973). "Active outward transport of daunomycin in resistant Ehrlich ascites tumor cells." Biochim Biophys Acta **323**(3): 466-83.

Davidson, A. L., H. A. Shuman, et al. (1992). "Mechanism of maltose transport in Escherichia coli: transmembrane signaling by periplasmic binding proteins." Proc Natl Acad Sci U S A **89**(6): 2360-4.

Dawson, R. J., K. Hollenstein, et al. (2007). "Uptake or extrusion: crystal structures of full ABC transporters suggest a common mechanism." Mol Microbiol **65**(2): 250-7.

Dawson, R. J. and K. P. Locher (2006). "Structure of a bacterial multidrug ABC transporter." Nature **443**(7108): 180-5.

Dawson, R. J. and K. P. Locher (2007). "Structure of the multidrug ABC transporter Sav1866 from Staphylococcus aureus in complex with AMP-PNP." FEBS Lett **581**(5): 935-8.

de Vries, S. J., A. D. van Dijk, et al. (2006). "WHISCY: what information does surface conservation yield? Application to data-driven docking." Proteins **63**(3): 479-89.

Dean, M., Y. Hamon, et al. (2001). "The human ATP-binding cassette (ABC) transporter superfamily." J Lipid Res **42**(7): 1007-17.
Denisov, A. Y., G. Chen, et al. (2006). "Structural model of the BCL-w-BID peptide complex and its interactions with phospholipid micelles." Biochemistry **45**(7): 2250-6.
Denning, G. M., M. P. Anderson, et al. (1992). "Processing of mutant cystic fibrosis transmembrane conductance regulator is temperature-sensitive." Nature **358**(6389): 761-4.
Diederichs, K., J. Diez, et al. (2000). "Crystal structure of MalK, the ATPase subunit of the trehalose/maltose ABC transporter of the archaeon Thermococcus litoralis." Embo J **19**(22): 5951-61.
Dominguez, C., R. Boelens, et al. (2003). "HADDOCK: a protein-protein docking approach based on biochemical or biophysical information." J Am Chem Soc **125**(7): 1731-7.
Dorman, G. and G. D. Prestwich (2000). "Using photolabile ligands in drug discovery and development." Trends Biotechnol **18**(2): 64-77.
Dunne, M. J., C. Kane, et al. (1997). "Familial persistent hyperinsulinemic hypoglycemia of infancy and mutations in the sulfonylurea receptor." N Engl J Med **336**(10): 703-6.
Ecker, G. F., E. Csaszar, et al. (2002). "Identification of ligand-binding regions of P-glycoprotein by activated-pharmacophore photoaffinity labeling and matrix-assisted laser desorption/ionization-time-of-flight mass spectrometry." Mol Pharmacol **61**(3): 637-48.
Ecker, G. F., K. Pleban, et al. (2004). "A three-dimensional model for the substrate binding domain of the multidrug ATP binding cassette transporter LmrA." Mol Pharmacol **66**(5): 1169-79.
Ecker, G. F., T. Stockner, et al. (2008). "Computational models for prediction of interactions with ABC-transporters." Drug Discov Today **13**(7-8): 311-7.
Fojo, T. and S. Bates (2003). "Strategies for reversing drug resistance." Oncogene **22**(47): 7512-23.
Foote, S. J., J. K. Thompson, et al. (1989). "Amplification of the multidrug resistance gene in some chloroquine-resistant isolates of P. falciparum." Cell **57**(6): 921-30.
Gaudet, R. and D. C. Wiley (2001). "Structure of the ABC ATPase domain of human TAP1, the transporter associated with antigen processing." Embo J **20**(17): 4964-72.
Gekeler, V., G. Frese, et al. (1992). "Mdr1/P-glycoprotein, topoisomerase, and glutathione-S-transferase pi gene expression in primary and relapsed state adult and childhood leukaemias." Br J Cancer **66**(3): 507-17.
Gekeler, V., S. Weger, et al. (1990). "mdr1/P-glycoprotein gene segments analyzed from various human leukemic cell lines exhibiting different multidrug resistance profiles." Biochem Biophys Res Commun **169**(2): 796-802.
Ghose, A. K. and G. M. Crippen (1987). "Atomic physicochemical parameters for three-dimensional-structure-directed quantitative structure-activity relationships. 2. Modeling dispersive and hydrophobic interactions." J Chem Inf Comput Sci **27**(1): 21-35.
Gottesman, M. M., T. Fojo, et al. (2002). "Multidrug resistance in cancer: role of ATP-dependent transporters." Nat Rev Cancer **2**(1): 48-58.
Gottesman, M. M. and I. Pastan (1993). "Biochemistry of multidrug resistance mediated by the multidrug transporter." Annu Rev Biochem **62**: 385-427.

Hartley, J. L., G. F. Temple, et al. (2000). "DNA cloning using in vitro site-specific recombination." Genome Res **10**(11): 1788-95.
Higgins, C. F. (2007). "Multiple molecular mechanisms for multidrug resistance transporters." Nature **446**(7137): 749-57.
Higgins, C. F., P. D. Haag, et al. (1982). "Complete nucleotide sequence and identification of membrane components of the histidine transport operon of S. typhimurium." Nature **298**(5876): 723-7.
Higgins, C. F., I. D. Hiles, et al. (1986). "A family of related ATP-binding subunits coupled to many distinct biological processes in bacteria." Nature **323**(6087): 448-50.
Higgins, C. F., I. D. Hiles, et al. (1985). "Nucleotide binding by membrane components of bacterial periplasmic binding protein-dependent transport systems." Embo J **4**(4): 1033-9.
Higgins, C. F. and K. J. Linton (2004). "The ATP switch model for ABC transporters." Nat Struct Mol Biol **11**(10): 918-26.
Higuchi, R., B. Krummel, et al. (1988). "A general method of in vitro preparation and specific mutagenesis of DNA fragments: study of protein and DNA interactions." Nucleic Acids Res **16**(15): 7351-67.
Ho, S. N., H. D. Hunt, et al. (1989). "Site-directed mutagenesis by overlap extension using the polymerase chain reaction." Gene **77**(1): 51-9.
Hobson, A. C., R. Weatherwax, et al. (1984). "ATP-binding sites in the membrane components of histidine permease, a periplasmic transport system." Proc Natl Acad Sci U S A **81**(23): 7333-7.
Holland, I. B. and M. A. Blight (1999). "ABC-ATPases, adaptable energy generators fuelling transmembrane movement of a variety of molecules in organisms from bacteria to humans." J Mol Biol **293**(2): 381-99.
Hollenstein, K., R. J. Dawson, et al. (2007). "Structure and mechanism of ABC transporter proteins." Curr Opin Struct Biol **17**(4): 412-8.
Hollenstein, K., D. C. Frei, et al. (2007). "Structure of an ABC transporter in complex with its binding protein." Nature **446**(7132): 213-6.
Hopfner, K. P., A. Karcher, et al. (2000). "Structural biology of Rad50 ATPase: ATP-driven conformational control in DNA double-strand break repair and the ABC-ATPase superfamily." Cell **101**(7): 789-800.
Hung, L. W., I. X. Wang, et al. (1998). "Crystal structure of the ATP-binding subunit of an ABC transporter." Nature **396**(6712): 703-7.
Hyde, S. C., P. Emsley, et al. (1990). "Structural model of ATP-binding proteins associated with cystic fibrosis, multidrug resistance and bacterial transport." Nature **346**(6282): 362-5.
Invitrogen. (2002). "Manual: Flp-In System." Retrieved 21.06.2009, from http://biochem.dental.upenn.edu/GATEWAY/Vector_manual/flpinsystem_man.pdf.
Invitrogen. (2002). "Manual: pEF5/FRT/V5-DEST Gateway Vector." Version C. Retrieved 21.06.2009, from http://biochem.dental.upenn.edu/GATEWAY/Vector_manual/pef5frtv5_dest_man.pdf.
Invitrogen. (2003). "Manual: Gateway Technologa." Version E. Retrieved 21.06.2009, from http://tools.invitrogen.com/content/sfs/manuals/gatewayman.pdf.
Invitrogen. (2004). "Manual: Baculovirus Expression System with Gateway Technology." Version E. Retrieved 21.06.2009, from http://wolfson.huji.ac.il/expression/baculogateway_man.pdf.

Invitrogen. (2004). "Manual: Gateway pENTR Vectors." Verion B. Retrieved 21.06.2009, from http://tools.invitrogen.com/content/sfs/manuals/pentr_man.pdf.
Invitrogen. (2006). "Lipofectamine 2000 Datasheet." Retrieved 21.06.2009, from http://tools.invitrogen.com/content/sfs/manuals/lipofectamine2000_man.pdf.
Invitrogen. (2006). "Manual: pENTR Directional TOPO Cloning Kits." Version G. Retrieved 21.06.2009, from http://tools.invitrogen.com/content/sfs/manuals/pentr_dtopo_man.pdf.
Invitrogen. (2007). "Manual: TRIZOL Reagent." Retrieved 21.06.2009, from http://tools.invitrogen.com/content/sfs/manuals/15596018%20pps%20Trizol%20Reagent%20061207.pdf.
Invitrogen. (2009). "Manual: Bac-to-Bac Baculovirus Expression System." Version E. Retrieved 21.06.2009, from http://tools.invitrogen.com/content/sfs/manuals/bactobac_man.pdf.
Jones, P. M. and A. M. George (1999). "Subunit interactions in ABC transporters: towards a functional architecture." FEMS Microbiol Lett **179**(2): 187-202.
Juliano, R. L. and V. Ling (1976). "A surface glycoprotein modulating drug permeability in Chinese hamster ovary cell mutants." Biochim Biophys Acta **455**(1): 152-62.
Kang, H., M. H. Fisher, et al. (2004). "Inhibition of MDR1 gene expression by chimeric HNA antisense oligonucleotides." Nucleic Acids Res **32**(14): 4411-9.
Karpowich, N., O. Martsinkevich, et al. (2001). "Crystal structures of the MJ1267 ATP binding cassette reveal an induced-fit effect at the ATPase active site of an ABC transporter." Structure **9**(7): 571-86.
Kreimer, D. I., K. P. Chai, et al. (2000). "Nonequivalence of the nucleotide-binding subunits of an ABC transporter, the histidine permease, and conformational changes in the membrane complex." Biochemistry **39**(46): 14183-95.
Landy, A. (1989). "Dynamic, structural, and regulatory aspects of lambda site-specific recombination." Annu Rev Biochem **58**: 913-49.
Linton, K. J. and C. F. Higgins (2007). "Structure and function of ABC transporters: the ATP switch provides flexible control." Pflugers Arch **453**(5): 555-67.
Liu, P. Q., C. E. Liu, et al. (1999). "Modulation of ATPase activity by physical disengagement of the ATP-binding domains of an ABC transporter, the histidine permease." J Biol Chem **274**(26): 18310-8.
Liu, R. and F. J. Sharom (1996). "Site-directed fluorescence labeling of P-glycoprotein on cysteine residues in the nucleotide binding domains." Biochemistry **35**(36): 11865-73.
Locher, K. P. (2004). "Structure and mechanism of ABC transporters." Curr Opin Struct Biol **14**(4): 426-31.
Locher, K. P., A. T. Lee, et al. (2002). "The E. coli BtuCD structure: a framework for ABC transporter architecture and mechanism." Science **296**(5570): 1091-8.
Loo, T. W., M. C. Bartlett, et al. (2003). "Simultaneous binding of two different drugs in the binding pocket of the human multidrug resistance P-glycoprotein." J Biol Chem **278**(41): 39706-10.
Loo, T. W., M. C. Bartlett, et al. (2003). "Substrate-induced conformational changes in the transmembrane segments of human P-glycoprotein. Direct evidence for the substrate-induced fit mechanism for drug binding." J Biol Chem **278**(16): 13603-6.
Loo, T. W., M. C. Bartlett, et al. (2004). "Disulfide cross-linking analysis shows that transmembrane segments 5 and 8 of human P-glycoprotein are close together on the cytoplasmic side of the membrane." J Biol Chem **279**(9): 7692-7.

Loo, T. W., M. C. Bartlett, et al. (2004). "Processing mutations located throughout the human multidrug resistance P-glycoprotein disrupt interactions between the nucleotide binding domains." J Biol Chem **279**(37): 38395-401.
Loo, T. W., M. C. Bartlett, et al. (2004). "Thapsigargin or curcumin does not promote maturation of processing mutants of the ABC transporters, CFTR, and P-glycoprotein." Biochem Biophys Res Commun **325**(2): 580-5.
Loo, T. W., M. C. Bartlett, et al. (2004). "Val133 and Cys137 in transmembrane segment 2 are close to Arg935 and Gly939 in transmembrane segment 11 of human P-glycoprotein." J Biol Chem **279**(18): 18232-8.
Loo, T. W., M. C. Bartlett, et al. (2005). "The dileucine motif at the COOH terminus of human multidrug resistance P-glycoprotein is important for folding but not activity." J Biol Chem **280**(4): 2522-8.
Loo, T. W., M. C. Bartlett, et al. (2005). "Rescue of DeltaF508 and other misprocessed CFTR mutants by a novel quinazoline compound." Mol Pharm **2**(5): 407-13.
Loo, T. W., M. C. Bartlett, et al. (2005). "Rescue of folding defects in ABC transporters using pharmacological chaperones." J Bioenerg Biomembr **37**(6): 501-7.
Loo, T. W., M. C. Bartlett, et al. (2006). "Transmembrane segment 1 of human P-glycoprotein contributes to the drug-binding pocket." Biochem J **396**(3): 537-45.
Loo, T. W., M. C. Bartlett, et al. (2006). "Transmembrane segment 7 of human P-glycoprotein forms part of the drug-binding pocket." Biochem J **399**(2): 351-9.
Loo, T. W., M. C. Bartlett, et al. (2007). "Nucleotide binding, ATP hydrolysis, and mutation of the catalytic carboxylates of human P-glycoprotein cause distinct conformational changes in the transmembrane segments." Biochemistry **46**(32): 9328-36.
Loo, T. W., M. C. Bartlett, et al. (2007). "Suppressor mutations in the transmembrane segments of P-glycoprotein promote maturation of processing mutants and disrupt a subset of drug-binding sites." J Biol Chem **282**(44): 32043-52.
Loo, T. W. and D. M. Clarke (1993). "Functional consequences of phenylalanine mutations in the predicted transmembrane domain of P-glycoprotein." J Biol Chem **268**(27): 19965-72.
Loo, T. W. and D. M. Clarke (1995). "Membrane topology of a cysteine-less mutant of human P-glycoprotein." J Biol Chem **270**(2): 843-8.
Loo, T. W. and D. M. Clarke (1996). "The minimum functional unit of human P-glycoprotein appears to be a monomer." J Biol Chem **271**(44): 27488-92.
Loo, T. W. and D. M. Clarke (1997). "Correction of defective protein kinesis of human P-glycoprotein mutants by substrates and modulators." J Biol Chem **272**(2): 709-12.
Loo, T. W. and D. M. Clarke (1998). "Superfolding of the partially unfolded core-glycosylated intermediate of human P-glycoprotein into the mature enzyme is promoted by substrate-induced transmembrane domain interactions." J Biol Chem **273**(24): 14671-4.
Loo, T. W. and D. M. Clarke (1999). "Determining the structure and mechanism of the human multidrug resistance P-glycoprotein using cysteine-scanning mutagenesis and thiol-modification techniques." Biochim Biophys Acta **1461**(2): 315-25.
Loo, T. W. and D. M. Clarke (1999). "The transmembrane domains of the human multidrug resistance P-glycoprotein are sufficient to mediate drug binding and trafficking to the cell surface." J Biol Chem **274**(35): 24759-65.
Loo, T. W. and D. M. Clarke (2001). "Defining the drug-binding site in the human multidrug resistance P-glycoprotein using a methanethiosulfonate analog of verapamil, MTS-verapamil." J Biol Chem **276**(18): 14972-9.

Loo, T. W. and D. M. Clarke (2002). "Location of the rhodamine-binding site in the human multidrug resistance P-glycoprotein." J Biol Chem **277**(46): 44332-8.
Loo, T. W. and D. M. Clarke (2005). "Do drug substrates enter the common drug-binding pocket of P-glycoprotein through "gates"?" Biochem Biophys Res Commun **329**(2): 419-22.
Loo, T. W. and D. M. Clarke (2008). "Mutational analysis of ABC proteins." Arch Biochem Biophys **476**(1): 51-64.
Lu, G., J. M. Westbrooks, et al. (2005). "ATP hydrolysis is required to reset the ATP-binding cassette dimer into the resting-state conformation." Proc Natl Acad Sci U S A **102**(50): 17969-74.
Luckow, V. A., S. C. Lee, et al. (1993). "Efficient generation of infectious recombinant baculoviruses by site-specific transposon-mediated insertion of foreign genes into a baculovirus genome propagated in Escherichia coli." J Virol **67**(8): 4566-79.
Lugo, M. R. and F. J. Sharom (2005). "Interaction of LDS-751 and rhodamine 123 with P-glycoprotein: evidence for simultaneous binding of both drugs." Biochemistry **44**(42): 14020-9.
Manciu, L., X. B. Chang, et al. (2003). "Intermediate structural states involved in MRP1-mediated drug transport. Role of glutathione." J Biol Chem **278**(5): 3347-56.
Mannering, D. E., S. Sharma, et al. (2001). "Demonstration of conformational changes associated with activation of the maltose transport complex." J Biol Chem **276**(15): 12362-8.
Martin, C., G. Berridge, et al. (2000). "Communication between multiple drug binding sites on P-glycoprotein." Mol Pharmacol **58**(3): 624-32.
Martin, C., G. Berridge, et al. (2000). "Drug binding sites on P-glycoprotein are altered by ATP binding prior to nucleotide hydrolysis." Biochemistry **39**(39): 11901-6.
Martin, C., C. F. Higgins, et al. (2001). "The vinblastine binding site adopts high- and low-affinity conformations during a transport cycle of P-glycoprotein." Biochemistry **40**(51): 15733-42.
Mihalek, I., I. Res, et al. (2004). "A family of evolution-entropy hybrid methods for ranking protein residues by importance." J Mol Biol **336**(5): 1265-82.
Miki, T., J. A. Park, et al. (1992). "Control of segregation of chromosomal DNA by sex factor F in Escherichia coli. Mutants of DNA gyrase subunit A suppress letD (ccdB) product growth inhibition." J Mol Biol **225**(1): 39-52.
Mimmack, M. L., M. P. Gallagher, et al. (1989). "Energy coupling to periplasmic binding protein-dependent transport systems: stoichiometry of ATP hydrolysis during transport in vivo." Proc Natl Acad Sci U S A **86**(21): 8257-61.
Moody, J. E., L. Millen, et al. (2002). "Cooperative, ATP-dependent association of the nucleotide binding cassettes during the catalytic cycle of ATP-binding cassette transporters." J Biol Chem **277**(24): 21111-4.
Mourez, M., M. Hofnung, et al. (1997). "Subunit interactions in ABC transporters: a conserved sequence in hydrophobic membrane proteins of periplasmic permeases defines an important site of interaction with the ATPase subunits." Embo J **16**(11): 3066-77.
Neumann, L., R. Abele, et al. (2002). "Thermodynamics of peptide binding to the transporter associated with antigen processing (TAP)." J Mol Biol **324**(5): 965-73.
Nikaido, K. and G. F. Ames (1999). "One intact ATP-binding subunit is sufficient to support ATP hydrolysis and translocation in an ABC transporter, the histidine permease." J Biol Chem **274**(38): 26727-35.
O'Gorman, S., D. T. Fox, et al. (1991). "Recombinase-mediated gene activation and site-specific integration in mammalian cells." Science **251**(4999): 1351-5.

O'Mara, M. L. and D. P. Tieleman (2007). "P-glycoprotein models of the apo and ATP-bound states based on homology with Sav1866 and MalK." FEBS Lett **581**(22): 4217-22.
Oldham, M. L., D. Khare, et al. (2007). "Crystal structure of a catalytic intermediate of the maltose transporter." Nature **450**(7169): 515-21.
Omote, H., R. A. Figler, et al. (2004). "Improved energy coupling of human P-glycoprotein by the glycine 185 to valine mutation." Biochemistry **43**(13): 3917-28.
Opitz, O. G., T. D. Jenkins, et al. (1998). "Transcriptional regulation of the differentiation-linked human K4 promoter is dependent upon esophageal-specific nuclear factors." J Biol Chem **273**(37): 23912-21.
Panagiotidis, C. H., M. Reyes, et al. (1993). "Characterization of the structural requirements for assembly and nucleotide binding of an ATP-binding cassette transporter. The maltose transport system of Escherichia coli." J Biol Chem **268**(31): 23685-96.
Payen, L. F., M. Gao, et al. (2003). "Role of carboxylate residues adjacent to the conserved core Walker B motifs in the catalytic cycle of multidrug resistance protein 1 (ABCC1)." J Biol Chem **278**(40): 38537-47.
Petronilli, V. and G. F. Ames (1991). "Binding protein-independent histidine permease mutants. Uncoupling of ATP hydrolysis from transmembrane signaling." J Biol Chem **266**(25): 16293-6.
Pind, S., J. R. Riordan, et al. (1994). "Participation of the endoplasmic reticulum chaperone calnexin (p88, IP90) in the biogenesis of the cystic fibrosis transmembrane conductance regulator." J Biol Chem **269**(17): 12784-8.
Pinkett, H. W., A. T. Lee, et al. (2007). "An inward-facing conformation of a putative metal-chelate-type ABC transporter." Science **315**(5810): 373-7.
Pleban, K., S. Kopp, et al. (2005). "P-glycoprotein substrate binding domains are located at the transmembrane domain/transmembrane domain interfaces: a combined photoaffinity labeling-protein homology modeling approach." Mol Pharmacol **67**(2): 365-74.
Pohl, A., P. F. Devaux, et al. (2005). "Function of prokaryotic and eukaryotic ABC proteins in lipid transport." Biochim Biophys Acta **1733**(1): 29-52.
Polgar, O. and S. E. Bates (2005). "ABC transporters in the balance: is there a role in multidrug resistance?" Biochem Soc Trans **33**(Pt 1): 241-5.
Possee, R. D. and S. C. Howard (1987). "Analysis of the polyhedrin gene promoter of the Autographa californica nuclear polyhedrosis virus." Nucleic Acids Res **15**(24): 10233-48.
Procko, E., I. Ferrin-O'Connell, et al. (2006). "Distinct structural and functional properties of the ATPase sites in an asymmetric ABC transporter." Mol Cell **24**(1): 51-62.
QIAGEN. (2005). "Manual: HiSpeed Plasmid Purification Handbook." Retrieved 21.06.2009, from http://kirschner.med.harvard.edu/files/protocols/QIAGEN_HiSpeedPlasmidKit_EN.pdf.
Quiocho, F. A. and P. S. Ledvina (1996). "Atomic structure and specificity of bacterial periplasmic receptors for active transport and chemotaxis: variation of common themes." Mol Microbiol **20**(1): 17-25.
Raymond, M. and P. Gros (1989). "Mammalian multidrug-resistance gene: correlation of exon organization with structural domains and duplication of an ancestral gene." Proc Natl Acad Sci U S A **86**(17): 6488-92.

Rees, D. C., E. Johnson, et al. (2009). "ABC transporters: the power to change." Nat Rev Mol Cell Biol **10**(3): 218-27.
Reyes, C. L. and G. Chang (2005). "Structure of the ABC transporter MsbA in complex with ADP.vanadate and lipopolysaccharide." Science **308**(5724): 1028-31.
Rihakova, L., M. Deraet, et al. (2002). "Methionine proximity assay, a novel method for exploring peptide ligand-receptor interaction." J Recept Signal Transduct Res **22**(1-4): 297-313.
Riordan, J. R., J. M. Rommens, et al. (1989). "Identification of the cystic fibrosis gene: cloning and characterization of complementary DNA." Science **245**(4922): 1066-73.
Rosenberg, M. F., R. Callaghan, et al. (1997). "Structure of the multidrug resistance P-glycoprotein to 2.5 nm resolution determined by electron microscopy and image analysis." J Biol Chem **272**(16): 10685-94.
Rosenberg, M. F., R. Callaghan, et al. (2005). "Three-dimensional structure of P-glycoprotein: the transmembrane regions adopt an asymmetric configuration in the nucleotide-bound state." J Biol Chem **280**(4): 2857-62.
Rosenberg, M. F., A. B. Kamis, et al. (2003). "Three-dimensional structures of the mammalian multidrug resistance P-glycoprotein demonstrate major conformational changes in the transmembrane domains upon nucleotide binding." J Biol Chem **278**(10): 8294-9.
Rosenberg, M. F., Q. Mao, et al. (2001). "The structure of the multidrug resistance protein 1 (MRP1/ABCC1). crystallization and single-particle analysis." J Biol Chem **276**(19): 16076-82.
Rosenberg, M. F., G. Velarde, et al. (2001). "Repacking of the transmembrane domains of P-glycoprotein during the transport ATPase cycle." Embo J **20**(20): 5615-25.
Ruth, A., W. D. Stein, et al. (2001). "Coordinate changes in drug resistance and drug-induced conformational transitions in altered-function mutants of the multidrug transporter P-glycoprotein." Biochemistry **40**(14): 4332-9.
Sanchez, C. P., A. Rotmann, et al. (2008). "Polymorphisms within PfMDR1 alter the substrate specificity for anti-malarial drugs in Plasmodium falciparum." Mol Microbiol **70**(4): 786-98.
Sauna, Z. E. and S. V. Ambudkar (2000). "Evidence for a requirement for ATP hydrolysis at two distinct steps during a single turnover of the catalytic cycle of human P-glycoprotein." Proc Natl Acad Sci U S A **97**(6): 2515-20.
Sauna, Z. E. and S. V. Ambudkar (2001). "Characterization of the catalytic cycle of ATP hydrolysis by human P-glycoprotein. The two ATP hydrolysis events in a single catalytic cycle are kinetically similar but affect different functional outcomes." J Biol Chem **276**(15): 11653-61.
Sauna, Z. E. and S. V. Ambudkar (2007). "About a switch: how P-glycoprotein (ABCB1) harnesses the energy of ATP binding and hydrolysis to do mechanical work." Mol Cancer Ther **6**(1): 13-23.
Sauna, Z. E., I. W. Kim, et al. (2007). "Catalytic cycle of ATP hydrolysis by P-glycoprotein: evidence for formation of the E.S reaction intermediate with ATP-gamma-S, a nonhydrolyzable analogue of ATP." Biochemistry **46**(48): 13787-99.
Saurin, W., M. Hofnung, et al. (1999). "Getting in or out: early segregation between importers and exporters in the evolution of ATP-binding cassette (ABC) transporters." J Mol Evol **48**(1): 22-41.
Schieborr, U., M. Vogtherr, et al. (2005). "How much NMR data is required to determine a protein-ligand complex structure?" Chembiochem **6**(10): 1891-8.

Schlemmer, S. R. and F. M. Sirotnak (1994). "Functional studies of P-glycoprotein in inside-out plasma membrane vesicles derived from murine erythroleukemia cells overexpressing MDR 3. Properties and kinetics of the interaction of vinblastine with P-glycoprotein and evidence for its active mediated transport." J Biol Chem **269**(49): 31059-66.

Schmid, D., G. Ecker, et al. (1999). "Structure-activity relationship studies of propafenone analogs based on P-glycoprotein ATPase activity measurements." Biochem Pharmacol **58**(9): 1447-56.

Schmid, D., D. L. Staudacher, et al. (2003). "A subset of highly effective propafenone-type multidrug resistance modulators lacks effects on cardiac action potential and mechanical twitch parameters of rat papillary muscles." J Pharmacol Exp Ther **307**(2): 589-96.

Schmitt, L., H. Benabdelhak, et al. (2003). "Crystal structure of the nucleotide-binding domain of the ABC-transporter haemolysin B: identification of a variable region within ABC helical domains." J Mol Biol **330**(2): 333-42.

Schmitt, L. and R. Tampe (2002). "Structure and mechanism of ABC transporters." Curr Opin Struct Biol **12**(6): 754-60.

Schneider, E. and S. Hunke (1998). "ATP-binding-cassette (ABC) transport systems: functional and structural aspects of the ATP-hydrolyzing subunits/domains." FEMS Microbiol Rev **22**(1): 1-20.

Seigneuret, M. and A. Garnier-Suillerot (2003). "A structural model for the open conformation of the mdr1 P-glycoprotein based on the MsbA crystal structure." J Biol Chem **278**(32): 30115-24.

Senior, A. E., M. K. al-Shawi, et al. (1995). "The catalytic cycle of P-glycoprotein." FEBS Lett **377**(3): 285-9.

Senior, A. E. and D. C. Gadsby (1997). "ATP hydrolysis cycles and mechanism in P-glycoprotein and CFTR." Semin Cancer Biol **8**(3): 143-50.

Serohijos, A. W., T. Hegedus, et al. (2008). "Phenylalanine-508 mediates a cytoplasmic-membrane domain contact in the CFTR 3D structure crucial to assembly and channel function." Proc Natl Acad Sci U S A **105**(9): 3256-61.

Shapiro, A. B., K. Fox, et al. (1999). "Stimulation of P-glycoprotein-mediated drug transport by prazosin and progesterone. Evidence for a third drug-binding site." Eur J Biochem **259**(3): 841-50.

Shapiro, A. B. and V. Ling (1997). "Extraction of Hoechst 33342 from the cytoplasmic leaflet of the plasma membrane by P-glycoprotein." Eur J Biochem **250**(1): 122-9.

Sharma, S. and A. L. Davidson (2000). "Vanadate-induced trapping of nucleotides by purified maltose transport complex requires ATP hydrolysis." J Bacteriol **182**(23): 6570-6.

Sigma-Aldrich. (2006). "Manual: GenElute Plasmid Miniprep Kit." Retrieved 21.06.2009, from http://www.sigmaaldrich.com/etc/medialib/docs/Sigma/Bulletin/pln10bul.Par.0001.File.tmp/pln10bul.pdf.

Smit, J. W., M. T. Huisman, et al. (1999). "Absence or pharmacological blocking of placental P-glycoprotein profoundly increases fetal drug exposure." J Clin Invest **104**(10): 1441-7.

Smith, P. C., N. Karpowich, et al. (2002). "ATP binding to the motor domain from an ABC transporter drives formation of a nucleotide sandwich dimer." Mol Cell **10**(1): 139-49.

Sonveaux, N., C. Vigano, et al. (1999). "Ligand-mediated tertiary structure changes of reconstituted P-glycoprotein. A tryptophan fluorescence quenching analysis." J Biol Chem **274**(25): 17649-54.
Stein, W. D. (1997). "Kinetics of the multidrug transporter (P-glycoprotein) and its reversal." Physiol Rev **77**(2): 545-90.
Stenham, D. R., J. D. Campbell, et al. (2003). "An atomic detail model for the human ATP binding cassette transporter P-glycoprotein derived from disulfide cross-linking and homology modeling." Faseb J **17**(15): 2287-9.
Stockner, T., S. J. de Vries, et al. (2009). "Data-driven homology modelling of P-glycoprotein in the ATP-bound state indicates flexibility of the transmembrane domains." Febs J **276**(4): 964-72.
Taguchi, Y., K. Kino, et al. (1997). "Alteration of substrate specificity by mutations at the His61 position in predicted transmembrane domain 1 of human MDR1/P-glycoprotein." Biochemistry **36**(29): 8883-9.
Tzakos, A. G., P. Fuchs, et al. (2004). "NMR and molecular dynamics studies of an autoimmune myelin basic protein peptide and its antagonist: structural implications for the MHC II (I-Au)-peptide complex from docking calculations." Eur J Biochem **271**(16): 3399-413.
Ueda, K., M. M. Cornwell, et al. (1986). "The mdr1 gene, responsible for multidrug-resistance, codes for P-glycoprotein." Biochem Biophys Res Commun **141**(3): 956-62.
Urbatsch, I. L., B. Sankaran, et al. (1995). "Both P-glycoprotein nucleotide-binding sites are catalytically active." J Biol Chem **270**(45): 26956-61.
Urbatsch, I. L., B. Sankaran, et al. (1995). "P-glycoprotein is stably inhibited by vanadate-induced trapping of nucleotide at a single catalytic site." J Biol Chem **270**(33): 19383-90.
Urbatsch, I. L., G. A. Tyndall, et al. (2003). "P-glycoprotein catalytic mechanism: studies of the ADP-vanadate inhibited state." J Biol Chem **278**(25): 23171-9.
van der Valk, P., C. K. van Kalken, et al. (1990). "Distribution of multi-drug resistance-associated P-glycoprotein in normal and neoplastic human tissues. Analysis with 3 monoclonal antibodies recognizing different epitopes of the P-glycoprotein molecule." Ann Oncol **1**(1): 56-64.
van Dijk, A. D., S. J. de Vries, et al. (2005). "Data-driven docking: HADDOCK's adventures in CAPRI." Proteins **60**(2): 232-8.
van Dijk, A. D., D. Fushman, et al. (2005). "Various strategies of using residual dipolar couplings in NMR-driven protein docking: application to Lys48-linked di-ubiquitin and validation against 15N-relaxation data." Proteins **60**(3): 367-81.
van Dijk, M., A. D. van Dijk, et al. (2006). "Information-driven protein-DNA docking using HADDOCK: it is a matter of flexibility." Nucleic Acids Res **34**(11): 3317-25.
van Veen, H. W., A. Margolles, et al. (2000). "The homodimeric ATP-binding cassette transporter LmrA mediates multidrug transport by an alternating two-site (two-cylinder engine) mechanism." Embo J **19**(11): 2503-14.
Verdon, G., S. V. Albers, et al. (2003). "Crystal structures of the ATPase subunit of the glucose ABC transporter from Sulfolobus solfataricus: nucleotide-free and nucleotide-bound conformations." J Mol Biol **330**(2): 343-58.
Volkov, A. N., D. Ferrari, et al. (2005). "The orientations of cytochrome c in the highly dynamic complex with cytochrome b5 visualized by NMR and docking using HADDOCK." Protein Sci **14**(3): 799-811.

Volpon, L., I. D'Orso, et al. (2005). "NMR structural study of TcUBP1, a single RRM domain protein from Trypanosoma cruzi: contribution of a beta hairpin to RNA binding." Biochemistry **44**(10): 3708-17.
Walker, J. E., M. Saraste, et al. (1982). "Distantly related sequences in the alpha- and beta-subunits of ATP synthase, myosin, kinases and other ATP-requiring enzymes and a common nucleotide binding fold." Embo J **1**(8): 945-51.
Ward, A., C. L. Reyes, et al. (2007). "Flexibility in the ABC transporter MsbA: Alternating access with a twist." Proc Natl Acad Sci U S A **104**(48): 19005-10.
Welch, W. J. and C. R. Brown (1996). "Influence of molecular and chemical chaperones on protein folding." Cell Stress Chaperones **1**(2): 109-15.
Yang, Z., D. Wu, et al. (2008). "A Novel Human Multi-Drug Resistance Gene MDR1 Variant G571A-Gly191Arg Modulates Cancer Drug Resistance and Efflux Transport." J Pharmacol Exp Ther.
Yang, Z., D. Wu, et al. (2008). "A novel human multidrug resistance gene MDR1 variant G571A (G191R) modulates cancer drug resistance and efflux transport." J Pharmacol Exp Ther **327**(2): 474-81.
Yuan, Y. R., S. Blecker, et al. (2001). "The crystal structure of the MJ0796 ATP-binding cassette. Implications for the structural consequences of ATP hydrolysis in the active site of an ABC transporter." J Biol Chem **276**(34): 32313-21.
Zolnerciks, J. K., C. Wooding, et al. (2007). "Evidence for a Sav1866-like architecture for the human multidrug transporter P-glycoprotein." Faseb J **21**(14): 3937-48.

8 List of abbreviations

ABC	ATP-binding cassette
ADP	Adenosine diphosphate
AMP-PNP	Adenosine 5'-(ß, γ-imido) triphosphate
APS	Ammonium persulphate
ATP	Adenosine triphosphate
ATP-γ-S	Adenosine 5'-(γ-thio) triphosphate
Å	Angstrom
BCRP	Breast cancer resistance protein
BSA	Bovine serum albumin
bp	Base pair
°C	Degree Celsius
cDNA	Complementary DNA
cryo-EM	Cryo-electron microscopy
C-terminal	Carboxy-terminal
DEPC	Diethylpyrocarbonate
DMEM	Dulbecco's modified Eagle's medium
DMSO	Dimethyl sulfoxide
DNA	Deoxyribonucleic acid
DBS	Donor bovine serum
EDTA	Ethylene diamine tetraacetic acid
ER	Endoplasmic reticulum
FACS	Fluorescence-activated cell sorting
GAM Ig FITC	Goat anti-mouse Ig fluorescein isothiocyanate
ICL	Intracellular loop
HADDOCK	High Ambiguity Driven DOCKing
HPRT	Hypoxanthine-guanine phosphoribosyltransferase
hr	Hour
ICL	Intracellular loop
Km	Michaelis-Menten constant
kb	Kilobase
kDa	Kilodalton
LB	Lysogeny broth

M	Molarity
MALDI-TOF	Matrix-assisted laser desorption/ionization time-of-flight
MDR	Multidrug resistance
MFU	Mean fluorescence units
ml	Milligram
min	Minute
MOPS	3-(N-Morpholino)propanesulphonic acid
MRP	Multidrug resistance-associated protein
mRNA	Messenger Ribonucleic acid
MSAs	Multiple sequence alignments
NBD	Nucleotide-binding domain
NMR	Nuclear magnetic resonance
Nt	Nucleotide
N-terminal	Amino-terminal
OE-PCR	Overlap extension polymerase chain reaction
PAGE	Polyacrylamide Gel Electrophoresis
PBS	Phosphate-buffered saline
PCR	Polymerase chain reaction
P-gp	P-glycoprotein
Real-time RT-PCR	Real-time reverse transcription PCR
Rh123	Rhodamine 123
RNA	Ribonucleic acid
RT	Room temperature
rvET	Real valued evolutionary trace
SDS	Sodium dodecyl sulphate
sec	Second
TAE	Tris-acetate EDTA buffer
TEMED	N, N, N´ ,N´ -tetramethylethane-1, 2-diamine
TM	Transmembrane helix
TMD	Transmembrane domain
Tris	Trihydoxymethylaminomethane
U	Unit
UV	Ultra violet
V	Voltage

Vmax	Maximum velocity
Wt	Wild-type

Symbols of amino acids

A	Ala	Alanine
C	Cys	Cysteine
E	Glu	Glutamic acid
H	His	Histidine
Q	Gln	Glutamine
R	Arg	Arginine
V	Val	Valine

9 Zusammenfassung

Das humane „multidrug resistance“ P-Glycoprotein, welches durch das *MDR1* Gen kodiert wird, gehört zu der Familie der ATP-binding cassette (ABC) Transporter, die unter ATP-Verbrauch zelltoxische, strukturell nicht näher verwandte Stoffe aus der Zelle pumpt. Dieses Protein hat klinisch eine große Bedeutung aufgrund des Phänomens der zellulären Resistenz gegen viele Wirkstoffe, auch „multidrug resistance“ genannt. Resistenzen gegen verschiedene Medikamente sind eines der Hauptprobleme in der Behandlung von Krebs. Das P-Glycoprotein besteht aus zwei homologen Hälften, die durch einen Linker miteinander verbunden sind. Jede Hälfte besteht aus einer Transmembrandomäne, die sechs Transmembransegmente besitzt, und einer hydrophilen Nukleotidbindungsdomäne, der Nukleotidbindungsstelle.

Ziel dieser Arbeit war die Identifizierung und Charakterisierung von TMD1/TMD2 Kontakt-Interface-Aminosäurenresten, die eine wichtige Rolle beim Transport von löslichen Substanzen spielen. Funktionelle Untersuchungen wurden mit P-gp Mutanten durchgeführt, deren TMD1/TMD2 Kontakt-Interface-Aminosäuren mittels zielgerichteter Mutagenese zu anderen Resten außer Cystein mutiert wurden. Die zielgerichtete Mutagenese basierte auf „overlap extension“ Polymerase-Kettenreaktion (OE-PCR). Das Mutationskonzept wurde durch Photoaffinitätsmarkierung, vorhandene Proteinhomologiemodelle, *in-silico* Vorhersage von wichtigen Aminosäure-Resten mittels der „real valued evolutionary trace“ Methode und „data-driven docking“, basierend auf Daten von vorhergegangenen zielgerichteten Mutationen, gesteuert.

Diesen Erkenntnissen zufolge wurden P-gp Mutanten hergestellt, die Aminosäure-Reste besitzen, die vom Protein toleriert werden, um eine hohe Anzahl von richtig gefalteten und funktionellen Transportern zu erhalten. Die Glutaminreste Q132 (TM2) in der N-terminalen Hälfte und Q773 (TM8) in der C-terminalen Hälfte wurden in Betracht gezogen. P-gp Homologiemodelle zeigen, dass diese beiden Q-Reste in der Nähe von stark photomarkierten Resten im TM2/11 Interface und im contralateralen TM5/8 Interface liegen.

In einigen Tierarten ist einer der beiden Q-Reste zu R oder E mutiert, was darauf hinweist, dass eine Ladung in dieser Position im Protein toleriert wird. Deshalb wurde Q132 zu Q132A, Q132E und Q132R, und Q773 zu Q773A, Q773E und Q773R mutiert. Zusätzlich wurden die Doppelmutanten Q132A/Q773A, Q132E/Q773E und Q132R/Q773R generiert. Alle Mutanten wurden mittels Efflux-Studien, MRK16 Fär-

bungen und Toxizitätstests charakterisiert. Die Q773R Mutante zeigte für das Substrat Rhodamin 123 einen mangelhaften Transport, während sowohl die Q773E Mutante als auch die Q773A Mutante einen aktiven Transport aufwiesen. Ein unbeeinträchtigten Rhodamin 123 Transport konnte für die A, E und R Mutanten in der Position 132 gezeigt werden. Die Q132R/Q773R Doppelmutante war wenig aktiv.

10 Curriculum Vitae

PERSONAL DATA

Date of birth:	15.11.1976
Family status:	unmarried
Nationality:	Austrian
Place of birth:	Vorrau, Austria

EDUCATION

Since March 2008 - present

- Project: “Development of protein substitution therapy for Rett syndrome” at the Department of Human Genetics, Medical University of Vienna

October 2004 – February 2008

- PhD thesis “Structure and function of P-glycoprotein” at the Institute of Medical Chemistry, Medical University of Vienna

April 2004 – September 2004

- Project:”Structure and function of *LmrA*” at the Institute of Medical Chemistry, Medical University of Vienna

June 2003

- Final examination

January 2002 – April 2003

- Master thesis “Identification of proteins associated with human plasma cell membrane glycoprotein 1 (PC-1) by means of 2-D gel electrophoresis and matrix-assisted laser desorption/ionization mass spectrometry” at the Institute of Chemistry; University of Vienna

October 1996 – December 2001

- Studies of Genetics, University of Vienna

October 1995 – June 1996

- Studies of Veterinary Medicine, University of Veterinary Medicine Vienna

September 1991 – June 1995

- Bundesoberstufenrealgymnasium Hartberg (Styria)

September 1987 – June 1991

- Wirtschaftliches Realgymnasium Mödling (Lower Austria)

September 1983 – June 1987

- Elementary school; Biedermannsdorf (Lower Austria)

TEACHING

- SE+PR BL9: Krankheit, Manifestation und Wahrnehmung, allgemeiner Arzneitherapie

POSTER PRESENTATIONS

- ÖGBM Joint meeting 2004, Innsbruck, Austria
  Structural and functional studies of MDR-related ABC-transporters by site-directed mutagenesis, photoaffinity labelling and protein homology modelling

- FEBS congress 2005, Budapest, Hungary
  Structural and functional studies of MDR-related ABC-transporters by site-directed mutagenesis, photoaffinity labelling and protein homology modelling

- ÖGBM Joint meeting 2005, Vienna, Austria
  Characterization of MDR-related ABC-transporters using protein homology modelling, site-directed mutagenesis and photoaffinity labelling

- FEBS Special Meeting, ABC 2006, Innsbruck, Austria
  Site directed mutagenesis studies of P-gp guided by *in silico* impotance prediction of residues and protein homology modelling

- Vfwf-Einladung (Verein zur Föderung von Wissenschaft und Forschung) 2006, Vienna, Austria
  The role of conserved glutamine residues in transmembrane segments of P-glycoprotein

- ÖGBM Joint meeting 2006, Vienna, Austria
  P-glycoprotein (ABCB1) mutants with altered substrate specificity are detected by using substrates/inhibitors as pharmacological chaperones